

Copyright
by
Junsang Nam
2007

**The Dissertation Committee for Junsang Nam Certifies that this is the approved
version of the following dissertation:**

**Variability in Industrial Hydrocarbon Emissions and Its Impact on
Ozone Formation in Houston, Texas**

Committee:

David T. Allen, Supervisor

Howard M. Liljestrand

Richard L. Corsi

Thomas F. Edgar

Elena C. McDonald-Buller

**Variability in Industrial Hydrocarbon Emissions and Its Impact on
Ozone Formation in Houston, Texas**

by

Junsang Nam, M.S., B.S.

Dissertation

Presented to the Faculty of the Graduate School of

The University of Texas at Austin

in partial fulfillment

of the requirements

for the degree of

Doctor of Philosophy

The University of Texas at Austin

May 2007

To My Family

Acknowledgements

The research presented in this dissertation was carried out at Center for Energy and Environmental Resources at the University of Texas at Austin. I would like to express my most sincere gratitude to Dr. David T. Allen for his guidance, support, and encouragement during the course of this research. I would like to thank Dr. Thomas F. Edgar, Dr. Howard M. Liljestrand, Dr. Richard L. Corsi, and Dr. Elena C. McDonald-Buller for serving on my dissertation committee. I would like to thank Dr. Yosuke Kimura for his technical assistance and dedication throughout the work that is presented here. This dissertation was dedicated to my family, especially to my wife, Soohee Seo, for her great support and encouragement. Finally, I want to thank God for his countless blessings.

April 2007

Junsang Nam

Variability in Industrial Hydrocarbon Emissions and Its Impact on Ozone Formation in Houston, Texas

Publication No. _____

Junsang Nam, Ph.D.

The University of Texas at Austin, 2007

Supervisor: David T. Allen

Ambient observations have indicated that ozone formation in the Houston area is frequently faster and more efficient, with respect to NO_x consumed, than other urban areas in the country. It is believed that these unique characteristics of ozone formation in the Houston area are associated with the plumes of reactive hydrocarbons, emanating from the industrial Houston Ship Channel area. Thus, accurate quantification of industrial emissions, particularly of reactive hydrocarbons, is critical to effectively address the rapid ozone formation and the consequent high levels of ozone in the area. Industrial emissions of hydrocarbons have significant temporal variability as evidenced by various measurements, but they have been assumed to be continuous at constant levels for air quality regulation and photochemical modeling studies. This thesis examines the effect of emission variability from industrial sources on ozone formation in the Houston-Galveston area. Both discrete emission events and variability in continuous emissions

are examined; new air quality modeling tools have been developed to perform these analyses. Also, this thesis evaluates the impact of emission variability on the effectiveness of emission control strategies in the Houston-Galveston area. Overall, the results indicate that industrial emission variability plays a substantial role in ozone formation and that controlling emission variability can be effective in ozone reduction. These results suggest that a quantitative treatment of emission variability should be included in the development of air quality plans for regions with extensive industrial activity, such as Houston.

Table of Contents

List of Tables	xi
List of Figures	xii
CHAPTER 1 INTRODUCTION	1
1.1 Background.....	1
1.2 Research Objectives.....	7
1.3 Dissertation Overview	8
1.4 References.....	9
CHAPTER 2 LITERATURE REVIEW	11
2.1 Overview of Emission Inventories	11
2.2 Temporal Variability in Emissions of NO _x	13
2.3 Temporal Variability in Industrial Emissions of Hydrocarbons.....	14
2.4 References.....	15
CHAPTER 3 Modeling the impacts of emission events on ozone formation in Houston, Texas	18
3.1 Introduction.....	18
3.2 Methods	19
3.2.1 Characterization of Emission Events.....	19
3.2.2 Development of Subdomain Model.....	20
3.2.3 Evaluation of the sub-domain model	26
3.2.4 Scenarios examined using the sub-domain model.....	34
3.3 Results and Discussion	35
3.3.1 Event Magnitude.....	35
3.3.2 Time of event occurrence	39
3.3.3 Event Duration	41
3.3.4 Event Composition	43
3.4 Summary.....	46

3.5	References.....	49
CHAPTER 4 The effect of variability in industrial emissions on ozone formation in Houston, Texas		
		51
4.1	Introduction.....	51
4.2	Methods	53
4.2.1	The stochastic emission inventory generator.....	53
4.2.2	Application of stochastic emission inventory to the HG area	62
4.2.3	Air quality modeling.....	64
4.3	Results and Discussion	67
4.3.1	Stochastic emission inventory	67
4.3.2	Impacts of VOC emission variability on ozone formation	71
4.4	References.....	78
CHAPTER 5 The effectiveness of control of industrial emission variability for ozone in Houston, Texas		
		80
5.1	Introduction.....	80
5.2	Methods	83
5.2.1	The stochastic emission inventory for the HG area.....	83
5.2.2	Control strategies associated with variability in industrial emissions ...	90
5.2.3	Air quality modeling.....	96
5.3	Results and Discussion	99
5.3.1	Control of allowable episodic emissions	99
5.3.2	Control of nearly constant emissions.....	109
5.4	Conclusions	118
5.5	References.....	119
CHAPTER 6 SUMMARY, CONCLUSIONS, AND RECOMMENDATIONS		
		121
6.1	Summary.....	121
6.2	Conclusions	122
6.3	Recommendations for future work	123
6.4	References.....	124

APPENDIX A Summary of emission events reported for TCEQ region 12 from 2003 to 2005	125
APPENDIX B Evaluation of the sub-domain model for 30 August, 2000	127
APPENDIX C Summary of linear relationships between maximum additional ozone formation and event characteristics examined for Monte-Carlo simulation in Chapter 3.....	132
APPENDIX D Impacts of variable continuous emissions on ozone formation using the regular emission inventory.....	133
APPENDIX E Impacts of VOC emission variability on effectiveness of ozone control strategies	139
E.1 Impacts of VOC emission variability using regular emission inventory.....	139
E.2 Impacts of VOC emission variability using imputed emission inventory....	146
REFERENCES	157
VITA	162

List of Tables

Table 4.1	Observations from emission sources and fitted parameters (Webster, et al., 2007)	63
Table 4.2	Mean, standard deviation, and selected facilities of point source VOC emissions (tons/hr) in Houston Galveston.	70
Table 5.1	Parameters used to develop base case stochastic emissions	89
Table 5.2	Parameters used to develop stochastic emissions with allowable episodic emissions from flares eliminated.	93
Table 5.3	Parameters used to develop stochastic emissions with nearly constant emissions from flares reduced.	95
Table A.1	Summary of emission events reported by industrial facilities in the TCEQ region 12 from 2003 to 2005 (TCEQ, 2006). TCEQ region 12 is 13 counties around Houston. HRVOC was defined as ethylene, propylene, 1,3-butadiene, and isomers of butene by Texas Air Quality regulation for their significant roles in ozone formation.	125

List of Figures

Figure 1.1	Time series of ozone concentrations at 38 monitoring sites within the HGB area on October 23, 2003 (TCEQ, 2006b); monitors with ozone peaks have concentrations up to 200 ppb higher than the background level.....	3
Figure 1.2	Time series of ozone concentrations at 19 monitoring sites in the Dallas-Fort Worth urban area on August 7, 2003 (TCEQ, 2006b); high ozone concentrations were observed in multiple monitors simultaneously for relatively long periods of time.	3
Figure 3.1	Modeling domain used in the study. The Regional, East Texas, Houston-Galveston-Beaumont-Port Arthur (HGBPA), and Houston Galveston (HG) nested domains had 36, 12, 4 and 1 km resolution, respectively.	22
Figure 3.2	(a) Plume of a tracer release from a point source in the industrial source region and location of the sub-domain used for the August 25, 2000 simulation day, indicated by the box in the left center of the 1-km sub-domain shown in Figure 3.1 (region in red in Figure 3.1). (b) Plume of a tracer release from a point source in the industrial source region and location of the sub-domain used in this study for August 30, 2000 simulation day indicated by the box in the right center of the 1-km sub-domain shown in Figure 3.1 (region in red in Figure 3.1).....	24
Figure 3.3	Ozone concentrations for August 25 from 1200 hr to 1500 hr using the basecase inputs, predicted by the sub-domain model (left column) and full domain (right column).....	28
Figure 3.4	Comparison of ozone concentration predictions for the August 25 base case simulation using the sub-domain and the full domain	29
Figure 3.5	Ozone difference plots between emission event case and basecase with sub-domain model (left column) and full CAMx (right column).....	31
Figure 3.6	Comparison of the difference between the emission event and the base case in the full domain simulation to the difference between the emission event and the base case in the sub-domain simulation. Emission event is a propylene release at a rate of 5,819 lbs per hour from 10 am to 12 pm near the center right portion of Figure 3.2a.	33

Figure 3.7	Emission event scenarios	34
Figure 3.8	Daily maximum of additional ozone formation due to emission events of ethylene and propylene; results are reported for 10 am releases (1-hour duration) on August 25 and August 30.....	36
Figure 3.9	Domain-wide maximum ozone concentration for emission events of ethylene (top 2 figures) and propylene (bottom 2 figures) beginning at 10 am for 1-hour duration with various magnitudes for both episode days	38
Figure 3.10	Maximum additional ozone formation due to emission events of 1 hour duration, beginning of various times on August 25 and August 30, 2000 ..	40
Figure 3.11	Maximum additional ozone formation due to emission events of 1 hour duration (1000 lb/hr) and 2-hour duration (500 lb/hr) beginning at 10 am for August 25 and August 30, 2000	42
Figure 3.12	Maximum of additional ozone formation due to emission events of a 500 lb release of ethylene, propylene, propane and xylene beginning at 10 am for 1-hour duration for August 25 and August 30, 2000	43
Figure 3.13	Maximum of additional ozone formation due to emission events of a 500 lb release of pure ethylene, pure propylene and a total of 1,000 lbs release of half ethylene and half propylene beginning at 10 am for 1-hour duration for August 25 and August 30, 2000	45
Figure 3.14	Distribution of maximum added ozone due to emission events, based on a Monte Carlo simulation of 763 events	48
Figure 3.15	Distribution of maximum added ozone due to emission events based on a Monte Carlo simulation of 763 events using emission rates calculated with hourly blocks instead of actual duration.....	48
Figure 4.1	Probability distribution function (PDF) and time series of mass flow rate to a flare at an industrial facility in the HG area.....	54
Figure 4.2	(a) Single probability distribution of mass flow rates to the flare shown in Figure 4.1a. (b) Time series of mass flow rate simulated with the probability distribution in Figure 4.2a, modeling the mass flow rate in Figure 4.1b.	54
Figure 4.3	Components of mass flows: emission event, allowable episodic, routinely variable and nearly constant.	57

Figure 4.4	Decomposition into three PDFs of emissions from flare shown in Figure 4.1. Inverse normal is expressed in the standard form (z) in relation to the mean and standard deviation $\left(z = \frac{Y - \bar{Y}}{s}\right)$. (Webster, et al., 2007) 57
Figure 4.5	(a) PDFs for each component of emissions from the flare in Figure 4.1 (b) normalized PDFs of three components based on the proportion of each emission component 58
Figure 4.6	Time within each emission component before transition to next component..... 60
Figure 4.7	Time series of actual and simulated flare flow in Figure 4.1. Note that simulated time series has approximately 2.4 times longer time scale than actual time series..... 61
Figure 4.8	Comparison of cumulative probability distribution functions for observed and simulated (10,000 hours) for three flares..... 61
Figure 4.9	Modeling domain used in the study. The Regional, East Texas, Houston-Galveston-Beaumont-Port Arthur (HGBPA), and Houston Galveston (HG) nested domains had 36, 12, 4 and 1 km resolution, respectively. 66
Figure 4.10	Variability of hourly VOC emission rates for a) all industrial point sources in the HG domain, b) all industrial flares in the HG domain, and c) for the industrial point sources within three 1 km ² grid cells. The map shows the geographic locations of the three example grid cells..... 69
Figure 4.11	The probability that N or more point source emissions are a factor of 2, 5, and 10 times their annual average within the same hour. 70
Figure 4.12	Difference in ozone concentration for 25 August from 700 hr to 1500 hr between using the 45 th stochastic imputed emission inventory and using the deterministic imputed inventory. 72
Figure 4.13	Maximum difference in ozone concentrations in one day simulations representing 25 August and 30 August, 2000. The difference is taken between the imputed inventory with constant industrial emissions and the stochastic inventory for 50 instances of the stochastic inventory. Ozone concentrations (ppb), using the stochastic inventory, at the time the maximum difference was observed are indicated on the top and bottom of each column. 75

Figure 4.14	Probability distributions of maximum difference in ozone concentrations in one day simulations representing 25 August and 30 August, 2000.....	76
Figure 5.1	Components of mass flow rates to a flare at an industrial facility in the HG area: nearly constant, routinely variable, allowable episodic, and emission event in order of magnitude.....	84
Figure 5.2	PDFs for each component of emissions from the flare in Figure 5.1 in (a) the original version of the stochastic inventory generator (Webster et al., 2007) and (b) the updated version of the stochastic inventory generator....	87
Figure 5.3	(a) Time series of flare flow in Figure 5.1 simulated with original version of the stochastic inventory generator. (b) Time series of flare flow in Figure 5.1 simulated with the revised version of the stochastic inventory generator. (c) Time series of actual flare flow.	88
Figure 5.4	Conceptual diagram for a typical refinery flare system (Shell Oil Products US, 2006).....	91
Figure 5.5	Modeling domain used in the study. The Regional, East Texas, Houston-Galveston-Beaumont-Port Arthur (HGBPA), and Houston Galveston (HG) nested domains had 36, 12, 4 and 1 km resolution, respectively.	98
Figure 5.6	Difference in ozone concentrations for 25 August from 700hr to 1500hr between predictions based on the 19 th stochastic inventory generated using the models shown in Table 5.1 and predictions based on the deterministic inventory.	100
Figure 5.7	Difference in ozone concentration for 25 August from 700hr to 1500hr between predictions based on the 10 th stochastic inventory generated using the models shown in Table 5.2 and predictions based on the deterministic inventory. Ozone concentrations are scaled to the results shown in Figure 5.6.	102
Figure 5.8	Maximum difference in ozone concentration in one day simulations representing 25 August, 2000. The difference is taken between the deterministic inventory with constant industrial emissions and the stochastic inventory for 50 instances of the stochastic inventory with allowable episodic emission control (a) and without the control (b).....	104
Figure 5.9	Probability distribution of maximum changes in ozone concentration in simulations representing 25 August, 2000 due to variable continuous emissions with allowable episodic emission control (red line) and	

	without the control (blue line) in positive direction (a) and negative direction (b).....	105
Figure 5.10	Histograms of daily maximum ozone concentration across the HG 1-km domain for no control cases (black) and allowable episodic emission control cases (red).....	107
Figure 5.11	Difference in ozone concentration for 25 August from 700hr to 1500hr between predictions based on the reduced deterministic inventory and predictions based on the deterministic inventory. Percentage reduction in emissions was same with that from allowable episodic emission control. Maximum difference, approximately 1.4 ppb, occurred in (59, 55) at 2000hr.	108
Figure 5.12	Difference in ozone concentration for 25 August from 700hr to 1500hr between predictions based on the 38 th stochastic inventory generated using the models shown in Table 5.3 and predictions based on the deterministic inventory. Ozone concentrations are scaled to the results shown in Figures 5.6 and 5.7.	110
Figure 5.13	Maximum difference in ozone concentration in one day simulations representing 25 August, 2000. The difference is taken between the deterministic inventory with constant industrial emissions and the stochastic inventory for 50 instances of the stochastic inventory with a 50% reduction in nearly constant flare emissions. Maximum difference in ozone concentration was scaled to the results shown in Figure 5.8.	112
Figure 5.14	Probability distributions of maximum changes in ozone concentration in simulations representing 25 August, 2000 due to variable continuous emissions with allowable episodic emission control (red line), with nearly constant emission control (blue line) and without the control (black line) in positive direction (a) and negative direction (b).	113
Figure 5.15	Histograms of daily maximum ozone concentration across the HG 1-km domain for no control cases (black), allowable episodic emission control cases (red), and nearly constant emission control cases (blue).....	115
Figure 5.16	Difference in ozone concentration for 25 August from 700hr to 1500hr between predictions based on the reduced deterministic inventory and predictions based on the deterministic inventory. Percentage reduction in emissions was same with that from nearly constant emission control. Maximum difference, approximately 9.4 ppb, occurred in (59, 55) at 2000hr.	117

Figure A.1	Cumulative distribution function of event emission rates for 2003, 2004, and 2005.....	126
Figure B.1	Ozone concentration for 30 August from 1100hr to 1600hr using the basecase inputs, predicted by the sub-domain model (top 6 figures) and full-domain model (bottom 6 figures)	128
Figure B.2	Comparison of ozone concentration predictions for the 30 August base case simulation using the sub-domain and the full domain	129
Figure B.3	Ozone difference plots for 30 August from 1000hr to 1500hr between emission event case and basecase with sub-domain model (top 6 figures) and full-domain model (bottom 6 figures).....	130
Figure B.4	Comparison of the difference between the emission event and the base case in the full domain simulation to the difference between the emission event and the base case in the sub-domain simulation. Emission event is a propylene release at a rate of 5819 lb h ⁻¹ from 10 am to 12 pm near the center left portion of Figure B.3.	131
Figure C.1	Slopes of linear relationships between maximum additional ozone formed and event magnitude for each compound, each day, and each time of release. Slopes are based on the results from zero release and 1,000 lb release of event, instead of trend line of multiple simulation results like those shown in Figure 3.8.....	132
Figure D.1	Difference in ozone concentration for 25 August from 800 hr to 1600 hr between using the 7 th stochastic regular emission inventory and using the regular inventory with constant VOC emission, regular inventory	134
Figure D.2	Maximum difference in ozone concentration in all hours of simulations representing 25 August and 30 August, 2000 between using regular inventory and stochastic regular inventory for 10 sets of stochastic inventory. Ozone concentrations using the stochastic regular inventory are indicated in ppb inside each column.....	136
Figure D.3	Domain-wide maximum ozone concentration for 10 sets of stochastic regular emission inventory for both episode days	138
Figure E.1	Ozone difference plots between using the 7 th stochastic regular inventory with 25% NO _x reduction and using the stochastic regular inventory without control	140

Figure E.2	Ozone difference plots showing difference in response of ozone to 25% NOx reduction across the sub-domain between using the 7 th stochastic inventory and using regular inventory	142
Figure E.3	Ozone difference plots showing difference in response of ozone to 50% NOx reduction across the sub-domain between using the 7 th stochastic inventory and using regular inventory	143
Figure E.4	Ozone difference plots between using the 7 th stochastic inventory with 25% VOC reduction and using the stochastic inventory without control..	144
Figure E.5	Ozone difference plots showing difference in response of ozone to 25% VOC reduction across the sub-domain between using the 7 th stochastic inventory and using regular inventory	145
Figure E.6	Ozone difference plots between using the 7 th stochastic imputed inventory with 25% NOx reduction and using the stochastic imputed inventory without control.....	148
Figure E.7	Ozone difference plots showing difference in response of ozone to 25% NOx reduction across the sub-domain between using the 7 th stochastic imputed inventory and using the imputed inventory with constant VOC emissions.....	150
Figure E.8	Ozone difference plots showing difference in response of ozone to 50% NOx reduction across the sub-domain between using the 7 th stochastic imputed inventory and using the imputed inventory without varying VOC emissions	152
Figure E.9	Ozone difference plots between using the 7 th stochastic imputed inventory with 25% VOC reduction and using the stochastic imputed inventory without control.....	154
Figure E.10	Ozone difference plots showing difference in response of ozone to 25% VOC reduction across the sub-domain between using the 7 th stochastic imputed inventory and using the imputed inventory without varying VOC emissions	155

CHAPTER 1

INTRODUCTION

1.1 Background

The Houston-Galveston-Brazoria (HGB) area is in nonattainment of the National Ambient Air Quality Standard (NAAQS) for ground-level ozone; Counties affected under this status include Harris, Galveston, Brazoria, Fort Bend, Waller, Montgomery, Chambers, and Liberty (TCEQ, 2006a). The region violates both the NAAQSs for ozone with concentrations averaged over 1 hour, and concentrations averaged over 8 hours. In an effort to identify ways to address these persistent ozone exceedances in the Houston metropolitan area, a large number of field measurements and modeling studies have been conducted. Observations from ground monitors and instrumented aircraft indicate that ozone formation and accumulation processes in the HGB area are often much different than those observed in other areas of the country (Berkowitz et al., 2004; Daum et al., 2003, 2004; Kleinman et al., 2003). In the HGB area, frequently only a small region is affected by an extremely high concentration of ozone that occurs for only a relatively short period of time, while in other areas, high ozone tends to occur over relatively large areas, typically over entire metropolitan areas, for much longer periods of time. Figures 1.1 and 1.2 show data characteristic of this unique feature of ozone formation in the HGB area. Although the background level of ozone concentration in the HGB area (Figure 1.1) is comparable to that of the Dallas-Fort Worth area (Figure 1.2), very rapid formation of ozone in the HGB area often leads to extremely high ozone concentrations, up to 200 ppb higher than the background level, in spatially isolated areas. Furthermore,

ozone formation in the HGB area is more efficient in terms of moles of NO_x consumed per mole of ozone formed than other areas with high ozone events.

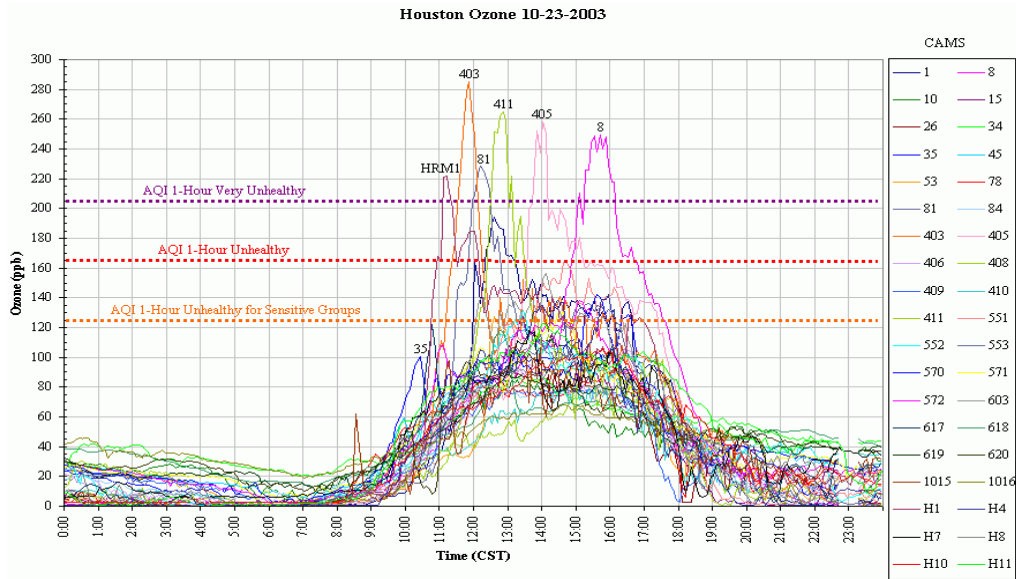


Figure 1.1 Time series of ozone concentrations at 38 monitoring sites within the HGB area on October 23, 2003 (TCEQ, 2006b); monitors with ozone peaks have concentrations up to 200 ppb higher than the background level.

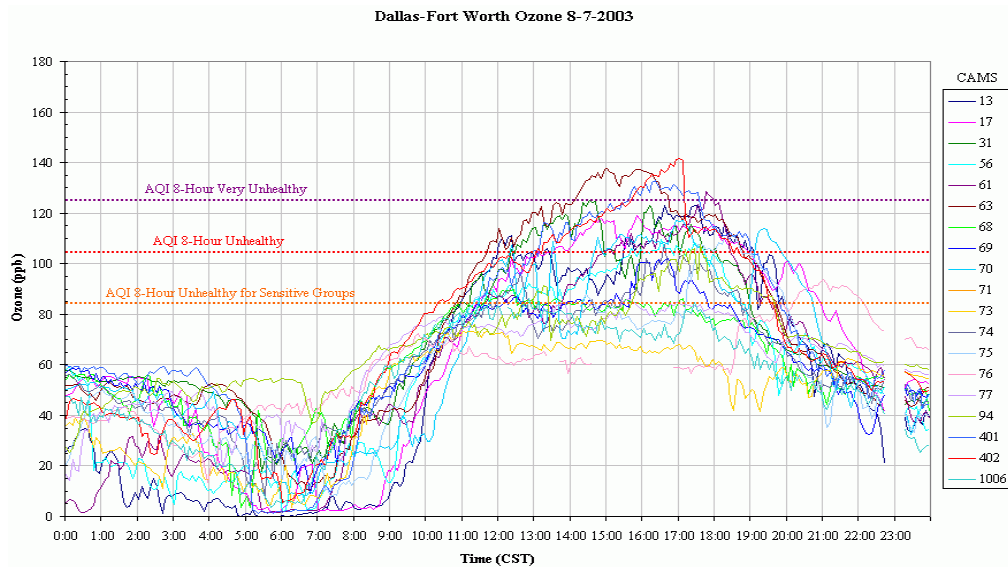


Figure 1.2 Time series of ozone concentrations at 19 monitoring sites in the Dallas-Fort Worth urban area on August 7, 2003 (TCEQ, 2006b); high ozone concentrations were observed in multiple monitors simultaneously for relatively long periods of time.

This uniqueness in ozone formation processes in the HGB area is associated with a geographically constrained region of sources emitting highly reactive hydrocarbons. The sources are most likely those surrounding the Houston Ship Channel (Kleinman et al., 2003; Ryerson et al., 2003). Observational data collected by aircraft show that high concentrations of ozone are, at times, formed rapidly in the plumes emanating from those industrial facilities (Kleinman et al., 2003). In order to address these rapid ozone formation events and the subsequent high ozone concentrations in the HGB area, the realistic quantification of industrial emissions, particularly of reactive hydrocarbons, is critical. Industrial emissions of volatile organic compounds (VOCs), largely from petroleum refineries and chemical manufacturing operations, are generally assumed to be continuous at constant levels. However, evidence from air emission event databases and evidence from measurements by ground monitors and aircraft demonstrated that the VOC emissions from industrial facilities can vary from annual average emissions by a factor of 10-1000 or more (Allen et al., 2004). In other words, when large emission events occur, they dominate local emissions of ozone precursors.

Texas air quality regulation defines highly reactive volatile organic compounds (HRVOC) as ethylene, propylene, isomers of butene, and 1,3-butadiene, since they play a significant role in ozone formation. Ozone formation potential of hydrocarbons is characterized using parameters such as the rate of reaction with hydroxyl radical ($\text{cm}^3 \text{ molecule}^{-1} \text{ s}^{-1}$) and incremental reactivity (amount of ozone formed per amount of VOC added to a base mixture; Carter, 1994). VOCs are removed and transformed in the atmosphere by photolysis and chemical reaction with hydroxyl radicals (Seinfeld and Pandis, 1998). In the presence of sunlight, the degradation reactions of VOCs lead to conversion of NO to NO₂ and the formation of ozone. However, different VOCs react at different rates in the atmosphere because of their differing rate constants for photolysis

and reaction with hydroxyl radicals. The rate of ozone production from a given VOC is largely a function of the species' atmospheric concentration and its rate of reaction with hydroxyl radicals. The product of a VOC's concentration and its OH rate constant determines in an approximate manner its relative role as an ozone precursor. A species with a large concentration will not necessarily be an important ozone precursor if it is unreactive. However, even small concentrations of HRVOCs can be important since they are extremely reactive. In addition, in terms of incremental reactivity, ozone formation by HRVOC can be greater by an order of magnitude than those due to unreactive species.

For emission events beginning on or after January 31, 2003, online data are available at an emission event database maintained by the Texas Commissions on Environmental Quality (TCEQ, 2006c). For this database, the threshold for reporting required was reduced from 5000 to 100 lb, in a 24-hour period, for most compounds emitted in the HGB area. Using this newly available database, Murphy and Allen (2005) investigated the characteristics of emission events in the HGB area, with a focus on HRVOC. From January 31, 2003 to January 30, 2004 (first full year of operation), a total of 1894 events were reported in the HGB area. The release of HRVOCs was involved in approximately 40% (759) of these events and the total release of HRVOC events constitute about 10% of both the total event release and annual HRVOC emissions. Individual HRVOC emission events have emission rates exceeding the annual average emission rate of all HRVOC emissions in the HGB area almost twice per month. Among the HRVOCs, ethylene exhibits the greatest frequency and magnitude of event emissions. Next most significant is propylene. More than half of the mass of HRVOC event emissions is attributable to ethylene and almost one third is due to propylene. Duration of emission events was relatively short; about 75% last 1 day or less and about 25% last

1 hour or less. Detailed information on the emission event database is provided in Appendix A.

Vizuete (2005) investigated the chemical and physical processes that control ozone formation during large industrial emission events by examining a small group of case studies; specifically, emission events of various compositions under different conditions of NO_x availability. He investigated emission events of ethylene, propylene, n-pentane and xylene, and suggested that emission events of 5819 lb propylene/hr for a 2-hour duration can contribute to increases in ozone concentrations by up to 100 ppb downwind of the release point in ozone conducive conditions. While this analysis provided important phenomenological information, it is limited in the sense that a small number of case studies cannot represent the diverse range of conditions associated with industrial emission events.

The variability in emissions from industrial facilities can be ascribed to variability in continuous emission as well as episodic emission events. Webster (2004) presented observational evidence of variability in continuous emissions from various industrial facilities in the HGB area. Based on the observations, he developed models to estimate variability in continuous emissions over the HGB area. He suggested that continuous emissions have significant variability with emissions varying by up to an order of magnitudes at single facilities.

1.2 Research Objectives

The overall goal of this study is to explore the impact, on ozone formation and accumulation in the Houston area, of variability in industrial hydrocarbon emissions.

The specific goals of this study will be:

1. to characterize the magnitude, composition, temporal and spatial patterns of industrial emission events in southeast Texas,
2. to assess the impact, on ozone formation, of industrial emission events utilizing the event characteristics,
3. to assess the variability in hydrocarbon emissions due to time-varying continuous emissions in southeast Texas,
4. to investigate potential changes in ozone formation and accumulation due to variability in continuous emissions of hydrocarbons,
5. and, to assess the impact of emission variability on the effectiveness of control strategies.

1.3 Dissertation Overview

The following chapter summarizes previous studies on variability in hydrocarbon emissions from various sources. Chapter 3 describes the characteristics of industrial emission events in southeast Texas, development of photochemical modeling tools with the computational efficiency needed for modeling many emission scenarios, and the impacts on ozone formation of the many possible types of emission events. Chapter 4 describes the variability in continuous emissions of hydrocarbons and potential changes in ozone formation and accumulation due to this variability in the Houston area. Chapter 5 describes the effectiveness of alternative control strategies for ozone, targeting significant variability in hydrocarbon emissions, relative to conventional strategies targeting emissions that are assumed to be time invariant. Finally, Chapter 6 will provide a summary and recommendations for further studies on modeling of emission variability and its impact on ozone formation and accumulation.

1.4 References

- Allen, D., Murphy, C., Kimura, Y., Vizuite, W., Edgar, T., Jeffries, H., Kim, B.-U., Webster, M., Symons, M., 2004. Inventories of HRVOC Emissions & Impact of Emission Magnitude & Variability on Ozone Formation in H/G Area. Houston Advanced Research Center, H13.2003 Final Report, April 16, 2004, available at <http://www.harc.edu/harc/Projects/AirQuality/Projects/ShowProject.aspx?projectID=27>
- Berkowitz, C.M., Jobson, T., Jiang, G., Spicer, C.W., Doskey, P.V., 2004. Chemical and meteorological characteristics associated with rapid increases of O₃ in Houston, Texas. J. Geophys. Res. 109, D10307
- Carter, W.P.L., 1994. Development of ozone reactivity scales for volatile organic compounds, J. Air & Waste Manage. Assoc., 44, 881-899.
- Daum, P.H., Kleinman, L.I., Springston, S.R., Nunnermacker, L.J., Lee, Y.-N., Weinstein-Loyd, J., Zheng, J., Berkowitz, C.M., 2003. A comparative study of O₃ formation in the Houston urban and industrial plumes during the 2000 Texas Air Quality Study. J. Geophys. Res. 108 (D23), 4715
- Daum, P.H., Kleinman, L.I., Springston, S.R., Nunnermacker, L.J., Lee, Y.-N., Weinstein-Loyd, J., Zheng, J., Berkowitz, C.M., 2004. Origin and properties of plumes of high ozone observed during the Texas 2000 Air Quality Study (TexAQS 2000). J. Geophys. Res. 109, D17306.
- Kleinman, L.I., Daum, P.H., Imre, D., Lee, Y.-N., Nunnermacker, L.J., Springston, S.R., 2003. Correction to "Ozone production rate and hydrocarbon reactivity in 5 urban areas: A cause of high ozone concentration in Houston". Geophys. Res. Lett. 30 (12).
- Murphy, C.F., Allen, D.T., 2005. Hydrocarbon emissions from industrial release events in the Houston-Galveston area and their impact on ozone formation. Atmospheric Environment 39(21), 3785-3798.
- Ryerson, T.B., Trainer, M., Angevine, W.M., Brock, C.A., Dissly, R.W., Fehsenfeld, F.C., Frost, G.J., Goldan, P.D., Holloway, J.S., Hubler, G., Jakoubek, R.O., Kuster, W.C., Neuman, J.A., Nicks, D.K., Parrish, D.D., Roberts, J.M., Sueper, D.T., Atlas, E.L., Donnelly, S.G., Flocke, F., Fried, A., Potter, W.T., Schauffler, S., Stroud, V., Weinheimer, A.J., Wert, B.P., Wiedinmyer, C., Alvarez, R.J., Banta, R.M., Darby, L.S., Senff, C.J., 2003. Effect of petrochemical industrial emissions of reactive alkenes and NO_x on tropospheric ozone formation in Houston, Texas. J. Geophys. Res. 108 (D8), 4249.

Seinfeld, J.H., Pandis, S.N., 1998. Atmospheric chemistry and physics. John Wiley & Sons, Inc. New York.

Texas Commission on Environmental Quality (TCEQ), 2006a. Houston-Galveston-Brazoria State Implementation Plan (SIP) Revision, Accessed March 2006 at <http://www.tceq.state.tx.us/implementation/air/sip/hgb.html>

Texas Commission on Environmental Quality (TCEQ), 2006b. General air pollution and meteorological data, Accessed May 2006 at <http://www.tceq.state.tx.us/assets/public/compliance/monops/air/sigevents/03/event2003-10-23hou.html>

Texas Commission on Environmental Quality (TCEQ), 2006c. Air emission event reports, Accessed March 2006 at http://www.tceq.state.tx.us/compliance/field_ops/eer/

Vizuite, W., 2005. Implementation of Process Analysis in a three dimensional air quality model, PhD thesis, University of Texas.

Webster, M., 2004. Stochastic Emission Inventories of Continuous Emissions. Houston Advanced Research Center, H13.2003 Final Report Appendix B, available at <http://files.harc.edu/Projects/AirQuality/Projects/H013.2003/H13AppendixB.pdf>

CHAPTER 2

LITERATURE REVIEW

2.1 Overview of Emission Inventories

The first step in developing strategies for decreasing ozone concentrations is to quantify emissions of nitrogen oxides (NO_x) and volatile organic compounds (VOCs), both of which are the precursors that lead to ozone formation and accumulation in the atmosphere. A compilation of emissions from various sources for a particular time period and a particular region is referred to as an emission inventory. While emission inventories have been improved over the past 30 years in terms of accuracy and completeness, they are still one of the weakest links in the air quality management and a major source of uncertainty in the development of ozone control strategies (NARSTO, 2005).

Emission inventories are generally developed using a combination of the direct measurements and emission models (EPA, 1998). The most accurate way to determine the rate at which a pollutant is emitted to the atmosphere is through emission monitoring. However, due to large number and varying types of sources, only the largest point sources, such as electricity generating units (EGU), are equipped with continuous emission monitoring (CEM) systems (NRC, 2004). For the majority of emissions sources, emission rates are estimated using emission models. Emission rates from stationary point sources, other than EGUs, are generally determined using emission factors combined with the facility-specific activity information. The U.S. Environmental Protection Agency (EPA, 2007) compiles and periodically updates emission factors for a wide variety of source types and a range of pollutants in its AP-42 document. Emissions

for non-point sources are estimated using emission models, such as MOBILE (EPA, 2003a), NONROAD (EPA, 2004), and BEIS (EPA, 2003b), among others.

Current emission inventories have a significant amount of uncertainty largely due to the use of emission models to develop the inventories. The application of an average emissions factor based on the measurements of a small subset of a total population necessarily introduces uncertainty (NRC, 2004). This uncertainty does not merit attention when the inventories are used to estimate annual average emissions on a national scale. Over a large number of sources and a long period of time, variations of emission rate are expected to even out so that the emission factor adequately reflects the average emission rate across the activity range. However, the same inventories can be more uncertain when used in other contexts, such as estimates of daily emissions in a local area or use as the emission data for air quality models (Miller et al., 2006). Since many ozone formation processes occur in the atmosphere on time scales of hours or less, these models require increasingly detailed information on the location and time of emissions, primarily of NO_x and VOCs. Uncertainty in emission factors and inventory development was extensively examined by various authors with a focus on uncertainty in mobile source emissions (Frey, 1997; Rhodes and Frey, 1997; Frey and Bammi, 2002; Frey and Zheng, 2002; Frey and Li, 2003; Frey and Song, 2003; Frey and Bammi, 2003; Chi et al., 2004; Frey and Zhao, 2004). While these studies used different approaches for quantifying uncertainty in emission inventories estimated from different emission models, they suggested that uncertainty in emission factors for mobile source emissions can generally vary from mean emission factors by up to an order of magnitude, depending on the pollutant, control technology, equipment age, and engine type.

2.2 Temporal Variability in Emissions of NO_x

Abdel-Aziz et al. (2003) investigated hourly variability in NO_x emissions from coal-fired power plants. They analyzed continuous emission monitoring data for 1995 and 1998 for 32 units from nine power plants in Charlotte, North Carolina. As in many air quality modeling domains, coal-fired power plants contribute substantially to the overall NO_x emissions in the area. Temporal variability in NO_x emissions from coal-fired power plants is due to variation in coal composition fed to the boilers, different boiler designs, and different operating conditions. The analysis indicated that there is significant variability in emissions of NO_x over all hours of the years and the coefficient of variation (the ratio of the standard deviation to the mean) can be up to 0.45 for a unit with highest variability.

In many urban areas, mobile emissions account for a significant portion of the overall emission inventories of ozone precursors. Temporal variability in mobile emissions has been investigated by several authors (Cardelino, 1998; Harley et al., 2005). Cardelino (1998) investigated daily variability of mobile emissions in rural and urban areas in the Atlanta metropolitan area. He estimated mobile emissions using emission factors, emission per miles traveled, derived from emission model and activity level, vehicle miles traveled, from traffic counter data collected during the 1992 Southern Oxidants Study Atlanta Intensive Study. Harley et al. (2005) described temporal patterns in NO_x emissions from on-road mobile sources using data collected from California for previous studies. They estimated mobile emissions using emission factors from on-road measurements and activity information, annual fuel sales data assigned to hours and days of the week based on traffic count data. Both studies indicated that weekday emissions of mobile sources display the typical double peak associated with the rush hours and

weekend emissions show a much broader single peak during daylight hours. Cardelino (1996) indicated that variability in mobile emissions is significant with the range of between -24 to 27% change with respect to the average emissions of the period studied.

2.3 Temporal Variability in Industrial Emissions of Hydrocarbons

As described in previous sections of this chapter, emissions of NO_x from both mobile and industrial sources have the potential to vary by approximately a factor of 2, and a number of investigators have examined this type of emission variability. In contrast, and as described in the previous chapter, industrial emissions of hydrocarbons can vary by factors of 10-1000 for a single facility (Allen et al., 2004; Murphy and Allen, 2005; Webster, 2004). Nationwide efforts are being made to quantify and reduce the variability in hydrocarbon emissions. The Bay Area Air Quality Management District (BAAQMD) enacted a flare monitoring rule to quantify the variability in hydrocarbon emissions and a flare minimization rule to reduce the significant variability in hydrocarbon emissions (BAAQMD, 2005; BAAQMD, 2006). The Texas Commission on Environmental Quality (TCEQ) has recognized a link between episodic emissions of the type associated with flaring and sudden increase in ozone concentration by enacting a new short-term limit on highly reactive volatile organic compound emissions. These programs are in their infancy, however, and the air quality impact of this type of emission variability is poorly understood. The primary goal of this thesis is to extend the development of quantitative tools for characterizing the impacts of industrial emission variability.

2.4 References

- Abdel-Aziz, A., Frey, H.C., 2003. Quantification of Hourly Variability in NOx Emissions for Baseload Coal-Fired Power Plants. *J. Air & Waste Manage. Assoc.* 53, 1401-1411.
- Allen, D., Murphy, C., Kimura, Y., Vizuete, W., Edgar, T., Jeffries, H., Kim, B.-U., Webster, M., Symons, M., 2004. Inventories of HRVOC Emissions & Impact of Emission Magnitude & Variability on Ozone Formation in H/G Area. Houston Advanced Research Center, H13.2003 Final Report, April 16, 2004, available at <http://www.harc.edu/harc/Projects/AirQuality/Projects/ShowProject.aspx?projectID=27>
- Bay Area Air Quality Management District, 2005. Flare Monitoring at Petroleum Refineries accessed February 2007 at <http://www.baaqmd.gov/dst/regulations/rg1211.pdf>
- Bay Area Air Quality Management District, 2006. Flares at Petroleum Refineries, Accessed January 2007 at <http://www.baaqmd.gov/dst/regulations/rg1212.pdf>
- Cardelino, C., 1998. Daily Variability of Motor Vehicle Emissions Derived from Traffic Counter Data. *J. Air & Waste Manage. Assoc.* 48, 637-645.
- Chi, T.R., Unal, A.D., Tian, R.A., 2004. Uncertainty of NONROAD emissions in Georgia. *13th Annual Emission Inventory Conference*, Clearwater, FL.
- Environmental Protection Agency, 1998. Handbook for Air Toxics Emission Inventory Development, Vol. 1. Stationary Sources. EPA 454/B-98-002. Office of Air Quality Planning and Standards, Research Triangle Park, NC.
- Environmental Protection Agency, 2003a. MOBILE6 Model, Accessed March 2007 at <http://www.epa.gov/otaq/models/mobile6/mobile62.zip>
- Environmental Protection Agency, 2003b. Biogenic Emission Inventory System (BEIS), Accessed March 2007 at <ftp://ftp.epa.gov/amd/asmd/beis3v12>
- Environmental Protection Agency, 2004. NONROAD2004 Model, Accessed March 2007 at <http://www.epa.gov/otaq/nonrdmdl.htm>
- Environmental Protection Agency, 2007. AP-42: Compilation of Air Pollutant Emission Factors, Accessed February 2007 at <http://www.epa.gov/ttn/chief/ap42/index.html>
- Frey, H.C., 1997. Variability and Uncertainty in Highway Vehicle Emission Factors. *Proceedings of the Air & Waste Management Association's Annual Meeting & Exhibition*, 208-219.

Frey, H.C., Bammi, S., 2002. Quantification of variability and uncertainty in lawn and garden equipment NOx and Total hydrocarbon emission factors. J. Air and Waste Manag. Assoc. 52(4), 435-448.

Frey, H.C., Bammi, S., 2003. Probabilistic Nonroad Mobile Source Emission Factors. J. Environmental Engineering. 129(2). 162-168.

Frey, H.C., Li, S., 2003. Methods for quantifying variability and uncertainty in AP-42 emission factors: case studies for natural gas-fueled engines. J. Air and Waste Manag. Assoc. 53(12).

Frey, H.C., Song, L., 2003. Methods for Quantifying Variability and Uncertainty in AP-42 Emission Factors: Case Studies for Natural Gas-Fueled Engines. J. Air & Waste Manage. Assoc. 53, 1436-1447.

Frey, H.C., Zhao, Y., 2004. Quantification of variability and uncertainty for air toxic emission inventories with censored emission factor data. Environ. Sci. Technol. 38, 6094-6100.

Frey, H.C., Zheng, J., 2002. Probabilistic Analysis of Driving Cycle-Based Highway Vehicle Emission Factors. Environ. Sci. Technol. 36, 5184-5191.

Harley, R.A., Marr, L.C., Lehner, J.K., Giddings, S.N., 2005. Changes in Motor Vehicle Emissions on Diurnal to Decadal Time Scales and Effects on Atmospheric Composition. Environ. Sci. Technol. 39, 5356-5362.

Miller, A.C., Hidy, G., Hales, J., Kolb, E.C., Werner, S.A., Haneke, B., Parrish, D., Frey, H. C., Rojas-Bracho, L., Deslauriers, M., Pennell, B., Mobley, D.J., 2006. Air Emission Inventories in North America: A Critical Assessment. J. Air & Waste Manage. Assoc. 56, 1115-1129.

Murphy, C.F., Allen, D.T., 2005. Hydrocarbon emissions from industrial release events in the Houston-Galveston area and their impact on ozone formation. Atmospheric Environment 39(21), 3785-3798.

NARSTO, 2000. An Assessment of Tropospheric Ozone Pollution: A North American Perspective. Palo Alto, CA: EPRI.

NARSTO, 2005. Improving Emission Inventory for Effective Air Quality Management Across North America: A NARSTO assessment, NARSTO-05-001.

National Research Council, 2004, Air Quality Management in the United States. National Academy Press, Washington, D.C.

Rhodes, D.S., Frey, H.C., 1997. Quantification of variability and uncertainty in AP-42 emission factors using bootstrap simulation. Presented at the *Emission Inventory Planning for the Future*. Air and Waste Management Association: Pittsburgh, Pennsylvania, October, 147-161.

Webster, M., 2004. Stochastic Emission Inventories of Continuous Emissions. Houston Advanced Research Center, H13.2003 Final Report Appendix B, available at <http://files.harc.edu/Projects/AirQuality/Projects/H013.2003/H13AppendixB.pdf>

Zhao, Y., Frey, H.C., 2004. Development of probabilistic emission inventories of air toxics for Jacksonville, Florida, USA. J. Air and Waste Manag. Assoc. 54(11), 1405-1421.

CHAPTER 3

Modeling the impacts of emission events on ozone formation in Houston, Texas*

3.1 Introduction

The Houston/Galveston region exceeds the National Ambient Air Quality Standards (NAAQSs) for ozone and has been designated as a severe ozone non-attainment area. Compared to other cities in the United States, Houston has a large concentration of industrial point sources, particularly chemical manufacturing facilities and petroleum refineries. Observational data collected during the 2000 Texas Air Quality study showed that high concentrations (>200 ppb) of ozone are, at times, formed rapidly in the plumes of these industrial facilities (Kleinman et al., 2002), and that the emissions from the facilities can be episodic (Murphy and Allen, 2005; Vizuite, 2005). The largest of these episodic emission events can have emission rates of reactive hydrocarbons that exceed 10,000 kg/hr; the events typically last only a few hours, can occur at all times of day, and can occur at any of dozens of facilities that are dispersed over a 10^4 - 10^5 km² region (Murphy and Allen, 2005). When large emission events occur, they dominate local emissions of ozone precursors, and therefore, in designing air quality management plans for attaining the NAAQSs for ozone, it is necessary to identify the limits that should be imposed on episodic emissions.

Vizuite (2005) examined the chemical and physical processes that control ozone formation during large industrial emission events by examining a small group of case studies. While this analysis provided important phenomenological information, it is

*Large parts of this chapter have been published in the journal, Atmospheric Environment, 40(28), 5329-5341

limited in the sense that a small number of case studies cannot represent the diverse range of conditions associated with industrial emission events. The goals of this work are (1) to characterize the magnitude, composition, temporal and spatial patterns of industrial emission events in southeast Texas, (2) to develop photochemical modeling tools capable of simulating the many possible types of emission events, and (3) to combine the characterization of the events and the modeling tools in an assessment of the impacts of industrial emission events on ozone formation in southeast Texas.

3.2 Methods

3.2.1 Characterization of Emission Events

Murphy and Allen (2005) have described emission events reported through an on-line database maintained by the Texas Commission on Environmental Quality (TCEQ). For the period from January 31st, 2003 to January 30th, 2004 (the first full year of operation of the database) a total of 1894 events were reported for TCEQ region 12, which includes the Houston-Galveston region. Approximately 40% (759) of the events involved highly reactive volatile organic compounds (HRVOCs, defined in Texas air quality regulations as ethylene, propylene, isomers of butene, and 1,3-butadiene), and 755 out of 759 HRVOC events occurred in only four counties, Harris, Brazoria, Galveston and Chambers. Total event HRVOC emissions within these 4 counties in the one year period was 851 tons while the total annual HRVOC emissions were approximately 8000 tons. Annual event emissions of volatile organic compounds

(VOCs) were 2066 tons (4.0% of the annual emissions of 52000 tons), and NO_x event emissions were 158 tons (0.12% of annual emissions of 133000 tons).

Murphy and Allen (2005) have reported on average properties of the events, including event magnitude, event duration and source types. The goal of this work is to assess the potential of events, with a variety of characteristics, to result in the formation and accumulation of ozone. The characteristics of emission events that will determine whether the events result in significant ozone formation and accumulation include the magnitude of the event, its duration, its composition, the time of day when the event occurs, and the meteorological conditions at the time of the event.

The emission event database described by Murphy and Allen (2005) was utilized to determine the distributions of these event characteristics. The magnitude of events was analyzed in terms of hourly emission rates of key species. Information on the composition and duration of events was extracted from the database.

3.2.2 Development of Subdomain Model

Thousands of possible combinations of emission event composition, duration, location, and timing are possible, and all of these permutations may lead to different ozone formation and accumulation patterns for emission events. In order to consider the full range of possible permutations of emission event characteristics, it is necessary to construct computationally efficient photochemical models. Ideally, these computationally efficient models would approximate, as closely as possible, the simulation that would be performed by a full 3-dimensional, regional air quality model, but do so with a small fraction of the computational effort of the full model.

In this work, computationally efficient models were constructed by taking advantage of the fact that the impacts of emissions events are spatially isolated. The overall strategy in developing the sub-domain model was to (1) identify a geographical region (sub-domain), from a full, 3-D photochemical model, that experienced the effects of emission events, (2) create a computationally efficient photochemical model of the sub-domain, and (3) analyze many permutations of emission events using the sub-domain model. Steps 1 and 2 in the development of the model are described in this section. Step 3 is described in the results section of this chapter.

The sub-domain model has the same basic structure as a full 3-D photochemical grid model, simulating emissions, advection, dispersion, chemical transformation and physical removal of air pollutants in the framework of a 3-dimensional grid. The photochemical model used in this work was the Comprehensive Air Quality Model, with extensions (CAMx) (Environ, 2004). The main difference between a typical 3-D photochemical model application and the sub-domain model used in this work is the size of the domain. Instead of incorporating several hundred thousand grid cells in the simulation, the subdomain uses only ~2000 grid cells to characterize a much smaller geographical region. Use of this smaller domain requires special efforts in determining boundary and initial conditions, as described below.

The first step in constructing the sub-domain model is to identify geographical regions (sub-domains) to be modeled. The full domain of interest used in the 3-D photochemical simulations used in this work, is shown in Figure 3.1.

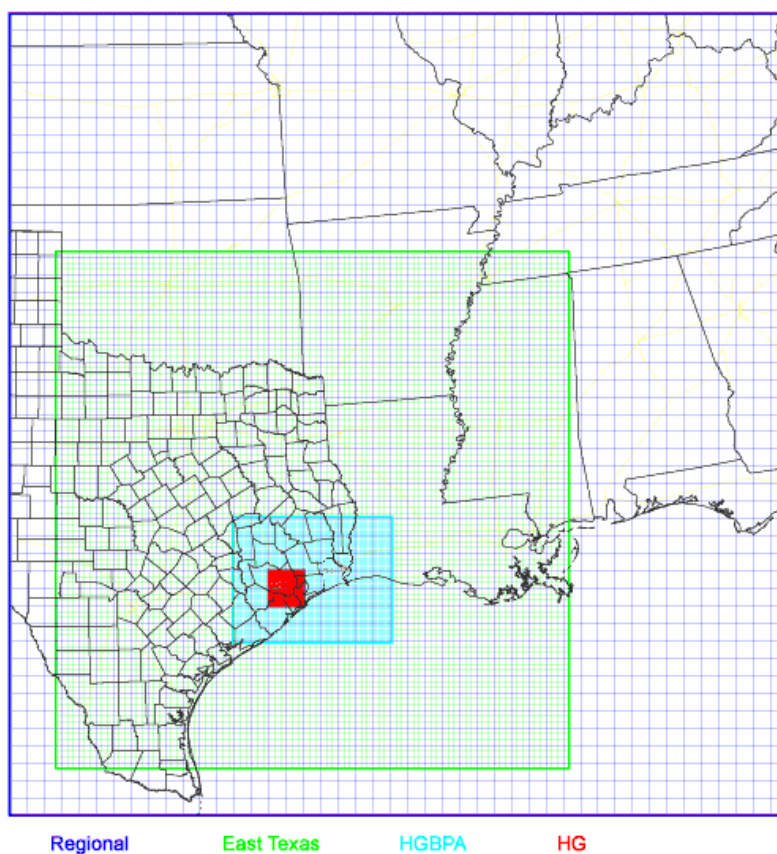


Figure 3.1 Modeling domain used in the study. The Regional, East Texas, Houston-Galveston-Beaumont-Port Arthur (HGBPA), and Houston Galveston (HG) nested domains had 36, 12, 4 and 1 km resolution, respectively.

Two sub-domains, shown in Figure 3.2, were selected to examine the impacts of industrial emission events on ozone formation. Both sub-domains will have the same point of origin for the emission event. This location was chosen because it is in an area where significant numbers of emission events are reported (Murphy and Allen, 2005) and because aircraft detected evidence of emission events at this location (Vizuite, 2005). For the sub-domains shown in Figures 3.2a and 3.2b, distinctly different meteorological

conditions on two different days (August 25, 2000 and August 30, 2000) had the potential to lead to different processes for ozone formation and accumulation for emissions events originating from a single location. On August 25, winds from the east in the late morning and early afternoon advected air from an industrial source region, referred to as the Ship Channel region (located in the center right portion of Figure 3.2a), toward downtown Houston. On August 30, winds from the north-northwest in the late morning and early afternoon advected air from the Ship Channel region toward Galveston Bay.

The size and shape of the domains shown in Figure 3.2 were determined by simulating the advection of an inert tracer release using the full 3-D photochemical model domain shown in Figure 3.1. The origin of modeling domain for August 25 (Figure 3.2a) is offset by 1 km to the east and 33 km to the north from the southwest corner of the region in red, shown in Figure 3.1, and the domain is 44 km by 24 km in size. The modeling domain for August 30 is offset by 33 km to the east and 13 km to the north from the southwest corner of the region in red, shown in Figure 3.1, and is 40 km by 44 km in size. The vertical structure of the sub-domains is identical to the full CAMx simulation; 24 vertical layers up to 5835.9 m above ground level (TCEQ, 2006).

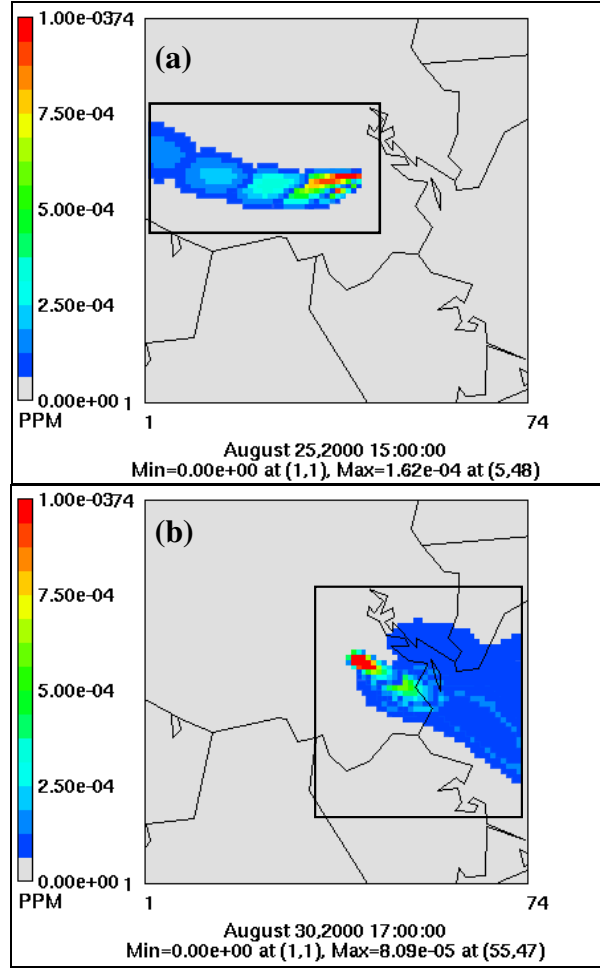


Figure 3.2 (a) Plume of a tracer release from a point source in the industrial source region and location of the sub-domain used for the August 25, 2000 simulation day, indicated by the box in the left center of the 1-km sub-domain shown in Figure 3.1 (region in red in Figure 3.1). (b) Plume of a tracer release from a point source in the industrial source region and location of the sub-domain used in this study for August 30, 2000 simulation day indicated by the box in the right center of the 1-km sub-domain shown in Figure 3.1 (region in red in Figure 3.1).

CAMx simulations using the full domain shown in Figure 3.1 were used to develop boundary and initial conditions for the sub-domain. Meteorological inputs for the full CAMx simulation were based on results from the NCAR/Penn State Mesoscale Meteorological Model version 5, MM5. The volatile organic compound (VOC), NO_x and CO emissions used as input for the modeling episode were prepared by the Texas Commission on Environmental Quality (TCEQ) in accordance with U.S. EPA guidance. A MOBILE6-based inventory was developed for on-road mobile source emissions. Emissions for non-road mobile and area sources were developed using emission factors and the U.S. EPA's NONROAD model, using local activity data when available. Biogenic emission inventories were estimated using the GLOBEIS emission model with locally developed land cover data. Point source emissions data were developed with TCEQ's point source database and special inventory. In some simulations, approximately 150 tons/day of reactive olefin species were added to approximately 100 point sources in the domain, based on ambient measurements made by aircraft (Ryerson et al., 2003). These point source inventory additions are commonly referred to as the imputed inventory, since the added emissions were estimated based on ambient measurements rather than reported inventories. The inventory without the added olefin emissions is commonly referred to as the regular inventory and is the inventory used as the base case in this work. Details of the meteorological modeling and the VOC and NO_x emission inventory development are available from the TCEQ (2006).

Both the sub-domain modeling and the full domain modeling in the region with industrial emissions (Figure 3.1) were performed at a 1 km spatial resolution. Analyses performed by the TCEQ (2006) and others (Allen et al., 2004) have indicated that this

level of spatial resolution is necessary to accurately model the concentration gradients observed in the industrial source region.

Several pre-processor programs, available from the CAMx website (Environ, 2006), were used in preparation of input data for the sub-domain model. Boundary and initial conditions for the sub-domain were extracted with BNDEXTR from the full model output. MM5 output meteorological fields were translated to input data for the sub-domain model using MM5CAMx and ground level emissions were extracted using the WINDOW program. Albedo/haze/ozone column and land use data were extracted from input data for the CAMx simulation on the full domain, with programs written for this work (University of Texas, 2006). Other input data, including photolysis rate, top boundary condition and elevated point source emissions were used directly from look-up tables in the full domain simulation. With these input data prepared, the sub-domain model was run for both episode days and contrasted with the results of the CAMx simulation using the full domain.

3.2.3 Evaluation of the sub-domain model

Figure 3.3 compares the spatial distribution of ozone concentrations predicted by the sub-domain model to ozone concentrations, for the same time and locations, predicted by the full domain simulation. Figure 3.4 presents a scatter plot, comparing predictions of ozone concentrations in all ground level cells from the full domain model and the sub-domain model. The data shown are for August 25. Similar results were obtained for the subdomain used for August 30. Details are provided in Appendix B. The slope of the scatter plot is 0.999, with the square of correlation coefficient of 0.997. The largest differences occurred at night, and near the boundary of the sub-domain.

Since the sub-domain uses only small number of grid cells relative to full domain simulation, it took about one tenth of the computation time required for the full domain simulation for the simulation of one day. This computational efficiency becomes more evident when we consider the fact that the full-domain simulation needs to be performed for a whole episode (from August 22 to September 1, 2000) for boundary condition and initial condition for simulation of a specific day; therefore, the sub-domain simulation is more than a hundred times computationally efficient than a typical simulation using the full domain.

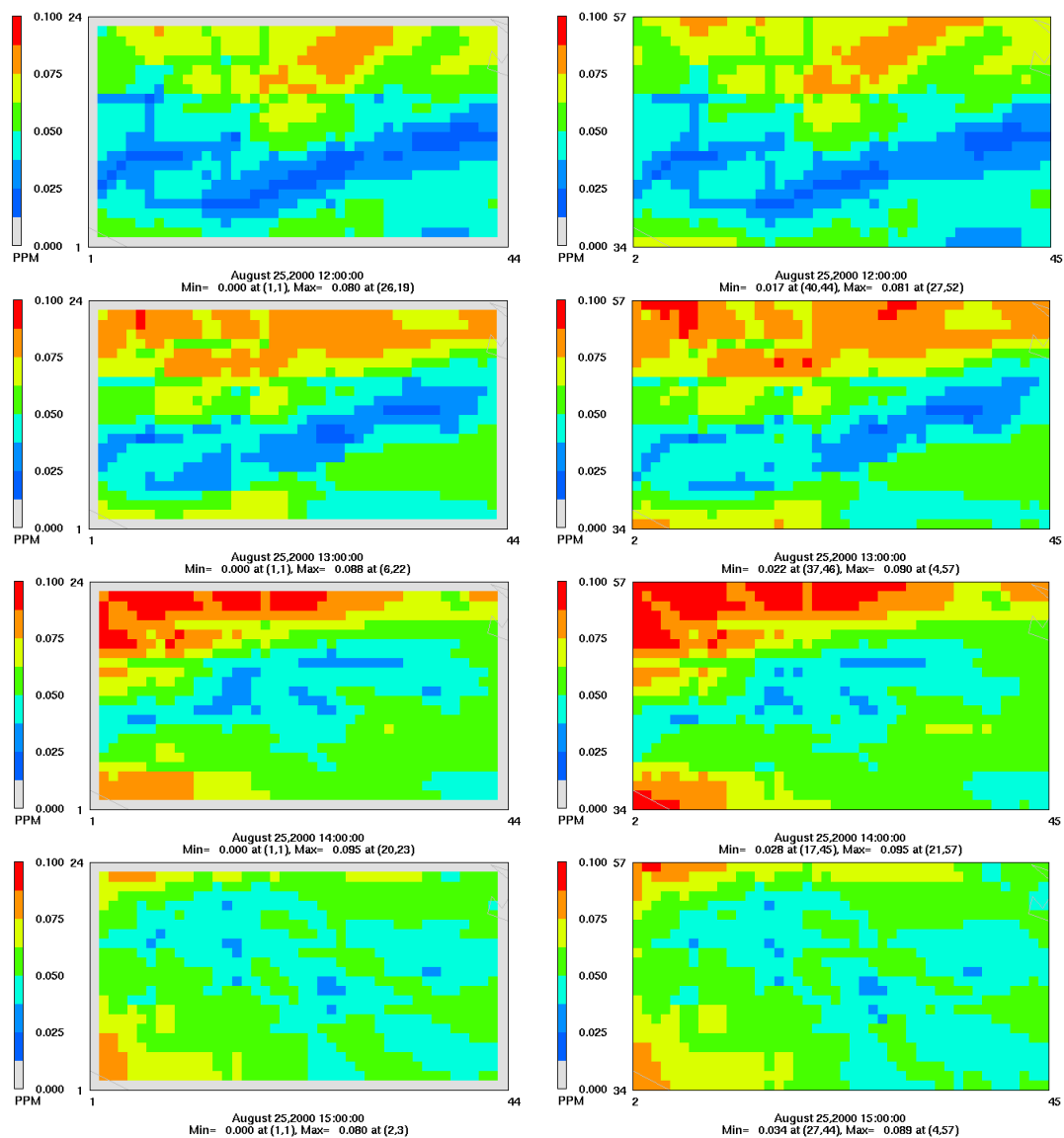


Figure 3.3 Ozone concentrations for August 25 from 1200 hr to 1500 hr using the basecase inputs, predicted by the sub-domain model (left column) and full domain (right column)

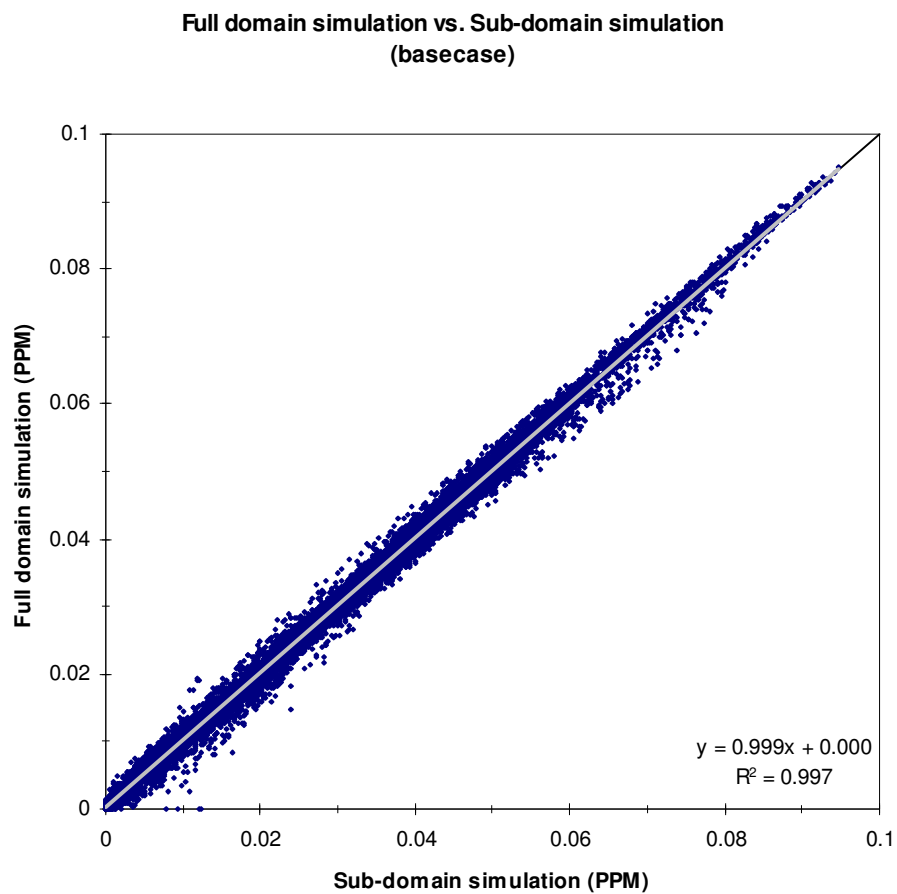


Figure 3.4 Comparison of ozone concentration predictions for the August 25 base case simulation using the sub-domain and the full domain

In order to determine if the sub-domain model would have the same response to emission events as the full domain simulation, a comparison similar to that shown in Figures 3.3 and 3.4 was performed, however, in this case an emission event was added. The event released 5,819 lbs per hour of propylene from 10 am to 12 pm August 25, 2000, at ground level, into the grid cell which is the 41st to the east and the 44th to the north from the southwest corner of the red portion of the domain shown in Figure 3.1. The particular composition and magnitude of this emission event was chosen to correspond to aircraft measurements made near the Ship Channel area on August 25, 2000, as described by Vizuite (2005). Figure 3.5 compares the changes in ozone concentrations due to the emission event, predicted by the sub-domain and full domain simulations.

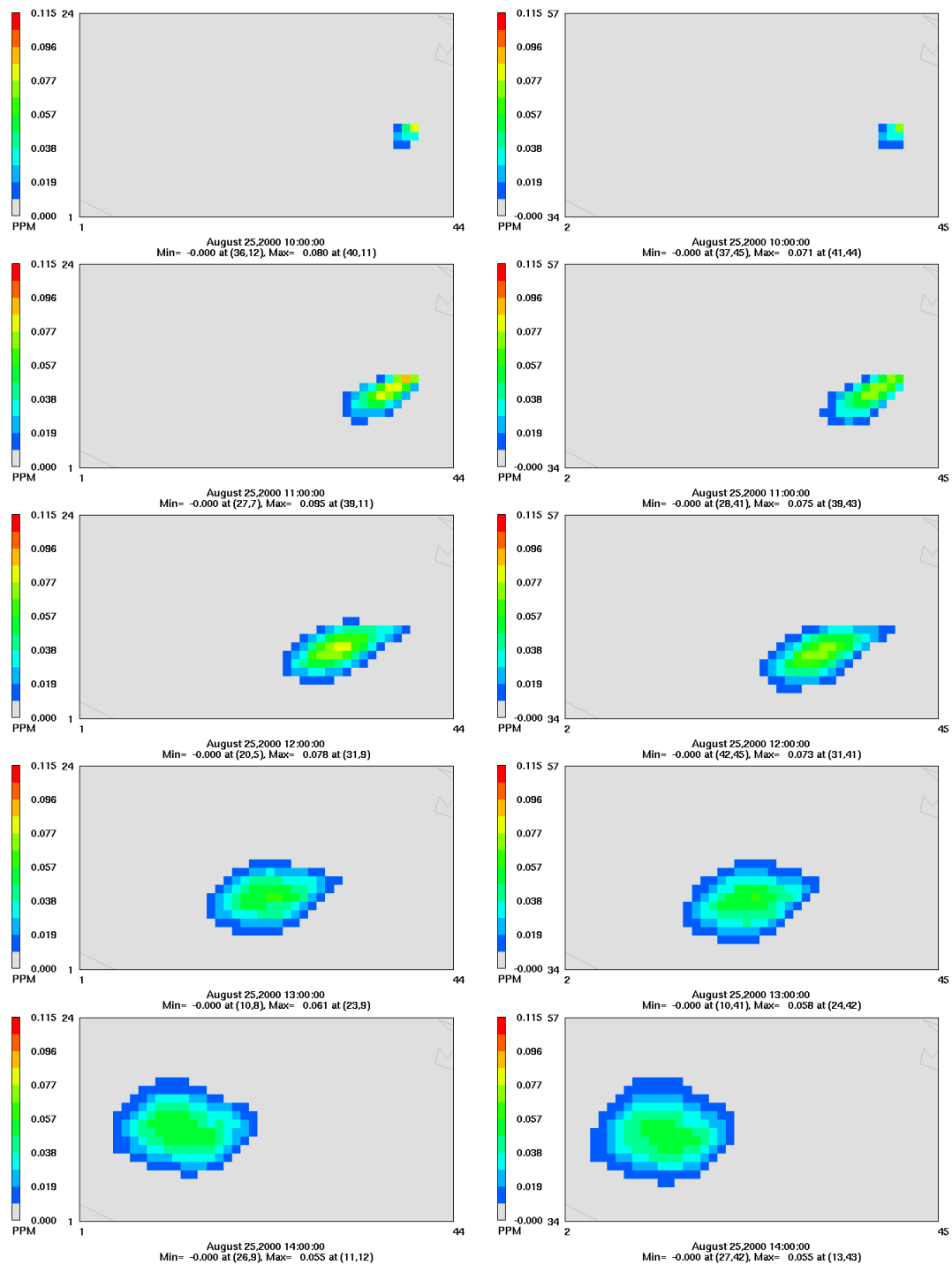


Figure 3.5 Ozone difference plots between emission event case and basecase with sub-domain model (left column) and full CAMx (right column)

Figure 3.6 shows a comparison of the differences in predicted ozone concentrations between the simulation that included the test emission event and the base case. The comparison is shown for all ground level cells. Although the scatter is greater than in the base case comparison, the correlation between the results of the sub-domain and full domain models still has a squared correlation coefficient of 0.967. The greatest differences in the predictions occurred at 11 AM, as the emission event plume was developing. The major cause of the differences is likely the process used in preparing boundary and initial condition for the sub-domain model. Boundary and initial conditions for the sub-domain model were extracted from the full domain model output file, with 1-hour averaged concentrations. This one hour averaging, rather than updating concentrations at all time steps, introduces the differences between the full domain and sub-domain simulations, particularly at the time of onset of the emission event.

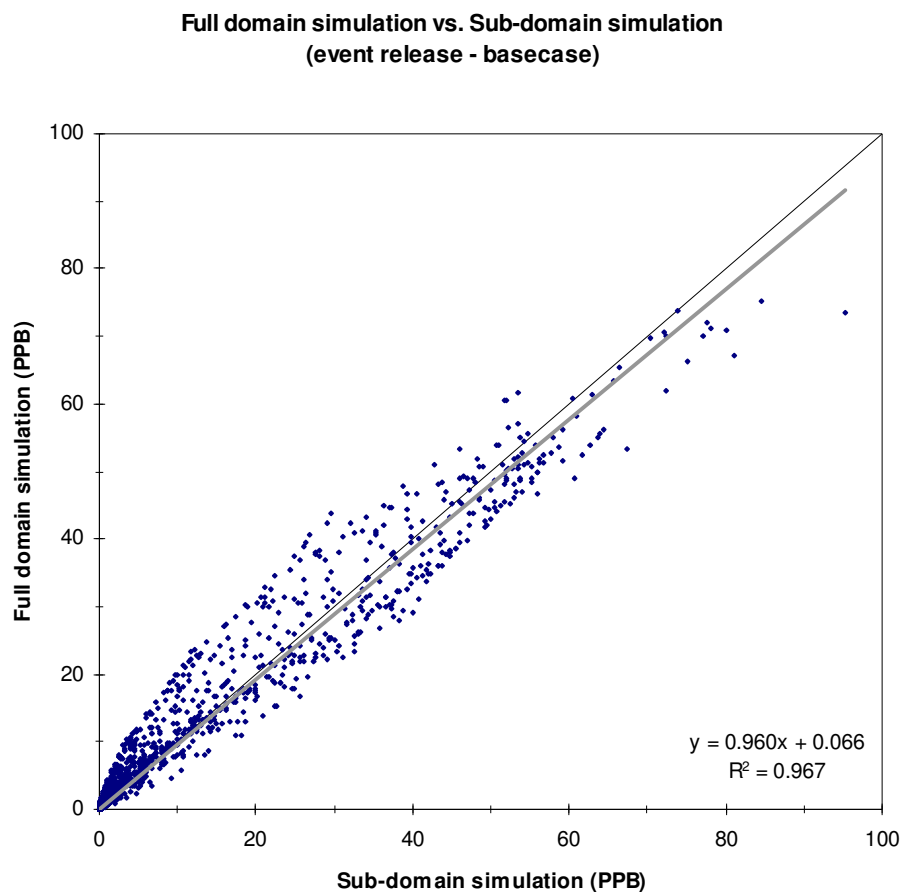


Figure 3.6 Comparison of the difference between the emission event and the base case in the full domain simulation to the difference between the emission event and the base case in the sub-domain simulation. Emission event is a propylene release at a rate of 5,819 lbs per hour from 10 am to 12 pm near the center right portion of Figure 3.2a.

3.2.4 Scenarios examined using the sub-domain model

The sub-domain model was used to examine the impact, on ozone formation, of the magnitude, duration, timing, and composition of industrial emission events in the Houston area. Figure 3.7 summarizes the scenarios that were examined. Eight different event magnitudes, two event durations, eight different times of event occurrence, and two event compositions were examined. Investigation of all permutations of these parameters would lead to 256 scenarios for each day that is investigated (2 days are reported in this work). This thesis will report on a subset of the set of all possible permutations that illustrate the basic features of the full range of scenarios.

$$\begin{array}{c}
 \text{magnitude} \times \text{duration} \times \text{time of occurrence} \times \text{composition} \\
 \left(\begin{array}{c} 100 \text{ lb} \\ 200 \text{ lb} \\ 300 \text{ lb} \\ 500 \text{ lb} \\ 1,000 \text{ lb} \\ 2,000 \text{ lb} \\ 3,000 \text{ lb} \\ 5,000 \text{ lb} \end{array} \right) \times \left(\begin{array}{c} 1 \text{ hr} \\ 2 \text{ hr} \end{array} \right) \times \left(\begin{array}{c} 4 \text{ hr} \\ 6 \text{ hr} \\ 8 \text{ hr} \\ 10 \text{ hr} \\ 11 \text{ hr} \\ 12 \text{ hr} \\ 15 \text{ hr} \\ 18 \text{ hr} \end{array} \right) \times \left(\begin{array}{c} \text{ethylene} \\ \text{propylene} \end{array} \right) = 8 \times 2 \times 8 \times 2 = 256 \text{ cases}
 \end{array}$$

Figure 3.7 Emission event scenarios

3.3 Results and Discussion

The sub-domain model was used to examine the impact, on ozone formation, of the magnitude, duration, timing, and composition of industrial emission events in the Houston area. The effects of each of these variables, in simulations representing August 25 and August 30, 2000, are discussed in the sub-sections below.

3.3.1 Event Magnitude

Event magnitudes ranging from 100-5,000 lb were examined. This range of emission spans the range from the smallest reportable emission events to events that are among the top 8% in emission rate (61 events out of 759 HRVOC events reported in 2003 had emission rates greater than 5,000 lb/hr). Figure 3.8 shows the maximum increase in predicted ozone concentration due to the emission event as a function of the amount of ethylene or propylene released. Specifically, the quantity reported is:

$$\text{Max}_{\text{all hours of simulation}} \{ \text{Ground level O}_3 \text{ event simulation} - \text{Ground level O}_3 \text{ base case} \} \quad (\text{Eqn. 3.1})$$

Results for both August 25 and August 30 are reported. In all of the simulations, the maximum additional ozone scales linearly with the amount of ethylene and propylene released, however, the slope of the linear relationship depends on the compound released and the meteorology the release encounters. The maximum additional ozone formed due to propylene releases (15 ppb per 1000 lb release) is two to three times greater than the amount formed from an ethylene release with the same mass (4-9 ppb per 1000 lb release). Meteorology is important in determining the ozone formation associated with an ethylene release; the ethylene release on August 25, which was advected over the

downtown area, generated half as large a change in maximum ozone as the release on August 30, which was advected over Galveston Bay.

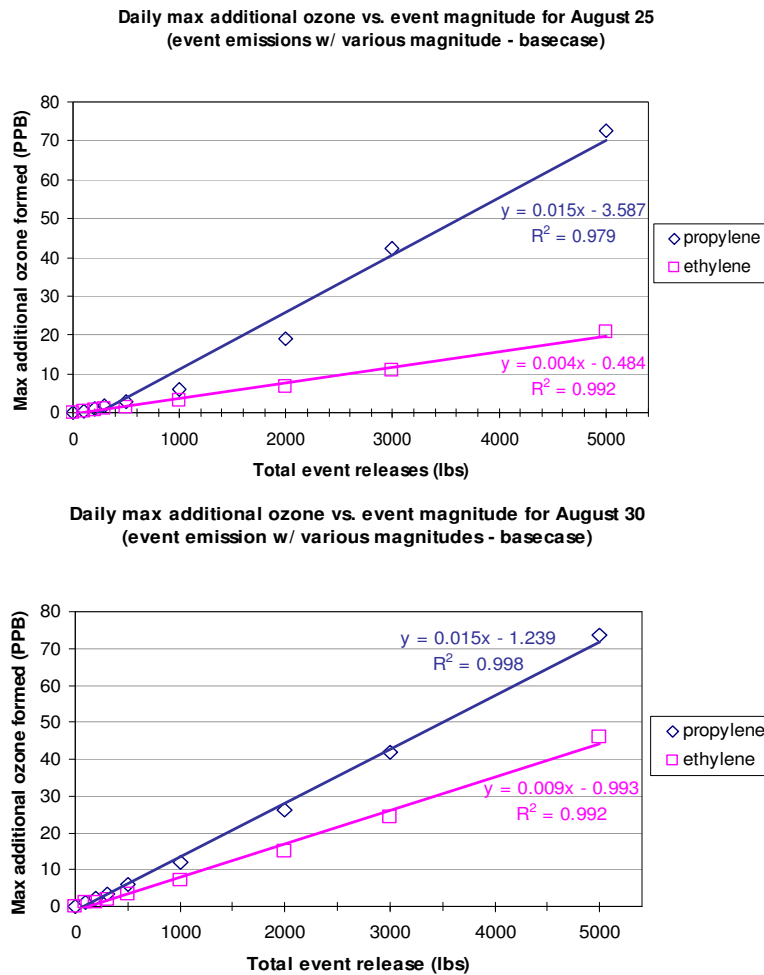


Figure 3.8 Daily maximum of additional ozone formation due to emission events of ethylene and propylene; results are reported for 10 am releases (1-hour duration) on August 25 and August 30

Figure 3.8 shows the maximum change in ozone concentrations between the event simulation and the base case. Figure 3.9 shows that these changes in ozone concentration did not always influence the peak ozone concentration, predicted in the sub-domain, over the course of the day. For example, on August 25, the daily maximum ozone concentration predicted in the sub-domain was not affected by the ethylene emission events, because the location of the maximum predicted ozone concentration was in a different portion of the sub-domain than the region affected by the plume. The simulated propylene events on August 25 did influence domain-wide maxima at some times of day, because they reacted more rapidly than the ethylene events. In contrast, on August 30, daily maximum ozone in the entire sub-domain was influenced by all of the emission events because the peak daily ozone concentration consistently occurred in areas affected by the event plumes. Daily maximum ozone concentration was increased by 8 ppb through the addition of a 5,000 lb event emission of ethylene, 5 ppb through the addition of a 3,000 lb event emission of propylene, and 33 ppb through the addition of a 5,000 lb event emission of propylene.

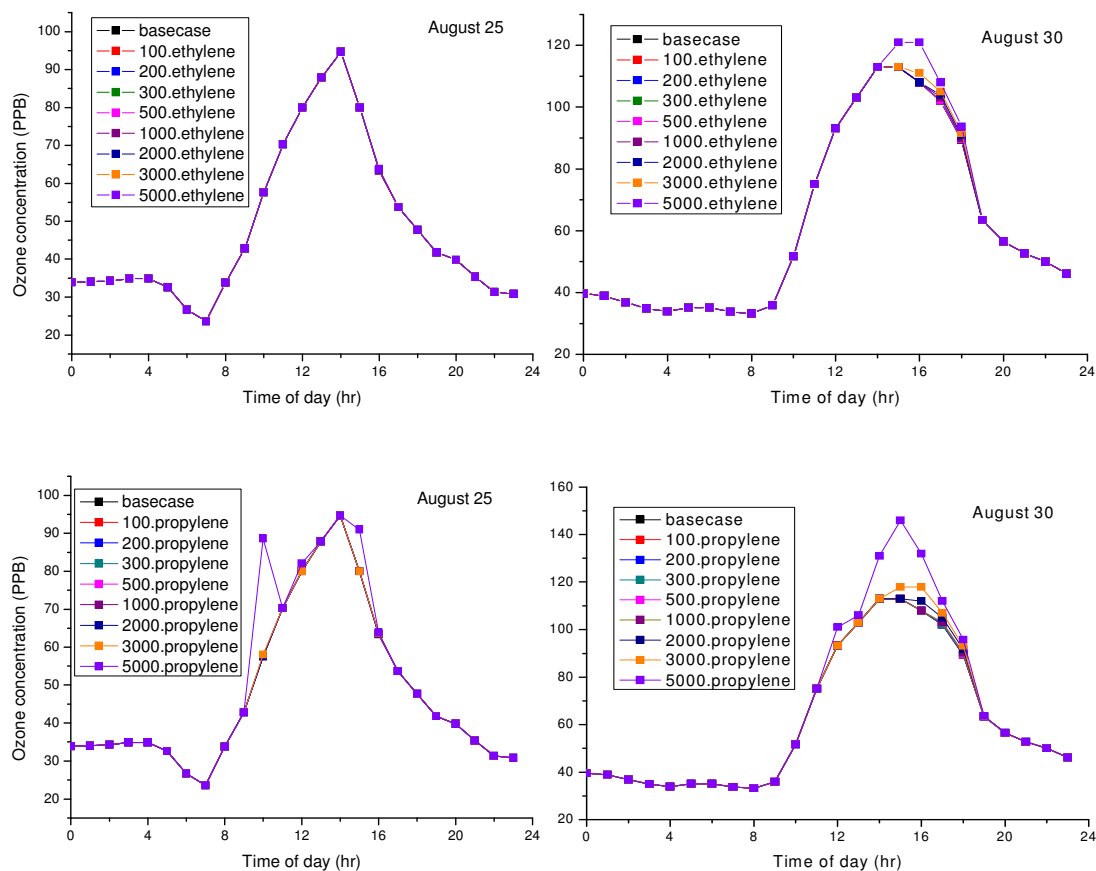


Figure 3.9 Domain-wide maximum ozone concentration for emission events of ethylene (top 2 figures) and propylene (bottom 2 figures) beginning at 10 am for 1-hour duration with various magnitudes for both episode days

The day to day differences between event emissions on August 25 and August 30, shown in Figures 3.8 and 3.9 are due to different meteorology and NO_x availability. As indicated above, the plumes of emission events on August 25 were transported to the west over downtown Houston, while the emission events of August 30 were transported over Galveston Bay. Low mixing heights over the Bay restricted vertical dilution of ozone and, therefore, led to higher ground level ozone concentrations on August 30 than on August 25; ozone titration by urban NO sources during morning hours also influenced ozone concentrations on August 25.

3.3.2 Time of event occurrence

The time of day that an event occurs has a large effect on ozone formation due to the event. For example, night-time releases tend to be widely mixed before the event can drive any significant differences in photochemistry, and events that are advected over urban areas during peak traffic periods will experience different NO_x availability than events that are released at mid-day. To investigate the impact of the time of day of an event on ozone formation, one-hour duration event releases of ethylene and propylene were simulated, beginning at 4 am, 6 am, 8 am, 10 am, 11 am, 12 pm, 3 pm, and 6 pm. Figure 3.10 shows the maximum additional ozone formed (Eqn. 3.1) due to simulated emission events of 1000 lbs, that began at various times of day, on August 25 and August 30, 2000. On August 25, peak ozone production for ethylene and propylene plumes occurred when the release began at 6 am, when the plume would experience the greatest NO_x availability due to traffic emissions. For August 30, ethylene and propylene releases in the afternoon, when wind speeds were slow and free radical availability from ozone photolysis was high, led to maximum ozone production.

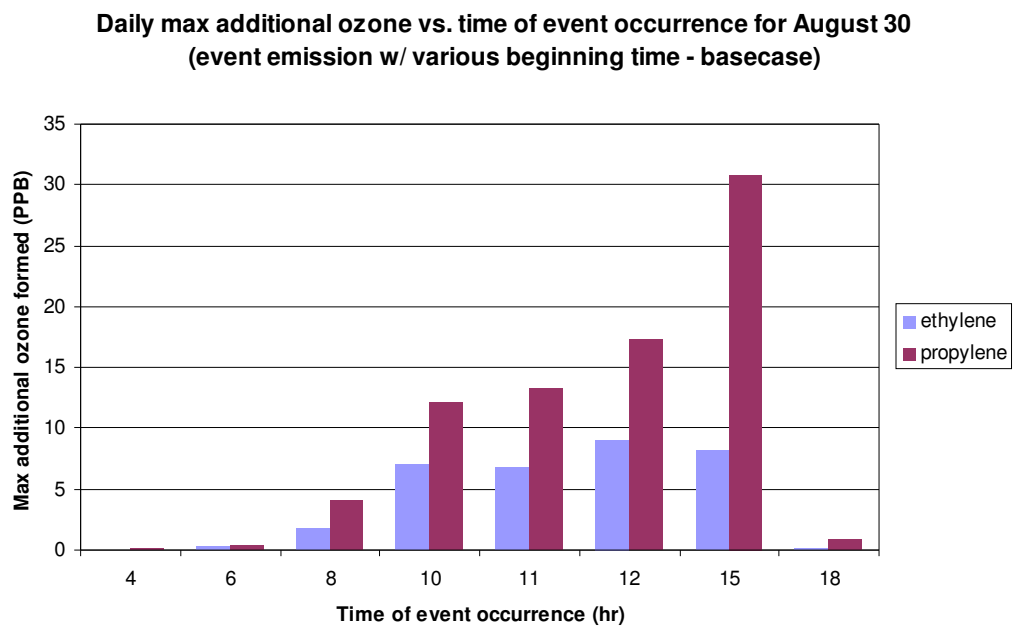
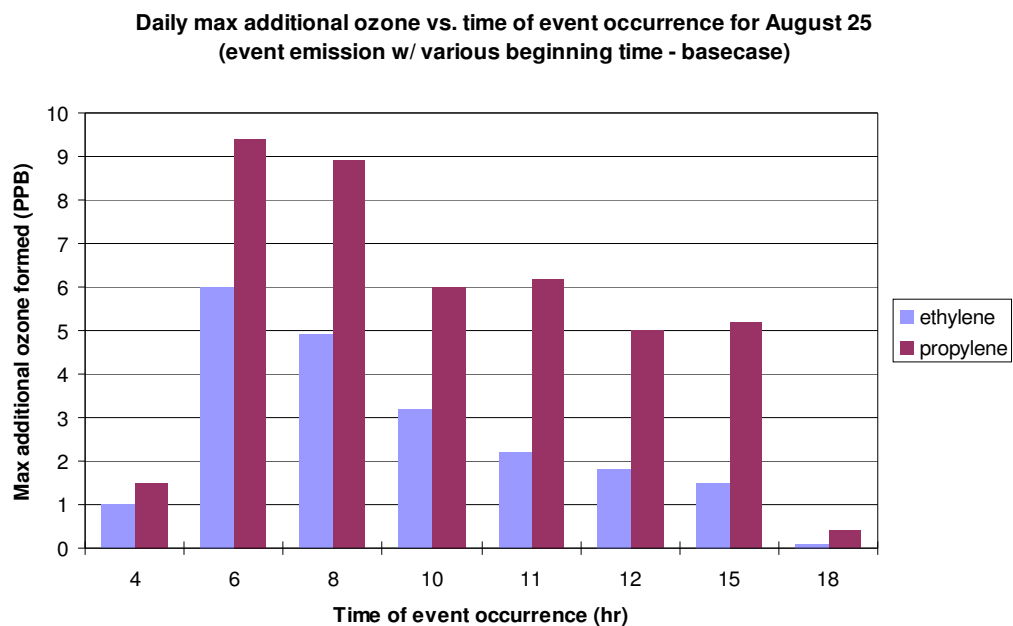


Figure 3.10 Maximum additional ozone formation due to emission events of 1 hour duration, beginning of various times on August 25 and August 30, 2000

3.3.3 Event Duration

Emission events of different durations produce different changes in ozone concentration. Figure 3.11 presents maximum changes in ozone concentration between the event simulation and the base case for August 25 and August 30, 2000 for events of 1 hour and 2 hour duration. In this set of simulations, the total amount of either ethylene or propylene released was fixed at 1,000 lbs for all the simulations, so a release rate of 1,000 lb per hour was used for a 1-hour duration events and a release rate of 500 lbs per hour was used for 2-hour duration events. The time of event onset was fixed at 10 am. The results presented in Figure 3.11 indicate that both total emission magnitude and emission rate influence the maximum change in ozone concentration; the 1-hour duration event (1000 lb/hr) led to greater changes in maximum ozone concentration than the 2-hour event (500 lb/hr), but the changes did not double.

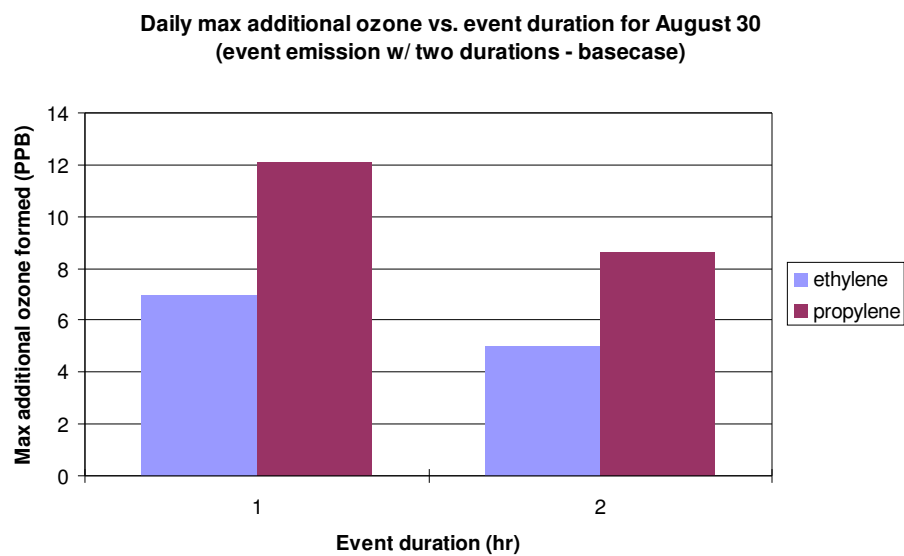
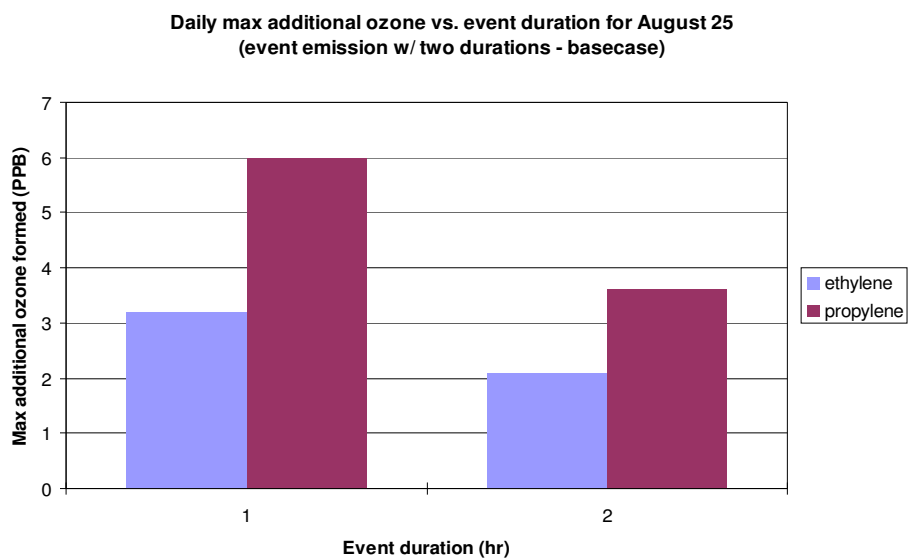


Figure 3.11 Maximum additional ozone formation due to emission events of 1 hour duration (1000 lb/hr) and 2-hour duration (500 lb/hr) beginning at 10 am for August 25 and August 30, 2000

3.3.4 Event Composition

Finally, the effect of the composition of emission events on ozone formation was examined. All of the simulations reported to this point have been for emission events of pure ethylene or pure propylene. These compounds were selected since 90% of the mass of the 759 HRVOC emission events reported in 2003 was accounted for by these two compounds. Figures 3.8 to 3.11 indicate that propylene events, per unit mass, consistently produce more ozone than ethylene events. Figure 3.12 compares the maximum additional ozone formed due to 1-hour duration, 500 lb emission events for ethylene, propylene, propane and xylene. The reactive olefins lead to maximum changes in ozone concentration that are 3 or more times greater than the maximum changes in ozone produced by a similar mass release of less reactive compounds.

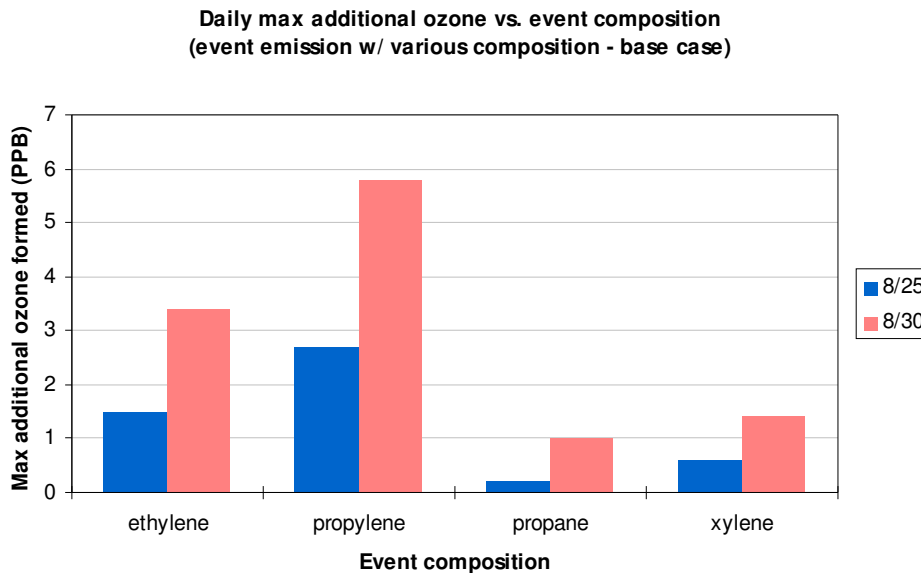


Figure 3.12 Maximum of additional ozone formation due to emission events of a 500 lb release of ethylene, propylene, propane and xylene beginning at 10 am for 1-hour duration for August 25 and August 30, 2000

The ratio of maximum changes in ozone concentration due to ethylene and propylene events is 0.56 (1.5 ppb / 2.7 ppb) for the simulation of 25 August and 0.59 (3.4 ppb / 5.8 ppb) for the simulation of 30 August. These ratios are 24% and 20% smaller than the ratio of Maximum Incremental Reactivity (MIR) for ethylene and propylene (0.73) reported by Carter (1994). The MIR scale is one of the measures used to quantify ozone forming capability of individual hydrocarbon species. This difference between the sub-domain modeling results and the MIR scale is primarily due to the fact that the MIR calculation is based on a representative high ozone episode under average conditions of urban areas.

Figure 3.13 examines the effect of considering emission events that are mixtures. All of the simulations reported to this point have been of single compounds. Figure 3.13 compares the combined maximum increases in ozone concentration due to 500 lb emission events of pure ethylene and pure propylene and those due to 1000 lb events of half ethylene and half propylene. On August 25, the sum of maximum increases in ozone concentration due to pure ethylene and pure propylene events were approximately same as the maximum increase due to a combined event. In contrast, on August 30, the sum of maximum increases in ozone concentration from pure ethylene and pure propylene events was more than 40% larger than maximum increase from one combined event.

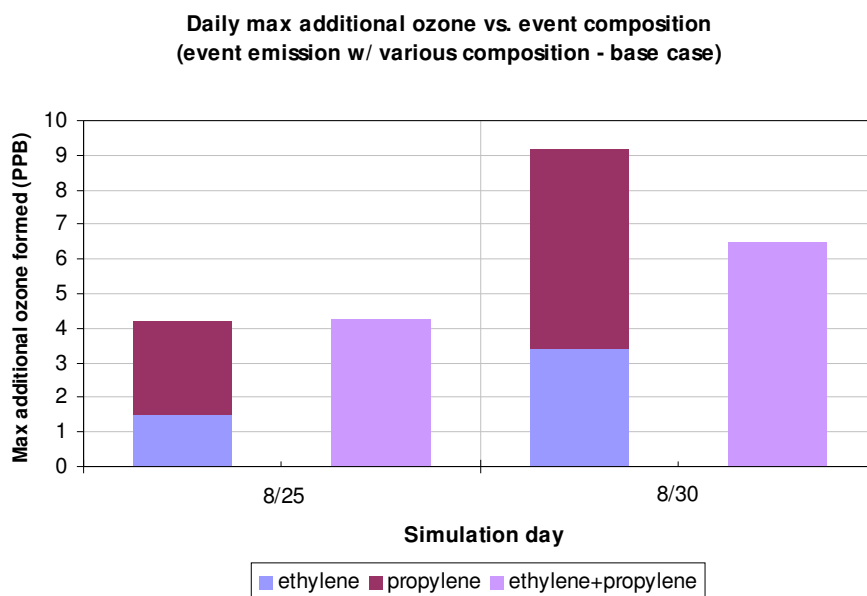


Figure 3.13 Maximum of additional ozone formation due to emission events of a 500 lb release of pure ethylene, pure propylene and a total of 1,000 lbs release of half ethylene and half propylene beginning at 10 am for 1-hour duration for August 25 and August 30, 2000

3.4 Summary

On average, five emission events per day occur in the Houston area and two of the five events include highly reactive volatile organic compounds. Because the ozone formation and accumulation due to emission events have a complex dependence on event magnitude, composition, duration and timing, as well as the specific meteorology at the time of the event, it is only possible to estimate likely probabilities of the impact of emission events. A simple Monte Carlo simulation of 759 events, the total number of HRVOC emission events reported in 2003, was conducted to examine the potential ozone impacts of a distribution of emission events. For each of the events in the Monte Carlo simulation, the event magnitude, composition, and timing were randomly selected based on the distribution of event magnitude, composition and timing reported by Murphy and Allen (2005). The magnitude of events was analyzed in terms of hourly emission rates. Half of the Monte Carlo emission events were assumed to occur on days with meteorology like August 25, and half on days like August 30. Once the event magnitude, composition and timing were selected in the Monte Carlo simulation, the maximum additional ozone associated with that event was calculated based on the results of the sub-domain modeling. To do this, the sub-domain modeling results were summarized by creating linear relationships (like those shown in Figure 3.8; all of the relationships are provided in Appendix C) between maximum additional ozone formed and event magnitude for each compound, each day, and each time of release. Two different sets of Monte Carlo calculations were performed, based on two different sets of assumptions. One set of calculations assumes that the emission rate is the most significant parameter in determining the amount of additional ozone formed. In this case,

the additional ozone formed by an event lasting 30 minutes would be estimated based on the emission rate (total mass released divided by 30 minutes). This might represent an over-estimate of the effect of short duration events, since the minimum time used in the simulations on which the Monte Carlo simulation is based is one hour. Figure 3.14 summarizes the results from this set of calculations in the form of a cumulative probability distribution. A second set of calculations assumes that the total mass emitted is divided over discrete one hour blocks, so the mass of an emission event lasting 30 minutes would be divided by a one hour duration to determine the emission rate. This is consistent with the one hour averaging of ozone concentrations and the minimum time resolution used in the modeling, however, it may represent an under-estimate of the effect of short duration events, since it underestimates the emission rate. Figure 3.15 summarizes the results from this set of calculations in the form of a cumulative probability distribution. The results in Figure 3.14 and 3.15 suggest that while most events lead to negligible ozone formation, a small number of events lead to extensive ozone formation; For Figure 3.14, a total of 15 out of the 763 events (~1.9%) had predicted maximum added ozone concentrations in excess of 100 ppb, and 46 out of the 763 events (~6%) in excess of 10 ppb. For Figure 3.15, a total of 2 out of the 763 events (~0.3%) had predicted maximum added ozone concentrations in excess of 70 ppb, and 11 out of the 763 events (~1.5%) in excess of 10 ppb.

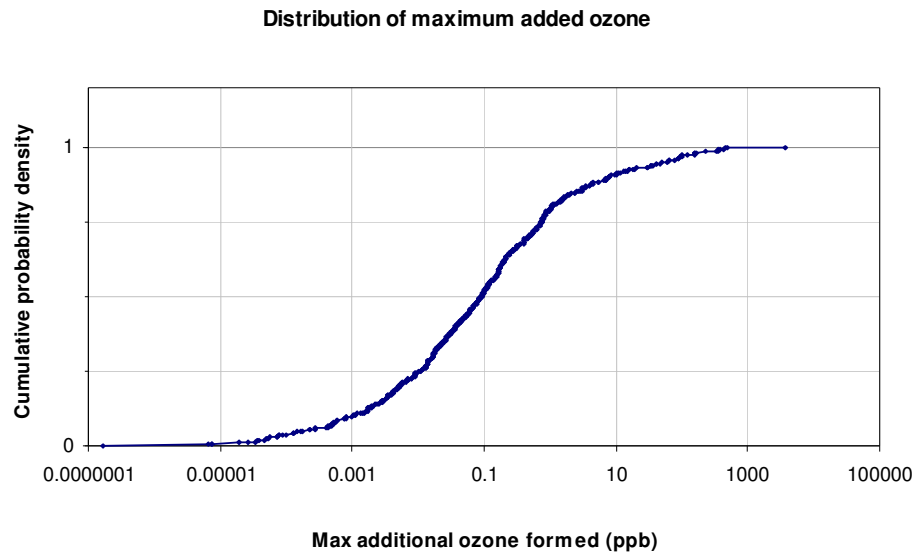


Figure 3.14 Distribution of maximum added ozone due to emission events, based on a Monte Carlo simulation of 763 events

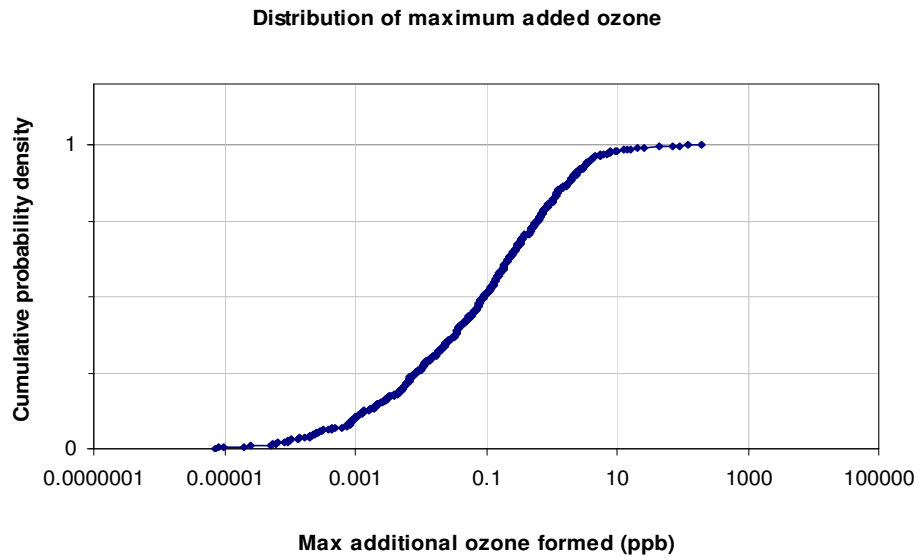


Figure 3.15 Distribution of maximum added ozone due to emission events based on a Monte Carlo simulation of 763 events using emission rates calculated with hourly blocks instead of actual duration.

3.5 References

Allen, D., Murphy, C., Kimura, Y., Vizuete, W., Edgar, T., Jeffries, H., Kim, B.-U., Webster, M., Symons, M., 2004. Inventories of HRVOC Emissions & Impact of Emission Magnitude & Variability on Ozone Formation in H/G Area. Houston Advanced Research Center, H13.2003 Final Report, April 16, 2004, available at <http://www.harc.edu/harc/Projects/AirQuality/Projects/ShowProject.aspx?projectID=27>

Carter, W.P.L., 1994. Development of ozone reactivity scales for volatile organic compounds, *J. Air & Waste Manage. Assoc.*, 44, 881-899.

Environ International Corporation (Environ), 2004. User's Guide: Comprehensive Air Quality Model with Extensions (CAMx), Version 4.03, Document and model are available online at <http://www.camx.com>

Environ International Corporation (Environ), 2006. Comprehensive Air Quality Model with Extensions (CAMx) Pre-processors, Accessed January 2006 at <http://www.camx.com/download/support.php>

Kleinman, L.I., Daum, P.H., Imre, D., Lee, Y.N., Nunnermacker, L.J., Springston, S.R., Weinstein-Lloyd, J., Rudolph, J., 2002. Ozone production rate and hydrocarbon reactivity in 5 urban areas: A cause of high ozone concentration in Houston. *Geophys. Res. Lett.* 29 (10).

Murphy, C.F., Allen, D.T., 2005. Hydrocarbon emissions from industrial release events in the Houston- Galveston area and their impact on ozone formation. *Atmospheric Environment* 39 (21), 3785-3798.

Ryerson, T.B., Trainer, M., Angevine, W.M., Brock, C.A., Dissly, R.W., Fehsenfeld, F.C., Frost, G.J., Goldan, P.D., Holloway, J.S., Hubler, G., Jakoubek, R.O., Kuster, W.C., Neuman, J.A., Nicks, D.K., Parrish, D.D., Roberts, J.M., Sueper, D.T., Atlas, E.L., Donnelly, S.G., Flocke, F., Fried, A., Potter, W.T., Schauffler, S., Stroud, V., Weinheimer, A.J., Wert, B.P., Wiedinmyer, C., Alvarez, R.J., Banta, R.M., Darby, L.S., Senff, C.J., 2003. Effect of petrochemical industrial emissions of reactive alkenes and NO_x on tropospheric ozone formation in Houston, Texas. *J. Geophys. Res.* 108 (D8), 4249.

Texas Commission on Environmental Quality (TCEQ), 2006. Houston-Galveston-Brazoria Ozone SIP Mid-Course Review Modeling, Accessed January 2006 at <http://www.tceq.state.tx.us/implementation/air/airmod/data/hgb1.html>

University of Texas at Austin, 2006. Comprehensive Air Quality Model with Extension (CAMx) Preprocessor for Albedo/haze/ozone column and Land use extraction

Vizuite, W., 2005. Implementation of Process Analysis in a three dimensional air quality model. Ph.D. Thesis, University of Texas.

CHAPTER 4

The effect of variability in industrial emissions on ozone formation in Houston, Texas

4.1 Introduction

Ambient observations have indicated that ozone formation in the Houston/Galveston (HG) area is faster and more efficient, with respect to NO_x consumed, than other urban areas in the United States. This results in highly localized but extreme ozone events, frequently in excess of the National Ambient Air Quality Standards (NAAQSs) for ozone. It is believed that these unique characteristics of ozone formation in the Houston metropolitan area are associated with plumes of highly reactive hydrocarbons, which have been observed in airborne measurements (Kleinman et al., 2003; Ryerson et al., 2003) over or near the industrial Houston Ship Channel area. Thus, accurate quantification of industrial emissions, particularly of reactive hydrocarbons, is critical to effectively address the rapid ozone formation and the consequent high ozone concentration events in the Houston metropolitan area.

Industrial emissions of hydrocarbons, from non-electricity generating units (NEGUs), have traditionally been assumed to be continuous at constant levels for the State Implementation Plan (SIP) development and photochemical modeling purposes. However, observational data collected during the Texas Air Quality Study in 2000 and emission event reports have shown that industrial emissions of hydrocarbons from NEGUs have significant temporal variability (Murphy and Allen, 2005; Vizuite, 2005).

Variability in industrial emissions of hydrocarbons can be ascribed to the occurrence of both episodic emission events and variable continuous emissions. Murphy and Allen (2005) have investigated characteristics of emission events in the HG area with a focus on highly reactive volatile organic compounds (HRVOCs; defined in Texas air quality regulation as ethylene, propylene, isomers of butene and 1,3-butadiene); characteristics of emission events examined included event magnitude, event duration and source types. These emissions events are discrete non-routine emissions events, of more than permitted amounts, with reporting required under Texas law. Since 2003, reporting is required of emissions events of over 100 lbs of a specific compound, or over 5000 lbs of VOCs if composed of less than 2% of individual highly reactive species.

Vizuete (2005) investigated the physical and chemical processes of ozone formation and accumulation in the HG area during a small number of large magnitude emission events. The previous chapter described development of computationally efficient photochemical models and the impact, on ozone formation in the HG area, of emission events using a stochastic characterization of the emission events described by Murphy and Allen (2005). While these previous studies provided important information on impacts of emission variability on ozone formation in the HG area, they are limited in the sense that the episodic emission events account for just a part of emission variability and contribute to just 10% of the mass of annual HRVOC emissions. As described in later sections of this chapter, data from emissions monitors for several industrial sources show that there is considerable variability in routine emissions that is not high enough to require reporting as an event, but may significantly impact ozone formation.

The overall goal of this chapter is to estimate potential changes in ozone formation and accumulation in the HG area due to variability in continuous hydrocarbon

emissions. Variability in VOC emissions will be simulated based on observations of emission variability from a group of industrial sources in the HG area, and a stochastic emission inventory generator, described in the Methods section of this chapter. The characterization of VOC emissions variability and the impacts of the variability on ozone formation in the Houston area are described in the Results section of this chapter.

4.2 Methods

4.2.1 The stochastic emission inventory generator

Observations from various emission sources and ambient measurements indicate that industrial emissions of VOC have significant temporal variability. For example, Figure 4.1 shows the hourly measurements of the mass flow rate to a typical flare at an industrial facility in the Houston area over the course of a year. Variability in mass flow to a flare represents the variability in emissions if combustion efficiency is constant and likely represents a lower bound on emission variability if combustion efficiency decreases at high or low flows. Although the annual average mass flow rate (blue horizontal line at 2.93 kilo-lb/hr) is below the permitted annual average mass flow rate (purple line at 3.43 kilo-lb/hr), the significant temporal variability in mass flow leads to frequent exceedances of the annual average emission rate. While temporal variability is large compared to the mean, this variability does not necessarily result in a reportable emission event. The maximum allowable flow to the flare of Figure 4.1, when averaged on a daily basis, is 34,700 lb/hr. Only a few of the instances of high flow rates exceed

this amount and are reportable as emission events. Data from other emission sources also exhibit high variability, with different temporal patterns.

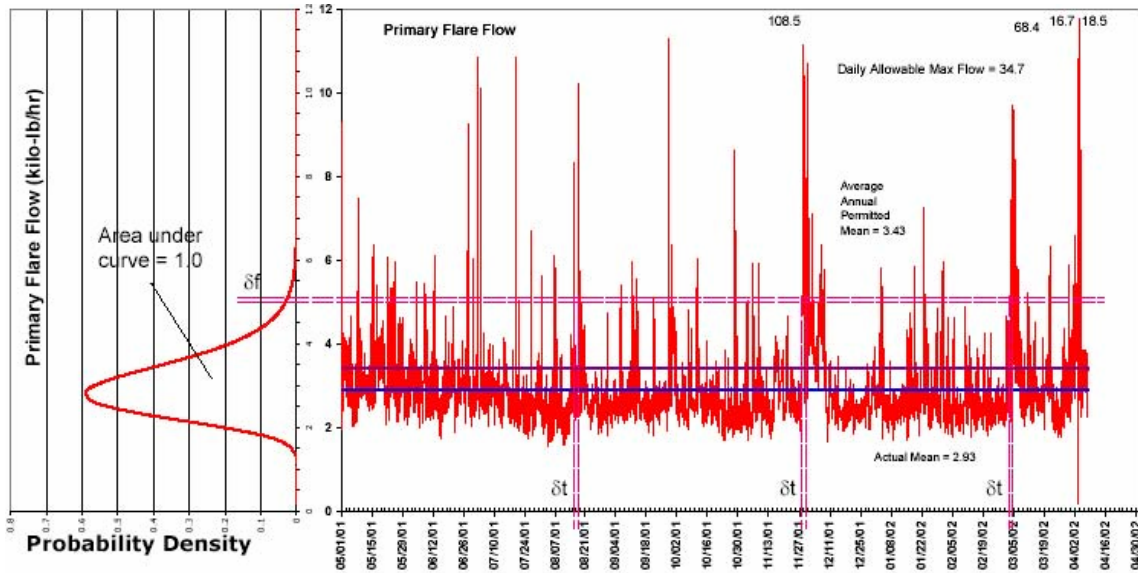


Figure 4.1 Probability distribution function (PDF) and time series of mass flow rate to a flare at an industrial facility in the HG area.

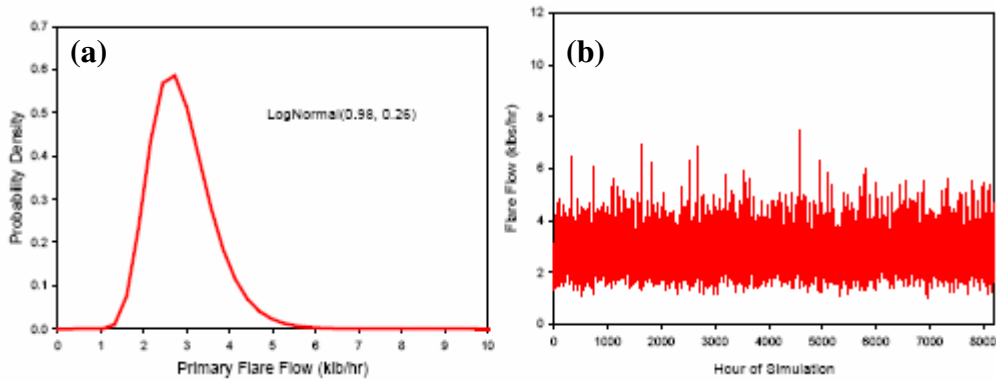


Figure 4.2 (a) Single probability distribution of mass flow rates to the flare shown in Figure 4.1a. (b) Time series of mass flow rate simulated with the probability distribution in Figure 4.2a, modeling the mass flow rate in Figure 4.1b.

In order to characterize the effect of these emissions on ozone formation, a model of the emissions must be constructed. For the flare described in Figure 4-1, a probabilistic model of the emissions was constructed. The simplest approach would be to assume that a single probability density function could be used to describe the emissions, however, sampling from a simple probability density function (PDF) is not sufficient to model the emissions. As shown in Figure 4.2, mass flow rates (Figure 4.2b) simulated with a single lognormal distribution (Figure 4.2a), fitted to the observations, has no resemblance to the time series of original data in Figure 4.1b. A single PDF cannot characterize the flare flow.

Mass flows to the flare in Figure 4.1 are composed of various components in magnitude, including nearly constant, routinely variable, and allowable episodic mass flow rates (Figure 4.3). Therefore the appropriate model for this process is a mixture of multiple PDFs (Cornell, 2002), each accounting for one of the components of the mass flow variability. Models of these emission rates were constructed by researchers at the University of North Carolina (UNC) (Webster et al., 2007). To determine the form of the PDF (normal or log-normal) that should be used for the nearly constant, routinely variable and allowable episodic mass flows, mass flow rates were sorted by the UNC group in order of size. The inverse normal of the mass flow rate was plotted against the mass flow rate or the logarithm of the mass flow rate. To characterize the inverse normal distribution function, a function z was calculated for each mass flow rate, where z is defined as $\left(z = \frac{Y - \bar{Y}}{s} \right)$, \bar{Y} is the mean emission rate and s is the standard deviation of the normal function that best fits the emission rate. In Figure 4.4, z is plotted against the mass flow rate and the natural logarithm of the mass flow rate. If the relationship is linear between the inverse normal (z) and the mass flow rate, it is reasonable to assume

that the emissions are normal. If the relationship is linear between the inverse normal and the logarithm of the mass flow rate, it is reasonable to assume that the mass flows are lognormal. Figure 4.4 shows the mass flows from the flare in Figure 4.1 graphed against their inverse normal (z). A total of three components of variable mass flows were identified by Webster, et al (2007); one normal distribution and two lognormal distributions. In addition, the mean and standard deviation of the distribution were obtained from the midpoint and slope of the fitted line, respectively. Figure 4.5 shows resultant PDFs for each component identified (Figure 4.5a) and the normalized PDFs based on the proportion of mass flow associated with each component (Figure 4.5b) for the mass flow rates shown in Figure 4.1. These distributions of mass flows were converted to emissions by assuming constant combustion efficiency.

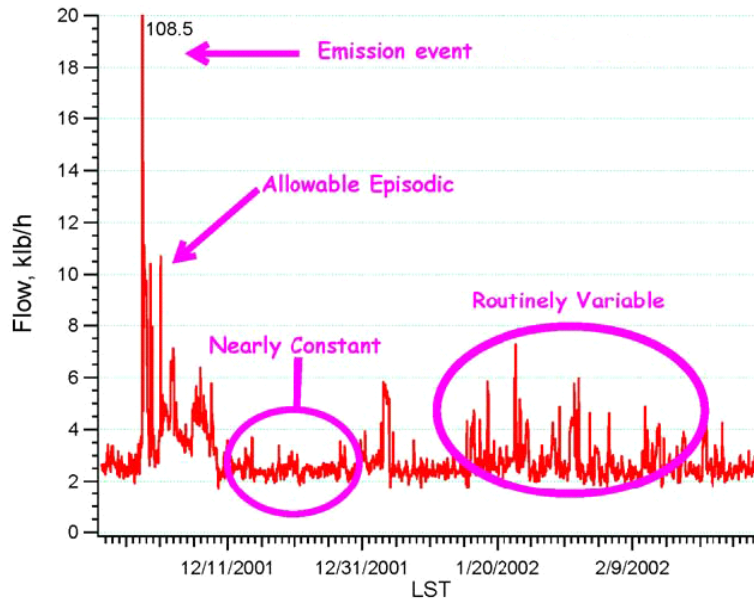


Figure 4.3 Components of mass flows: emission event, allowable episodic, routinely variable and nearly constant.

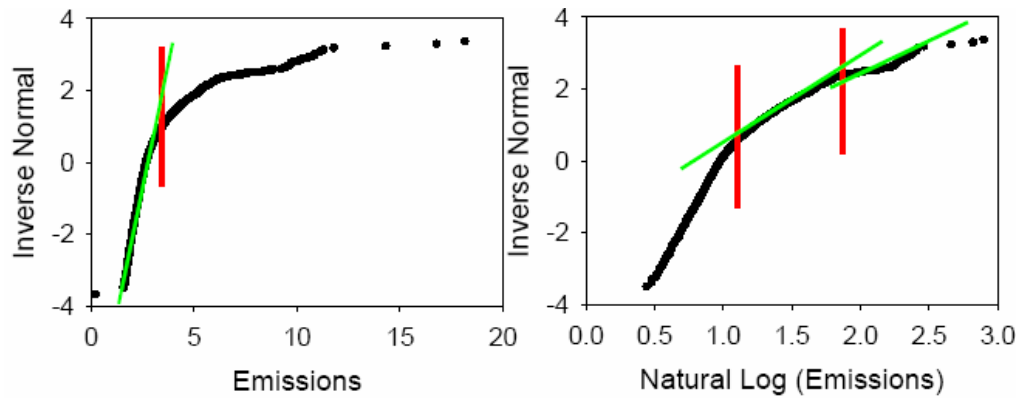


Figure 4.4 Decomposition into three PDFs of emissions from flare shown in Figure 4.1. Inverse normal is expressed in the standard form (z) in relation to the mean and standard deviation $\left(z = \frac{Y - \bar{Y}}{s} \right)$. (Webster, et al., 2007)

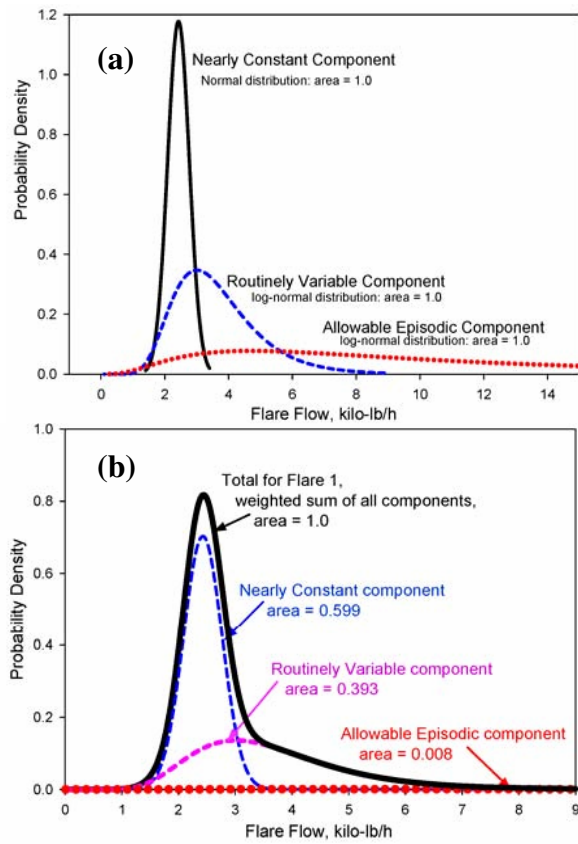


Figure 4.5 (a) PDFs for each component of emissions from the flare in Figure 4.1 (b) normalized PDFs of three components based on the proportion of each emission component

Once PDFs for each emission mode are calculated, the duration of emissions in one mode, before transition to another mode, was simulated by the UNC group using an exponential distribution function. Exponential distributions are probability distributions widely used to model the time between events. A mean time for the exponential distribution was calculated by sorting flow rates by time and averaging durations in mode for each emission mode. For the flare flow in Figure 4.1, mean time was calculated as 7.41, 4.41 and 1.15 hour for the nearly constant, routinely variable, and allowable episodic emission components, respectively, and the distribution of the duration in each component is shown in Figure 4.6.

Overall, the algorithm for generating emission samples, created by the UNC group, is to (1) randomly sample the mode of emissions using the proportions of each emission mode, (2) randomly sample the number of hours to remain in the current mode using the exponential distributions for the selected emission mode, and (3) randomly sample the emission rate for each hour based on the PDF of emission rates for the current mode. In sampling emissions in step (3), an autocorrelation of 0.99 with the emission rate of the previous hour is imposed. The autocorrelation was estimated from the observations, and is a reasonable model of a continuous industrial process, since the best predictor of one hour's activity level and operating conditions is the previous hour's. Based on the number of hours selected in step (2), step (3) is repeated. For example, if the first component, nearly constant, was selected in step (1) and two-hour duration was selected in step (2), then emission rates were randomly sampled from the PDF of the first component for two hours before randomly selecting the next component. A comparison between observed mass flow rates and those simulated with this model are shown in Figure 4.7. This method produces samples of emissions that closely match the

cumulative distribution properties of the observations. Note that this model of emissions includes only permit allowable emission rates. Emission events above permitted levels are not included. The nature and impacts of these emission events have been described in the previous chapter and by Murphy and Allen (2005).

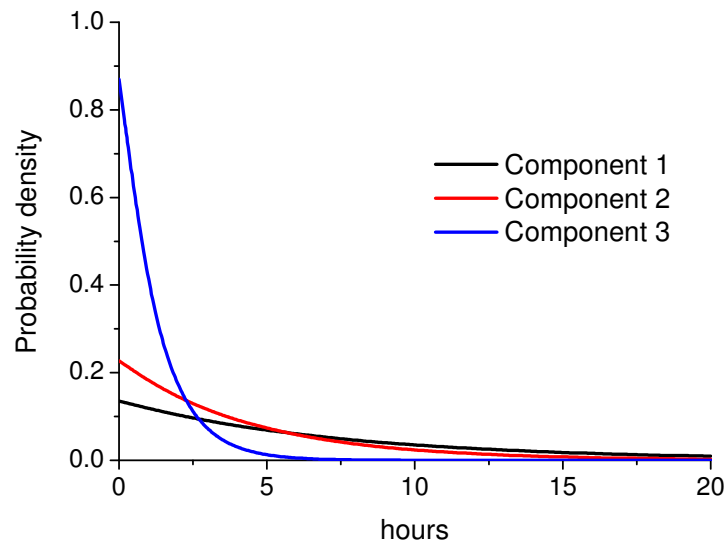


Figure 4.6 Time within each emission component before transition to next component

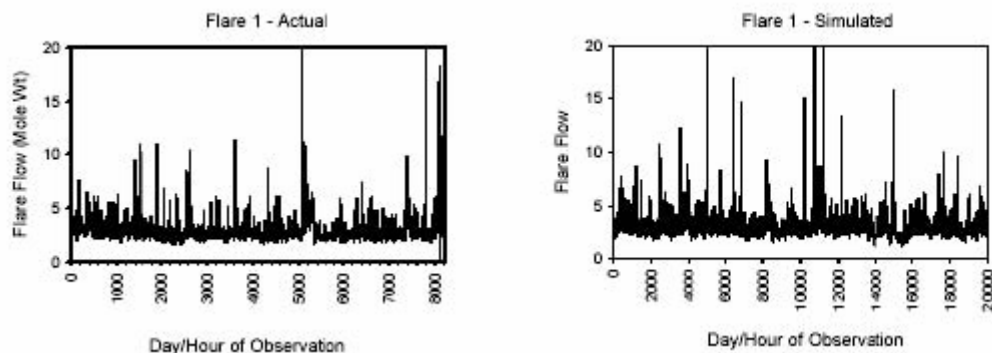


Figure 4.7 Time series of actual and simulated flare flow in Figure 4.1. Note that simulated time series has approximately 2.4 times longer time scale than actual time series.

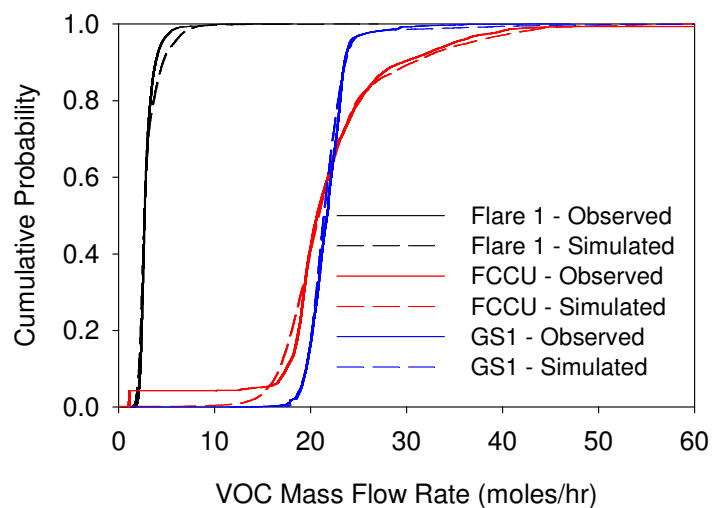


Figure 4.8 Comparison of cumulative probability distribution functions for observed and simulated (10,000 hours) for three flares.

4.2.2 Application of stochastic emission inventory to the HG area

A set of observations similar to that shown in Figure 4.1 were obtained from various flares and cooling towers in the HG area. The models to simulate emission variability were developed, by the UNC group, using the process described in the previous section of this chapter. Table 4.1 summarizes these observations and parameters for the models developed by the UNC team. Emissions from different sources exhibit different patterns of variability, but only limited data on that variability is available. For this thesis, therefore, individual flares, cooling towers and other point sources in the HG area were assigned one of the unit operation models developed by UNC and overall time-varying emissions from the point sources were simulated with the model. Cooling towers were randomly assigned one of the cooling tower models. Flares were randomly assigned one of the flare models. Stack and fugitive emissions were assumed to be lognormally distributed, as shown in Table 4.1. The mean of the selected model for simulating emissions is scaled to be equal to the average emission rates in the inventory for each emission source. In addition, the standard deviation of the models was scaled to preserve the coefficient of variation (the ratio of the standard deviation to the mean) shown in Table 4.1. In the work done for this thesis, for emission sources other than flares, all emissions except VOCs were kept intact throughout the simulation. For flares, both VOC and NO_x emissions were assumed to scale with flow rate, so for flares, the same pattern of variability was assumed for both VOC and NO_x emissions. The composition of the emissions from all sources was assumed to be constant, with only the temporal variability in the magnitude of emissions changing.

Table 4.1 Observations from emission sources and fitted parameters (Webster, et al., 2007)

Source name (number of observations)	Type	Component	Number of observations	Normalized proportion	Mean time	Normal or Lognormal	Standard deviation	Mean or Mean (LN Value)
Flare 1 (8208)	Flare	1	4913	0.599	7.41	N	0.34	2.43
		2	3223	0.393	4.41	LN	0.36	1.23
		3	68	0.008	1.15	LN	0.8	2.19
Flare 2 (720)	Flare	1	360	0.501	3.34	N	0.8	1.89
		2	331	0.460	3.5	N	2.5	4.99
		3	28	0.039	2.63	LN	0.33	2.45
Flare 5 (3624)	Flare	1	1757	0.486	3.09	N	225.52	758.83
		2	1706	0.472	5.36	N	1197.5	1721.7
		3	147	0.041	1.04	LN	0.71	8.08
HC Flare (1800)	Flare	1	128	0.071	0.52	LN	1.12	0.07
		2	1625	0.903	15.28	LN	0.26	0.9
		3	46	0.026	1.35	LN	0.3	1.58
Olefins Flare (1800)	Flare	1	1078	0.599	14.18	N	0.53	1.6
		2	700	0.389	10.58	N	3.1	4.91
		3	21	0.012	6.5	LN	0.42	2.95
FCCU (17533)	Flare	1	12383	0.743	195.31	N	3	20
		2	4270	0.256	17.85	N	11.93	29.38
		3	12	0.001	12.6	LN	1.2	3.97
Merox Flare (17543)	Flare	1	307	0.056	10.65	N	874.78	4.63
		2	15705	0.914	200.07	N	100.19	494.09
		3	1152	0.03	45.6	LN	0.001	6.63
Low Pressure Flare (17543)	Flare	1	200	0.011	9.37	LN	0.48	3.04
		2	16830	0.971	229.58	LN	0.05	3.23
		3	314	0.018	132.63	LN	0.52	3.46
General Service #1 (17543)	Flare	1	16892	0.964	155.47	N	1.66	21.45
		2	405	0.023	2	LN	0.38	3.26
		3	233	0.013	5.78	LN	0.43	3.47
General Service #2 (17543)	Flare	1	17322	0.67	508.65	N	1.31	17.8
		2	141	0.25	4	LN	0.08	3.05
		3	70	0.08	2.9	LN	0.7	3.26
Cooling Tower 1 (314)	Cooling Tower	1	243	0.779	5.72	LN	0.2	-2.69
		2	64	0.221	0.8	LN	0.3	-0.73
Cooling Tower 2 (340)	Cooling Tower	1	98	0.291	4.26	N	6.3	0.23
		2	148	0.439	2.61	N	0.39	0.67
		3	91	0.270	2.29	LN	0.68	0.28
Stacks/ Fugitives		1	NA	1	NA	LN	0.56	-0.15

4.2.3 Air quality modeling

The impact of industrial point source variability on ozone formation was assessed using the Comprehensive Air Quality Model with extensions (CAMx) (Environ, 2004). In this work, a computationally efficient version of CAMx, referred to as a sub-domain model, described in the previous chapter, was used. The overall strategy in developing the sub-domain model was to (1) identify a geographical region (sub-domain), from a full, 3-D photochemical model, (2) create a computationally efficient photochemical model of the sub-domain, and (3) analyze many scenarios or snapshots of variable emissions using the sub-domain model. Steps 1 and 2 in the development of the model are analogous to the methods used in the previous chapter and are only summarized here. Step 3 is described in the results section of this chapter.

The geographical region (sub-domain) to be modeled is the HG 1 km domain, shown as the region in red in Figure 4.9. CAMx simulations using the full domain, shown in Figure 4.9, were used to develop boundary and initial conditions for the sub-domain. Details of the meteorological modeling and the VOC and NO_x emission inventory development for simulation of the full domain are available from the TCEQ (2006) and are described in the previous chapter. Briefly, meteorological inputs were based on results from the NCAR/Penn State Mesoscale Meteorological Model version 5, MM5. Emission inventories were prepared by the Texas Commission on Environmental Quality (TCEQ). A MOBILE6-based inventory was developed for on-road mobile source emissions. Emissions for non-road mobile and area sources were developed using the U.S. EPA's NONROAD model, using local activity data when available. Biogenic emission inventories were estimated using the GLOBEIS emission model with locally developed land cover data. Point source emissions data were developed with TCEQ's

point source database and special inventory. Approximately 150 tons/day of reactive olefin species were added to approximately 100 point sources in the domain, based on ambient measurements made by aircraft (Ryerson et al., 2003). These point source inventory additions are commonly referred to as the imputed inventory, since the added emissions were estimated based on ambient measurements rather than reported inventories. The imputed point source inventory and the other components of the emission inventory, described above, were used as the base case in this work and will be collectively referred to as the imputed inventory. Both the sub-domain modeling and the full domain modeling in the region with industrial emissions were performed at a 1 km spatial resolution.

The full domain model was used to establish initial conditions and time varying boundary conditions for the sub-domain model. Calculations reported in the previous chapter indicate that the sub-domain model responds to temporal variability in industrial emissions in a manner that correlates ($r^2 > 0.96$) with the response of the full domain model.

The sub-domain model was run for two episode days: 25 August and 30 August, 2000. These two days were selected because there was rapid ozone formation on both days and distinctly different meteorological conditions on the two days had the potential to lead to different processes for ozone formation and accumulation. Details of the meteorological conditions on these two days have been described in the previous chapter.

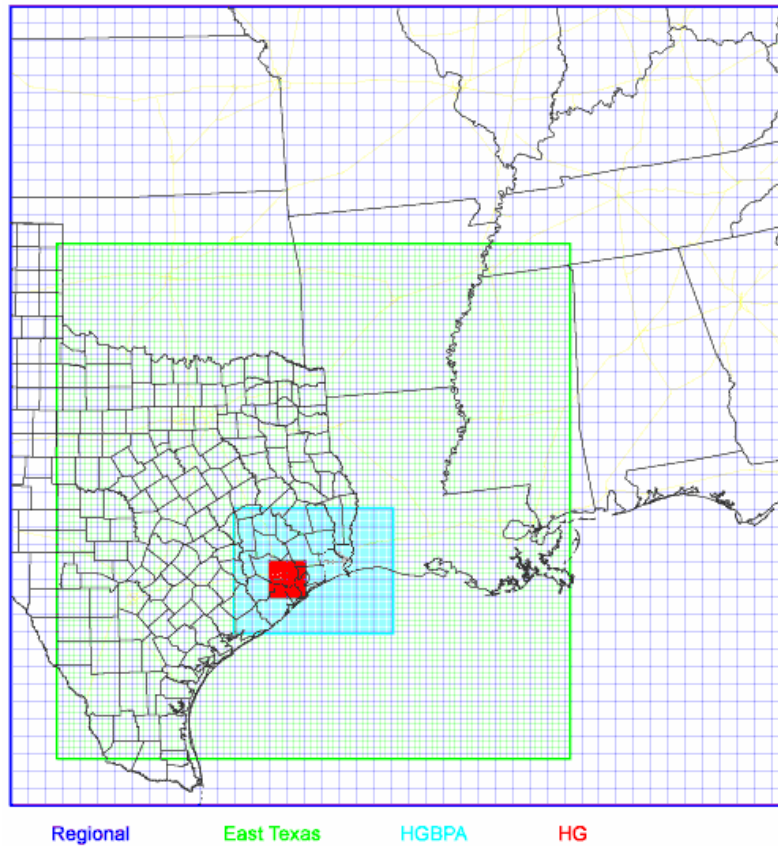


Figure 4.9 Modeling domain used in the study. The Regional, East Texas, Houston-Galveston-Beaumont-Port Arthur (HGBPA), and Houston Galveston (HG) nested domains had 36, 12, 4 and 1 km resolution, respectively.

4.3 Results and Discussion

The Results and Discussion will be presented in two parts. The first part summarizes the stochastic emission inventories; the second part describes the air quality modeling based on those inventories.

4.3.1 *Stochastic emission inventory*

Figure 4.10 shows probability distributions for 500 random realizations of one day's emissions (12,000 samples of hourly emissions), and numerical values of the mean, standard deviation, and selected percentiles are given in Table 4.2. The total VOC emissions from the industrial point sources show relatively little variation in any given hour (Figure 4.10a). This is a consequence of the Law of Large Numbers: the variance of a sum is significantly smaller than the variance of any individual component. Similarly, the sum of all hydrocarbon flares in Houston Galveston shows a relatively small variance. The mean of these distributions is virtually equal to the values from the deterministic emissions inventory.

As the area and the time period over which emissions are reported decrease, however, emission variability becomes more evident. The VOC emissions from two 1-km by 1-km grid cells near the Ship Channel, where significant VOC sources are concentrated, have 95% probability bounds that span more than a factor of two (Figure 4.10c; Table 4.2). A third grid cell near downtown Houston has 95% bounds that span a factor of 1.6. The three largest flares in the Houston Galveston region have 95% probability bounds that span factors of 9, 4, and 16, respectively (Table 4.2).

In addition to variability of any individual source, which can be quite large, it is important to explore other statistical properties of the combination of point sources. Figure 4.11 shows the probability, in any given hour, that at least N sources have emissions greater than or equal to a factor of 2, 5, or 10 times its annual average emissions, examining N over the range from 1 to 9. These probabilities were calculated by the UNC team. Only the 50 largest point sources, in terms of annual average emission rates, are considered. These sources comprise 20% of the total VOC emissions. For example, there is a 41% chance in any one hour that 8 or more of these large sources are emitting at greater than twice their average value. There is an 8.6% chance that at least 2 sources will emit more than five times their average in the same hour, and there is a 12% chance that in any hour, one of these sources will be emitting 10 times their average rate.

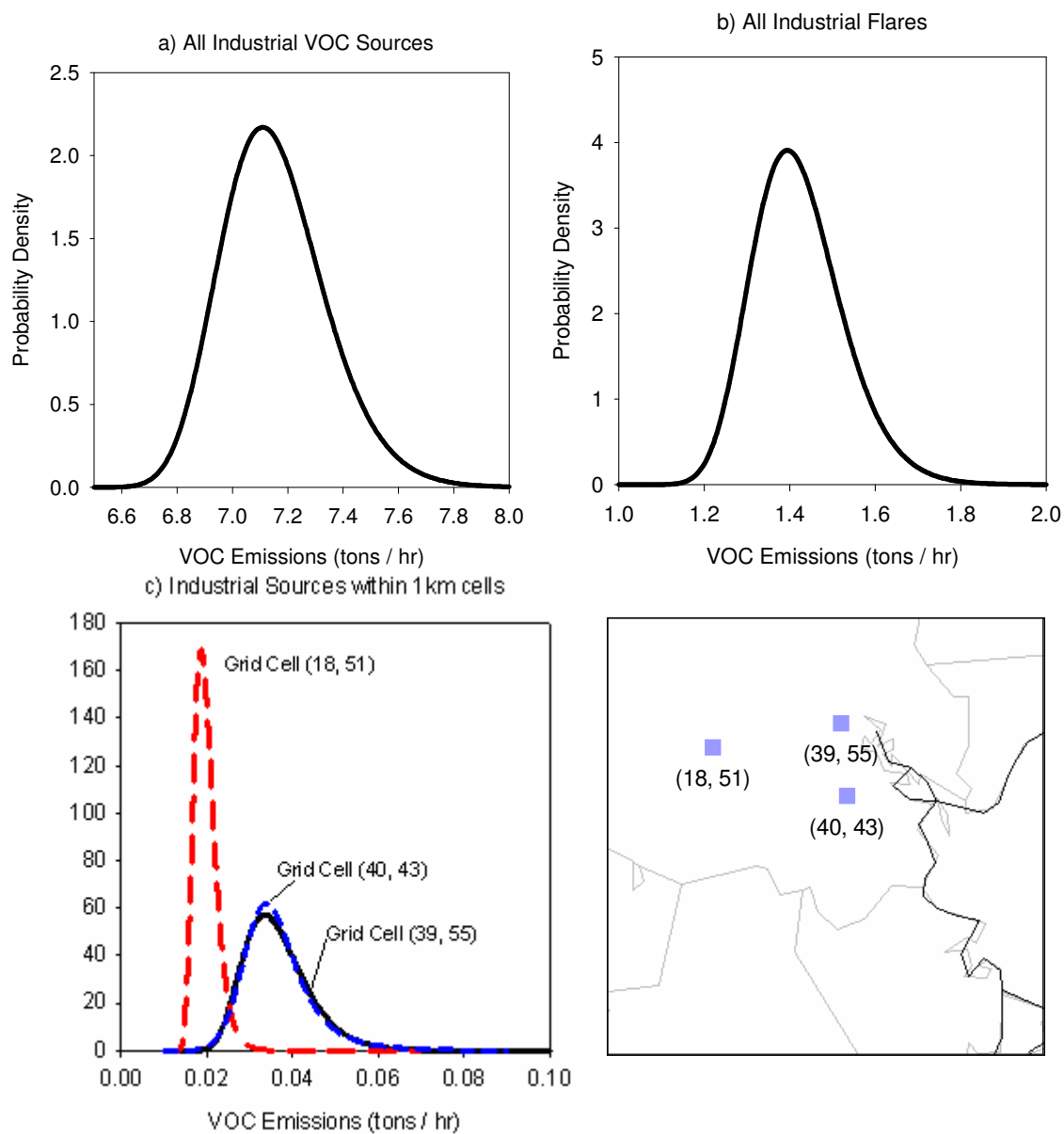


Figure 4.10 Variability of hourly VOC emission rates for a) all industrial point sources in the HG domain, b) all industrial flares in the HG domain, and c) for the industrial point sources within three 1 km² grid cells. The map shows the geographic locations of the three example grid cells.

Table 4.2 Mean, standard deviation, and selected facilities of point source VOC emissions (tons/hr) in Houston Galveston.

Percentile	All Sources ^a	All Flares	(18, 51)	(40, 43)	(39, 55)	3 Flares with Highest Avg Emi.		
0.01	6.77	1.21	0.015	0.023	0.023	0.043	0.049	0.005
0.025	6.83	1.24	0.016	0.024	0.024	0.052	0.061	0.010
0.05	6.87	1.27	0.016	0.026	0.026	0.062	0.077	0.023
0.25	7.02	1.35	0.018	0.031	0.031	0.107	0.096	0.056
0.5	7.14	1.41	0.019	0.035	0.035	0.156	0.101	0.069
0.75	7.27	1.48	0.021	0.041	0.041	0.229	0.106	0.083
0.95	7.48	1.61	0.024	0.051	0.051	0.391	0.216	0.131
0.975	7.57	1.66	0.026	0.055	0.055	0.469	0.249	0.157
0.99	7.69	1.73	0.028	0.061	0.060	0.558	0.283	0.202
mean	7.15	1.42	0.020	0.037	0.037	0.183	0.112	0.074
stdev	0.19	0.11	0.003	0.008	0.008	0.109	0.042	0.045

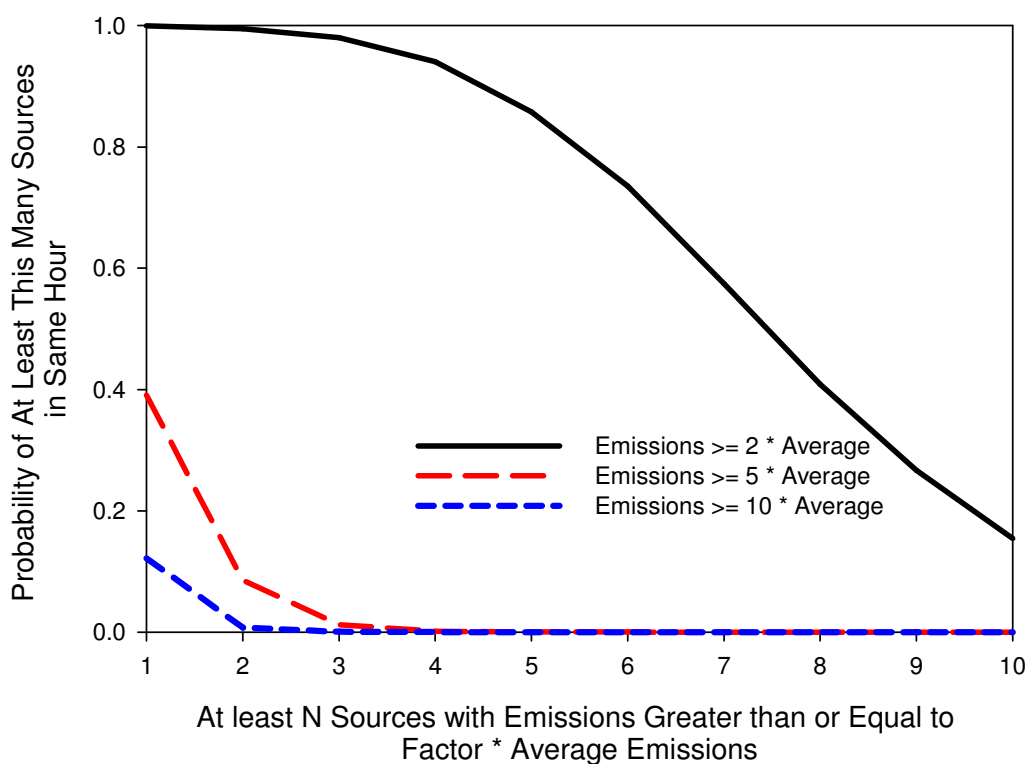


Figure 4.11 The probability that N or more point source emissions are a factor of 2, 5, and 10 times their annual average within the same hour.

4.3.2 Impacts of VOC emission variability on ozone formation

A total of 50 sets of stochastic emission inventories were generated with the models described in the Methods section and simulations representing 25 August and 30 August, 2000 were performed using these inventories, for a total of 100 simulations. Figure 4.12 shows the differences in ozone concentration on 25 August between using the 45th stochastic inventory and the deterministic imputed inventory. The 45th stochastic inventory showed the largest increase in ozone concentration for the August 25 meteorology, as shown in Figure 4.13. Since the stochastic inventory has both higher and lower VOC emissions across the HG area over the course of the day, ozone concentrations using the stochastic inventory are both higher and lower than using the imputed inventory without VOC emission variability depending on time of day and location. At conditions that lead to maximum difference in ozone concentration, ozone concentrations predicted using the stochastic inventory are approximately 82 ppb higher than using the imputed inventory without variable VOC emissions. Ozone concentrations are also up to 6 ppb lower using stochastic inventory than using the imputed inventory with constant industrial emissions.

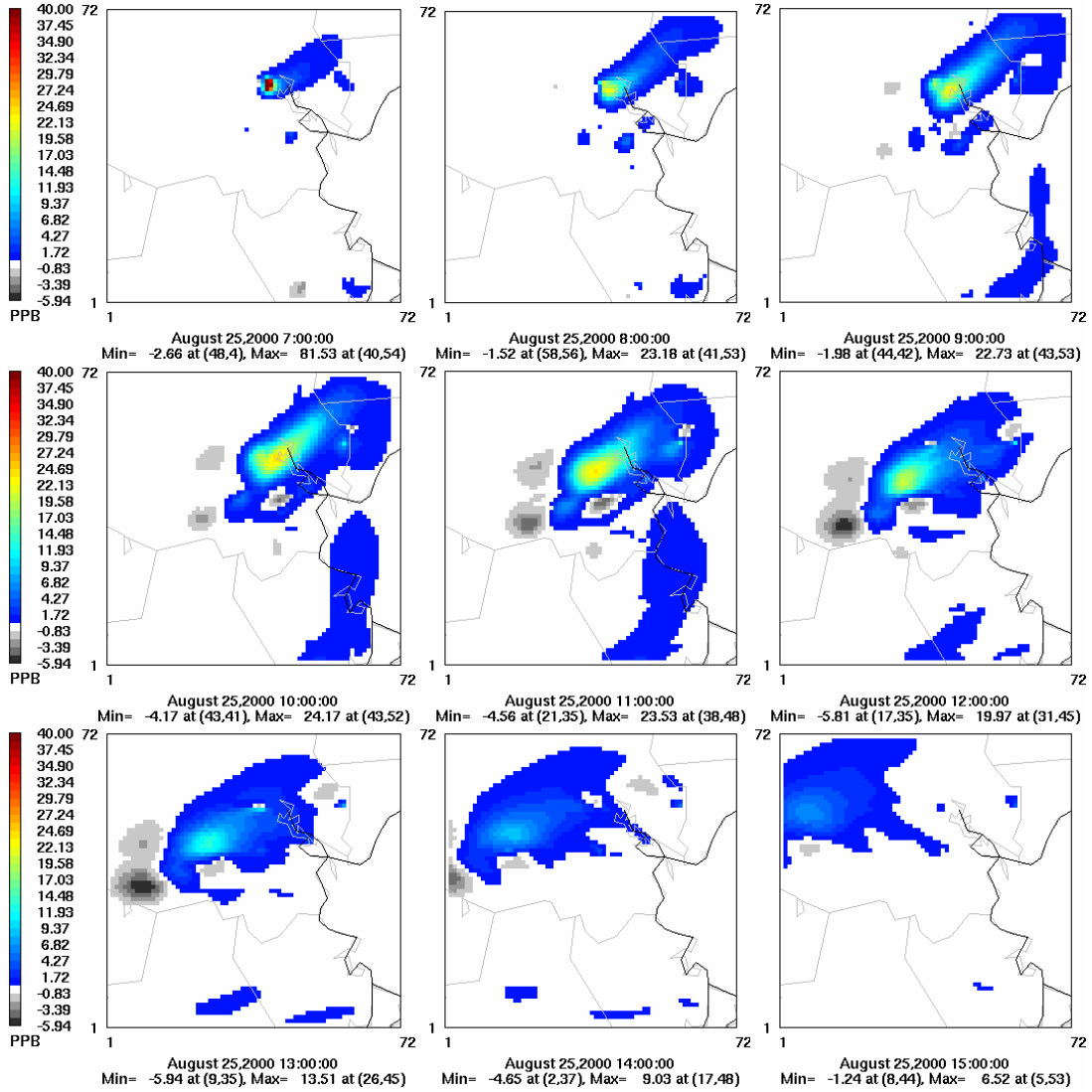


Figure 4.12 Difference in ozone concentration for 25 August from 700 hr to 1500 hr between using the 45th stochastic imputed emission inventory and using the deterministic imputed inventory.

Figure 4.13 summarizes the maximum changes in ozone concentrations that were observed, both positive and negative, when all 50 stochastic emission inventories were used for simulations on 25 August and 30 August, 2000. Specifically, the quantity presented is the maximum difference in ozone concentration between using the stochastic inventory and the deterministic inventory. On the top and bottom of each column, the ozone concentration for the stochastic inventory, at the time when the maximum difference occurred, is indicated in ppb. In the simulations of 25 August, the maximum difference in ozone concentration is largest when the 45th stochastic emission inventory was used; the ozone concentrations are 24 ppb and 106 ppb when the imputed and the stochastic inventory were used, respectively, at conditions that lead to the maximum increase in ozone concentration. In the simulations of 30 August, the largest maximum difference in ozone concentration occurred when the 7th stochastic inventory was used; a 64 ppb decrease in ozone concentration relative to the imputed inventory without variable VOC emissions was predicted. The probability distributions of maximum difference in ozone concentration for both days are shown in Figure 4.14. The maximum increase in ozone concentration at any hour and location from including the variability in VOC point-source emissions has 90% bounds (an interval within which 90% of the area falls under the curve in Figure 4.14) of 11-52 ppb for the August 25 meteorology and 8-22 ppb for the August 30 meteorology.

Simulations of the two episode days exhibit different responses of ozone formation due to variable VOC emissions. For example, the 45th stochastic inventory led to a maximum difference in ozone concentration of 82 ppb in a grid cell which is the 40th to the east and the 54th to the north from the southwest corner of the region in red, shown in Figure 4.12, at 7am 25 August. At the same time of day and location on 30 August,

the ozone concentration was not affected by variable VOC emissions. Distinctly different meteorological conditions on the two days led to these different behaviors of ozone formation for the same stochastic emission inventory.

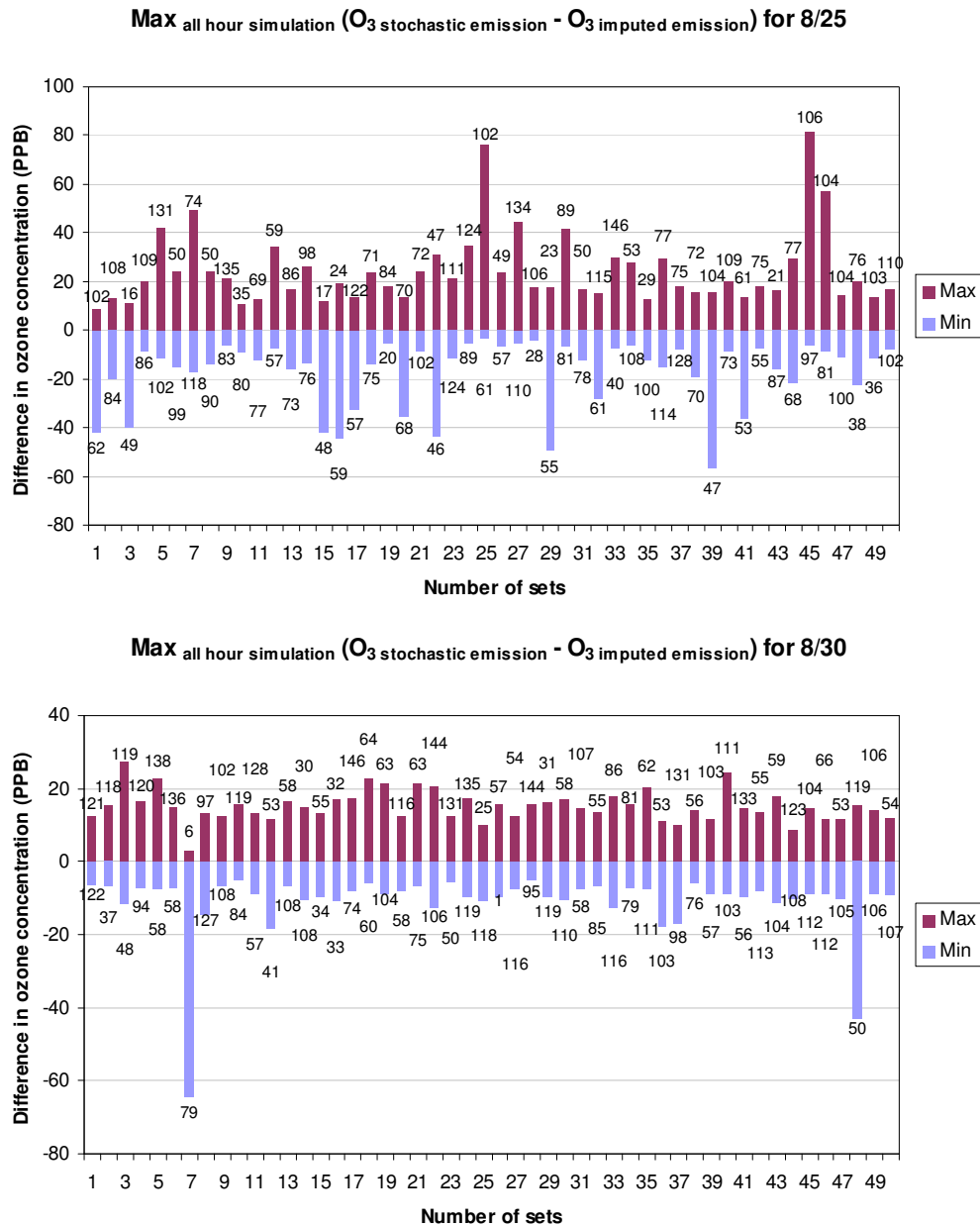


Figure 4.13 Maximum difference in ozone concentrations in one day simulations representing 25 August and 30 August, 2000. The difference is taken between the imputed inventory with constant industrial emissions and the stochastic inventory for 50 instances of the stochastic inventory. Ozone concentrations (ppb), using the stochastic inventory, at the time the maximum difference was observed are indicated on the top and bottom of each column.

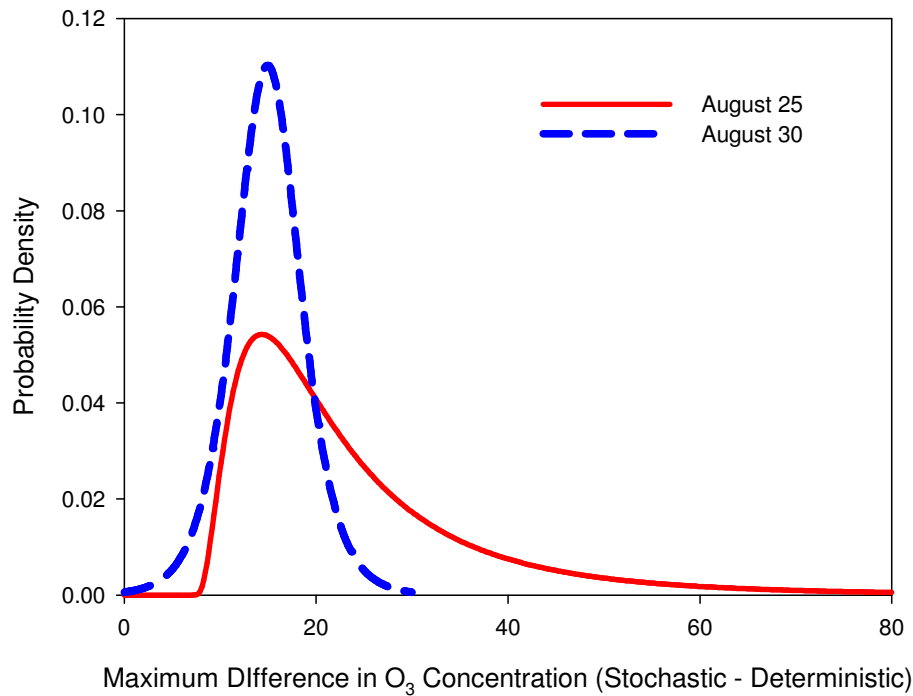


Figure 4.14 Probability distributions of maximum difference in ozone concentrations in one day simulations representing 25 August and 30 August, 2000.

This change in ozone concentration did not always increase the peak ozone concentration in the 1-km domain over the course of the day. For example, on 25 August the daily maximum ozone concentration using the stochastic inventory is up to 11.9 ppb higher and up to 6 ppb lower than when the non-stochastic imputed inventory was used, depending on the stochastic inventory used. The average and standard deviations for the increases and decreases in the sub-domain wide daily maximum ozone concentrations were 3.3 ± 2.9 and 2.4 ± 1.7 , respectively. These results can be contrasted with a maximum increase of 82 ppb and a maximum decrease of 56 ppb, shown in Figure 4.13, and average increases and decreases of 24 ± 15 and 17 ± 14 , respectively. A total of 31 out of

the 50 sets of stochastic inventories led to increases in daily maximum ozone concentration in the sub-domain. For 30 August, the daily maximum ozone concentration increased for 36 sets of stochastic inventories. The maximum increase in the peak ozone concentration in the 1-km domain was approximately 10.7 ppb and maximum decrease was approximately 4.5 ppb. The average and standard deviations for the increases and decreases in the sub-domain wide daily maximum ozone concentrations were 3.3 ± 2.6 and 1.4 ± 1.2 , respectively.

In summary, variability in continuous industrial VOC emissions has the potential to have a significant impact on ozone formation in the Houston-Galveston area. Increases and decreases of 20-50 ppb or more in ozone concentration are possible as a result of emission variability. The largest of these differences are restricted to regions of 10-20 km² (see Figure 4.12), but the variability also has the potential to increase region wide maxima in ozone concentrations by to 7-12 ppb.

These results raise important questions about effective ozone control strategies for ozone in the Houston Galveston region, and perhaps other regions with significant petrochemical industrial facilities such as Baton Rouge or New Jersey. If some of the high ozone episodes are the result of less frequent higher than average emission rates, rather than the mean emissions, control strategies that lower the annual average may prove ineffective at reducing ozone exceedances. Further, strategies that target the upper tails of the distribution may have very different, perhaps lower, compliance costs than traditional approaches. This is an important area for future inquiry and, therefore, described in the next chapter.

4.4 References

Cornell, J., 2002. *Experiments with mixtures: designs, models, and the analysis of mixture data*. Wiley, New York.

Environ International Corporation (Environ), 2004. User's Guide: Comprehensive Air Quality Model with Extensions (CAMx), Version 4.03, Document and model are available online at <http://www.camx.com>

Environ International Corporation (Environ), 2006. Comprehensive Air Quality Model with Extensions (CAMx) Pre-processors, Accessed January 2006 at <http://www.camx.com/download/support.php>

Kleinman, L.I., Daum, P.H., Imre, D., Lee, Y.N., Nunnermacker, L.J., Springston, S.R., Weinstein-Lloyd, J., Rudolph, J., 2002. Correction to "Ozone production rate and hydrocarbon reactivity in 5 urban areas: A cause of high ozone concentration in Houston". *Geophys. Res. Lett.* 30 (12), 1639.

Murphy, C.F., Allen, D.T., 2005. Hydrocarbon emissions from industrial release events in the Houston- Galveston area and their impact on ozone formation. *Atmospheric Environment* 39 (21), 3785-3798.

Ryerson, T.B., Trainer, M., Angevine, W.M., Brock, C.A., Dissly, R.W., Fehsenfeld, F.C., Frost, G.J., Goldan, P.D., Holloway, J.S., Hubler, G., Jakoubek, R.O., Kuster, W.C., Neuman, J.A., Nicks, D.K., Parrish, D.D., Roberts, J.M., Sueper, D.T., Atlas, E.L., Donnelly, S.G., Flocke, F., Fried, A., Potter, W.T., Schauffler, S., Stroud, V., Weinheimer, A.J., Wert, B.P., Wiedinmyer, C., Alvarez, R.J., Banta, R.M., Darby, L.S., Senff, C.J., 2003. Effect of petrochemical industrial emissions of reactive alkenes and NO_x on tropospheric ozone formation in Houston, Texas. *J. Geophys. Res.* 108 (D8), 4249.

Texas Commission on Environmental Quality (TCEQ), 2006. Houston-Galveston-Brazoria Ozone SIP Mid-Course Review Modeling, Accessed January 2006 at <http://www.tceq.state.tx.us/implementation/air/airmod/data/hgb1.html>

University of North Carolina, 2004. Stochastic Emission Inventories of Continuous Emissions. Houston Advanced Research Center, H13.2003 Final Report Appendix B, available at <http://files.harc.edu/Projects/AirQuality/Projects/H013.2003/H13AppendixB.pdf>

Vizuete, W., 2005. Implementation of Process Analysis in a three dimensional air quality model, PhD thesis, University of Texas.

CHAPTER 5

The effectiveness of control of industrial emission variability for ozone in Houston, Texas

5.1 Introduction

The Houston/Galveston (HG) area has been classified as nonattainment by the National Ambient Air Quality Standards (NAAQS) for ground-level ozone with concentrations averaged over 1 hour and 8 hours. Meeting the ozone standard is especially challenging for the HG area due to unique ozone formation chemistry as well as complex meteorological conditions, induced by the land/sea/bay effects. Ozone formation in the HG area is frequently faster and more efficient, with respect to NO_x consumed, than other urban areas with high ozone events. It is believed that these unique characteristics of ozone formation in the HG area are associated with plumes of reactive hydrocarbons, emanating from the industrial Houston Ship Channel area (Kleinman et al., 2003; Ryerson et al., 2003). Therefore, understanding industrial emissions, particularly of reactive hydrocarbons, is critical in the development of control measures for mitigation of high ozone concentrations in the area.

Industrial emissions of hydrocarbons have traditionally been assumed to be continuous at constant levels for air quality regulation and photochemical modeling purposes. However, ambient observations and industrial process data have shown that industrial emissions of hydrocarbons have significant temporal variability (Murphy and Allen, 2005; Vizuete, 2005). Variability in industrial emissions of hydrocarbons can be ascribed to both the occurrence of episodic emission events and variable continuous

emissions. The episodic emission events are non-routine discrete emission events, of more than permitted amounts, with reporting required under Texas law. Episodic events occur relatively infrequently; an emission event of more than 1000 kg occurs, on average, a few times a week somewhere among the hundreds of facilities in the Houston area. Variable continuous emissions are not as significant in magnitude as an emission event, but occur at all times at all facilities, and therefore also have the potential to increase the magnitude of ozone concentration in the area.

Murphy and Allen (2005) have investigated characteristics of emission events in the HG area with a focus on highly reactive volatile organic compounds (HRVOCs; defined in Texas air quality regulation as ethylene, propylene, isomers of butene and 1,3-butadiene); characteristics of emission events examined include event magnitude, composition, duration and source types. Vizuete (2005) investigated physical and chemical processes of ozone formation and accumulation in the HG area during a small number of large emission events. Chapter 3 describes development of computationally efficient photochemical models and the impact of emission events on ozone formation in the HG area using a stochastic characterization of emission events described by Murphy and Allen (2005).

The effect of variability in continuous emissions from industrial sources on ozone formation in the HG area was described in the previous chapter using the computationally efficient version of photochemical models described in Chapter 3. As indicated in the previous chapter, multiple components of variability in routine hydrocarbon emission exist for each individual source and, therefore, variability in industrial emissions can be simulated with statistical mixture models, multiple models each accounting for one of the components. Physical causes of these different

components of emission variability are not fully understood, but efforts are being made to identify the causes and reduce the variability in industrial emissions of hydrocarbons (BAAQMD, 2005; BAAQMD, 2006).

Flares are one focus of efforts to reduce variable industrial emissions. For example, Flare Minimization Plans (FMPs) have been prepared by petroleum refineries in the San Francisco Bay Region. The Bay Area Air Quality Management District (BAAQMD) required petroleum refineries with one or more flares to submit a FMP including a detailed process description, previous and planned reduction and prevention measures for large flaring events (BAAQMD, 2006). Significant variability in mass flow rates to a flare, leading to flaring of vent gas, is due to start-ups, shutdowns, and other maintenance related events. Refineries in the BAAQMD have reduced both the frequency of large emission events and the annual magnitude of flared gases. Reductions in large flaring events have been accomplished largely through changes in operating practices, particularly during start-up, shut-down and scheduled maintenance of process units. Annual magnitudes of flared gases have been increased by increasing the capacity of flaring systems to recompress gases for use in refinery fuel systems. The changes in operating practices generally involve relatively modest capital expenditures, while the changes in capacity for compressing potentially flared gases involve large capital costs.

This chapter will use these two flare reduction scenarios as examples of alternative strategies for reducing ozone concentrations due to variable industrial emissions. One type of control strategy involves reducing large magnitude events, and an alternative strategy involves reducing continuous, and relatively constant, emissions. Control strategies for ground-level ozone have been focused on reducing annual average emissions of ozone precursors, and photochemical modeling of emission control

strategies has generally assumed constant emissions from industrial sources (non-electricity generating units). However, as evidenced by various measurements and the modeling studies described in the previous chapters, industrial emissions of hydrocarbons have significant temporal variability and the variability can have a variety of effects on ozone formation in Houston. Variable emissions result in a distribution of ozone concentrations, both above and below the ozone concentrations that would be expected with constant industrial emissions. In this chapter, alternative control strategies for ozone, consistent with FMPs, will be applied to emissions in Houston and the effects on the expected distributions of ozone concentrations in the region will be examined.

5.2 Methods

5.2.1 The stochastic emission inventory for the HG area

The previous chapter indicated that industrial emissions of VOC have significant temporal variability and the variability is composed of multiple components in magnitude, including nearly constant, routinely variable, allowable episodic, and emission events (Figure 5.1). For this chapter, as in the previous chapter, emission events above permitted levels were excluded from analysis. In order to simulate a whole emission or emission surrogate (e.g., mass flow rates to flares), probability distribution functions (PDF) for each component of emission variability were identified. For a total of 12 sets of observations collected from various flares and cooling towers in the HG area, the models to simulate emission variability, referred to as the stochastic emission inventory generator, were developed (Table 5.1). Individual sources in the HG area were

randomly assigned one of the unit operation models by source type (flare, cooling tower, stack, or fugitive) and emission inventories with overall time-varying emissions were constructed for the HG area. For emission sources other than flares, all emissions except VOCs were kept intact throughout the simulation. For flares, both VOC and NO_x emissions were assumed to scale with flow rate having the same pattern of variability. Details on the development of the stochastic emission inventory generator and application of the stochastic inventory to the HG area are described in the previous chapter.

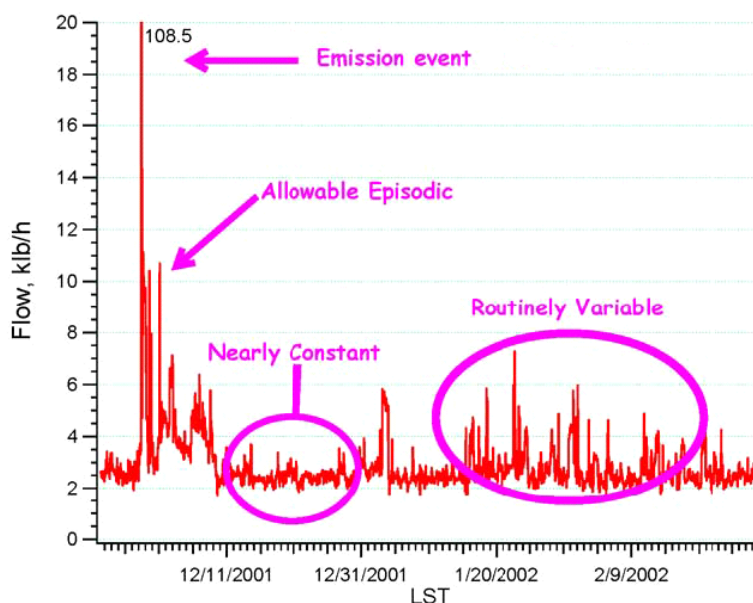


Figure 5.1 Components of mass flow rates to a flare at an industrial facility in the HG area: nearly constant, routinely variable, allowable episodic, and emission event in order of magnitude.

For this study, the stochastic emission inventory generator has been updated (Webster, 2007). The original version of the stochastic emission inventory generator, described in the previous chapter, randomly selects emission mode (from nearly constant, routinely variable, and allowable episodic modes), duration in the mode and, then, emission rates based on the emission mode and duration selected in the previous steps; emission modes, durations in each mode, and emission rates were selected based on PDFs of observations. The revised version of the stochastic inventory generator uses the transition matrix shown in Table 5.1, to determine probability of transition from current mode to the next mode for every time step. This method is based on the assumption of Markov chain. A Markov chain is a series of states of a system in which the conditional probability distribution of a future state is dependent on the current state. This is a reasonable assumption for a model of a continuous industrial process. In the transition matrix the row index (i) represents the current mode and the column index (j) represents the next mode; the entries in the matrix represents the probability of transition from current mode (i) to the next mode (j), P_{ij} . For example, for Flare 1 shown in Table 5.1, probabilities of transition from current mode 1 to modes 1, 2, and 3, in the next time step, are 0.883, 0.115, and 0.001, respectively. This simplified algorithm allows the model to be readily adapted to model control strategies that eliminate one or more modes. For example, modeling the elimination of allowable episodic emissions only requires that the probability of the system initially being in that mode be set to zero and that the probability of transition to that mode be set equal to zero.

In addition, the revised version of the stochastic inventory generator shifts the distributions for lognormal components of the models. Lognormal distributions are, in general, positively skewed; they have their peak likelihood at relatively small values and

have long tails in the probability distribution at higher values. However, we are modeling the emission rates, often starting at a much higher emission rates for some components of emission variability than for other components of emission variability. For example, allowable episodic emissions in Figure 5.1 were defined as mass flow rates greater than 6.4 kilo-lb/h and less than 34.7 kilo-lb/h, while routinely variable emission in Figure 5.1 were defined as mass flow rates between 2.8 kilo-lb/h and 6.4 kilo-lb/h. While the models for each component were designed to simulate emission rates with the two discrete ranges, probabilities of emission rates, areas under the two probability density curves, have emission rate values in common in the range of routinely variable emissions, particularly when lognormal distributions were used. Therefore, lognormal distributions were shifted to larger emission rates, reducing this region of overlap; specifically, the shift value was added to all values in the distributions. Figure 5.2 shows probability distribution functions (PDFs) for each component of emissions from the flare in Figure 5.1 in the original version and the revised version of the stochastic inventory generator. Similarly, all models with lognormal distributions shown in Table 5.1 shifted the emissions by the shift values (in units of kilo-lb/h) to better approximate the distribution of observations. Figure 5.3 shows mass flow rates to the flare in Figure 5.1 simulated with the original version and the revised version of the stochastic inventory generator and observed mass flow rates to this flare. This updated version of stochastic emission inventory generator was used for the study in this chapter.

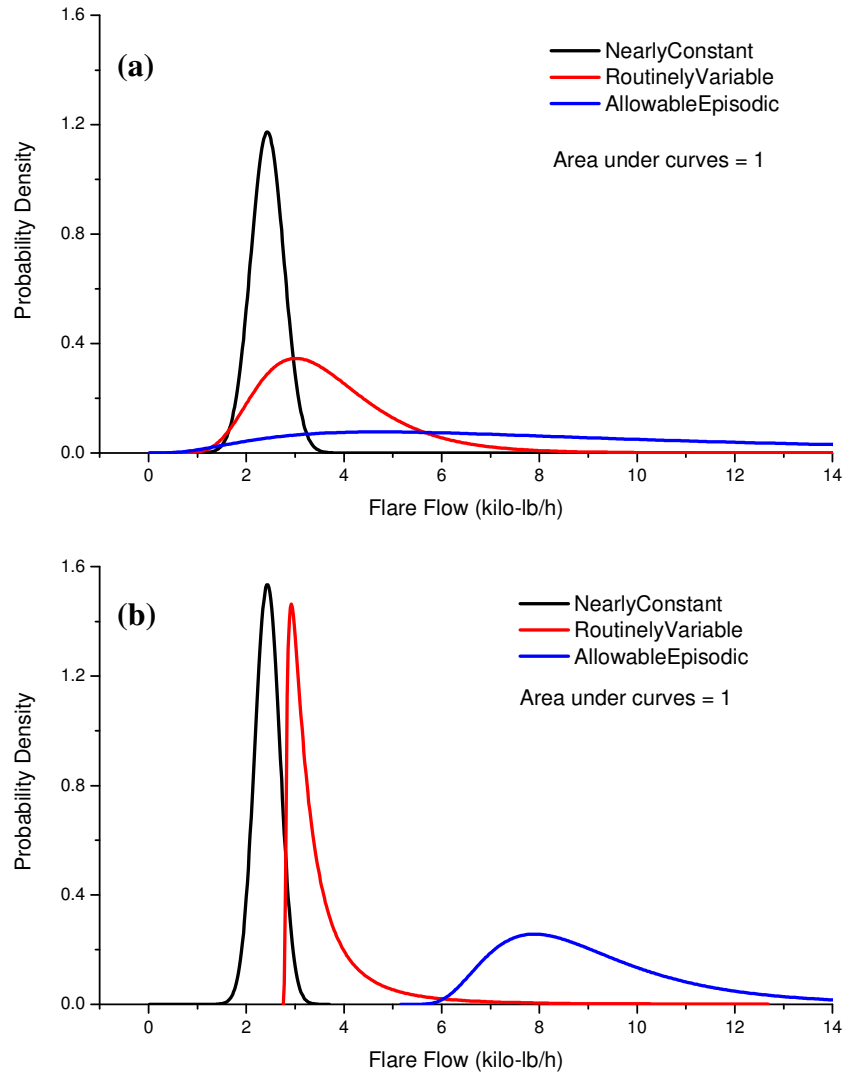


Figure 5.2 PDFs for each component of emissions from the flare in Figure 5.1 in (a) the original version of the stochastic inventory generator (Webster et al., 2007) and (b) the updated version of the stochastic inventory generator

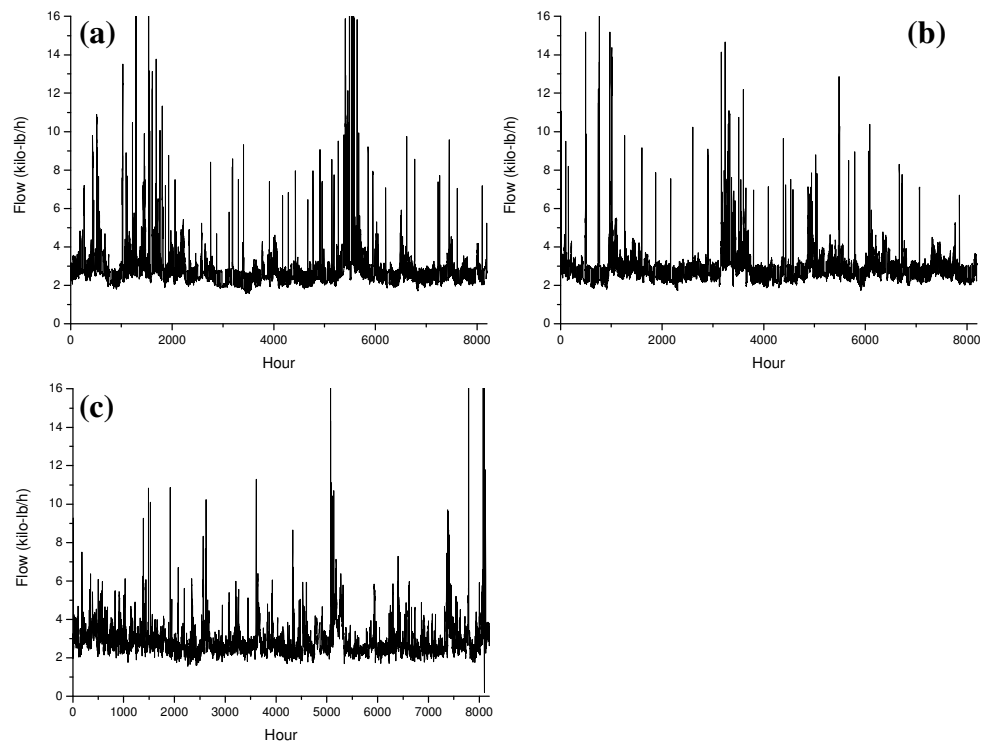


Figure 5.3 (a) Time series of flare flow in Figure 5.1 simulated with original version of the stochastic inventory generator. (b) Time series of flare flow in Figure 5.1 simulated with the revised version of the stochastic inventory generator. (c) Time series of actual flare flow.

Table 5.1 Parameters used to develop base case stochastic emissions

Source Name (Type)	Component	Normal or Lognormal	Mean or Mean (LN Value)	Standard deviation	Normalized proportion	Transition Matrix			Shift	Expected value
Flare1 (FL)	1	N	2.43	0.26	0.603	0.883	0.115	0.001	0	2.43
	2	LN	-0.798	1.05	0.389	0.179	0.813	0.008	2.76	3.54
	3	LN	1.26	0.5	0.008	0.085	0.38	0.535	5.14	9.13
Flare2 (FL)	1	N	1.97	0.64	0.544	0.798	0.196	0.005	0	1.97
	2	LN	0.54	0.97	0.426	0.252	0.729	0.02	2.81	5.56
	3	LN	-0.75	1.65	0.029	0.048	0.333	0.619	11	12.84
Flare5 (FL)	1	LN	6.8	0.305	0.7632	0.951	0.022	0.027	42.64	983.22
	2	N	2017	114.8	0.061	0.29	0.557	0.154	0	2017
	3	LN	5.98	0.72	0.1758	0.113	0.058	0.829	2153.2	2665.6
FCCU (FL)	1	N	21.1	3.01	0.9063	0.997	0.002	0.001	0	21.10
	2	N	33.67	2.14	0.0719	0.032	0.958	0.01	0	33.67
	3	LN	0.95	0.69	0.0217	0.003	0.058	0.939	37.56	40.84
General Service1 (FL)	1	N	21.4	1.51	0.9462	0.99	0.009	0.001	0	21.40
	2	LN	-0.572	1.44	0.0402	0.218	0.762	0.02	23.99	25.58
	3	LN	0.404	1.41	0.0135	0.046	0.068	0.886	28.85	32.90
General Service2 (FL)	1	N	17.08	0.94	0.67	0.97	0.027	0.003	0	17.08
	2	N	19.18	0.16	0.25	0.072	0.869	0.059	0	19.18
	3	LN	-1.61	1.48	0.08	0.022	0.186	0.792	19.48	20.08
HCF (FL)	1	N	2.41	0.62	0.974	0.989	0.011		0	2.41
	2	LN	-0.3	0.64	0.026	0.426	0.574		4.01	4.92
Low Pressure (FL)	1	N	24.64	0.918	0.6918	0.988	0.012	0	0	24.64
	2	LN	0.158	0.712	0.298	0.027	0.972	0.001	25.78	27.29
	3	LN	0.079	0.558	0.0102	0.011	0.039	0.95	34.76	36.02
Merox (FL)	1	N	31.9	16.23	0.056	0.896	0.091	0.012	0	31.90
	2	N	500.4	89.45	0.914	0.006	0.991	0.003	0	500.4
	3	LN	4.891	0.242	0.03	0.019	0.082	0.899	622.5	759.5
Olefins Flare (FL)	1	N	1.67	0.41	0.661	0.973	0.027	0	0	1.67
	2	LN	0.98	0.51	0.327	0.053	0.944	0.003	2.34	5.37
	3	LN	0.38	1.02	0.012	0.045	0.045	0.909	16.88	19.34
Cooling Tower1 (CT)	1	N	0.07	0.029	0.656	0.746	0.19	0.063	0	0.07
	2	LN	-2.778	1.023	0.194	0.623	0.295	0.082	0.13	0.24
	3	LN	-1.811	0.945	0.15	0.298	0.085	0.617	0.39	0.65
Cooling Tower2 (CT)	1	N	0.23	0.077	0.29	0.835	0.155	0.01	0	0.23
	2	N	0.67	0.131	0.438	0.095	0.73	0.176	0	0.67
	3	LN	-1.013	0.963	0.272	0.022	0.272	0.707	0.86	1.44
STs/FUs	1	LN	-0.15	0.56	1	NA				1.01

5.2.2 Control strategies associated with variability in industrial emissions

As described in the previous section of this chapter, nationwide, efforts are being made to estimate and reduce the variability in industrial emissions of hydrocarbons. The Bay Area Air Quality Management District (BAAQMD) enacted a flare monitoring rule (2005) and a flare minimization rule (2006) to characterize emission variability from flares and to reduce the significant variability in hydrocarbon emissions from flares, respectively. The Texas Commissions on Environmental Quality (TCEQ) has recognized a link between episodic emissions of the type associated with flaring and rapid increases in ozone concentration by enacting a new short-term limit on HRVOC emissions. In order to characterize the magnitude of air quality improvements that might be expected from these programs, photochemical modeling of a variety of flare emission scenarios was performed.

In order to understand how flare emissions can be minimized, it is useful to have a conceptual understanding of how a typical industrial flare system works. In many industrial operations, a flare serves multiple process units. The flare collects these multiple inputs through a collection system, or plenum, that is maintained at low pressure so that the plenum will always be at a lower pressure than the process units that it serves. Many systems that are designed to flare material with fuel value (e.g., refinery gases) are served by a compressor. If the flow to the flare is less than the capacity of the compressor, refinery gases that are sent to the flare system are recompressed and recycled to a process unit that uses refinery gas as fuel. If the flow is larger than can be handled by the compressor, then the refinery gas is flared. This refinery flare system is shown conceptually in Figure 5.4.

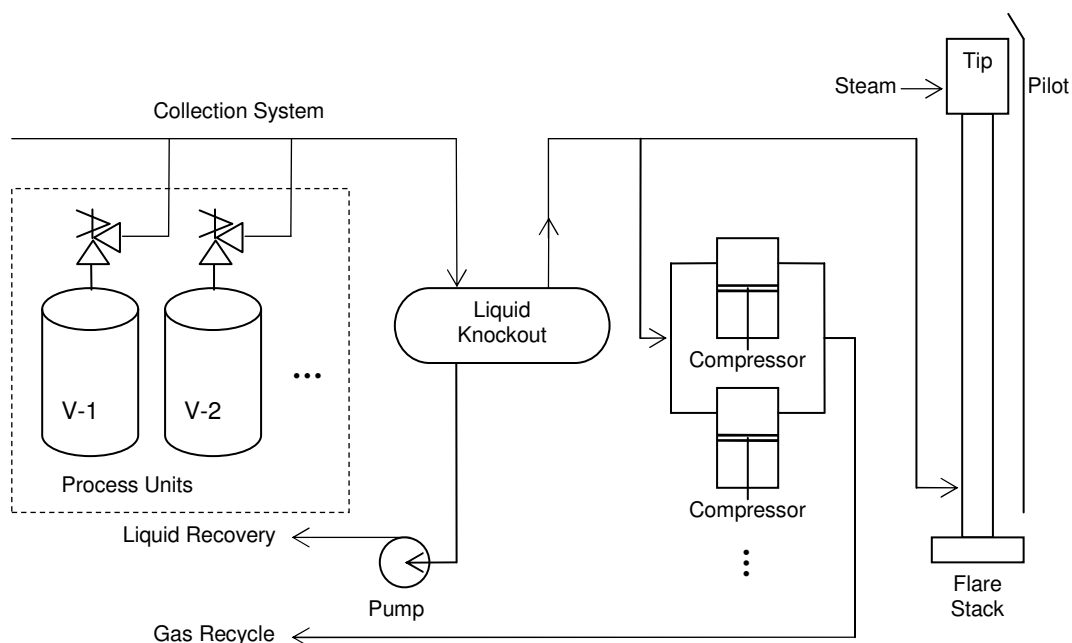


Figure 5.4 Conceptual diagram for a typical refinery flare system (Shell Oil Products US, 2006)

With this conceptual model of flare systems in mind, two options for reducing flare emissions are (1) to add temporary storage for flared gases, so that if the flow rate to the flare goes above the capacity of the compressor, the gases can be temporarily stored, and (2) to add additional compressor capacity to a flare system.

In general, adding storage capacity for flared gases is an expensive control option, however, temporary storage is sometimes available during start-up, shut-down and maintenance activities. A flare minimization scenario that has been reported in Flare Minimization Plans by petroleum refineries is to use process vessels that are temporarily empty during start-up, shut-down and scheduled maintenance as temporary storage for gases that would otherwise be flared during these events. This requires careful

management of the scheduling of operations during start-ups, shut-downs and maintenance activities, but it can reduce what are often large flaring events.

Adding additional compressor capacity to a flare system can also be expensive, if the compressor only recovers fuel during relatively rare emission events. However, if compressor capacity can be added to capture and recycle nearly constant flare emissions, it becomes more cost effective.

Based on these ideas, two approaches were evaluated for reducing flare emissions. The first approach is to control the large magnitude, infrequent emissions from flares (allowable episodic mode). This corresponds to eliminating large flaring events during start-up, shut-down and maintenance activities. In modeling this approach, the allowable episodic emissions for all of the flares in the HG area were assumed to be eliminated. For this task, the stochastic inventory generator was modified to reflect this control approach as shown in Table 5.2 and the stochastic inventory generated from this modified model was used to investigate the impacts on ozone formation of this emission control approach.

Table 5.2 Parameters used to develop stochastic emissions with allowable episodic emissions from flares eliminated.

Source Name (Type)	Component	Normal or Lognormal	Mean or Mean (LN Value)	Standard deviation	Normalized proportion	Transition Matrix			Shift	Expected value
Flare1 (FL)	1	N	2.43	0.26	0.608	0.884	0.115		0	2.43
	2	LN	-0.798	1.05	0.392	0.179	0.821		2.76	3.54
Flare2 (FL)	1	N	1.97	0.64	0.561	0.803	0.196		0	1.97
	2	LN	0.54	0.97	0.439	0.252	0.749		2.81	5.56
Flare5 (FL)	1	LN	6.8	0.305	0.926	0.978	0.022		42.64	983.2
	2	N	2017	114.8	0.074	0.29	0.711		0	2017
FCCU (FL)	1	N	21.1	3.01	0.926	0.998	0.002		0	21.1
	2	N	33.67	2.14	0.074	0.032	0.968		0	33.67
GeneralService1 (FL)	1	N	21.4	1.51	0.959	0.991	0.009		0	21.4
	2	LN	-0.572	1.44	0.041	0.218	0.782		23.99	25.58
GeneralService2 (FL)	1	N	17.08	0.94	0.728	0.973	0.027		0	17.08
	2	N	19.18	0.16	0.272	0.072	0.928		0	19.18
HCFlare (FL)	1	N	2.41	0.62	1	0			0	2.41
LowPressure (FL)	1	N	24.64	0.918	0.699	0.988	0.012		0	24.64
	2	LN	0.158	0.712	0.301	0.027	0.973		25.78	27.20
Merox (FL)	1	N	31.9	16.23	0.058	0.908	0.091		0	31.9
	2	N	500.4	89.45	0.942	0.006	0.994		0	500.4
OlefinsFlare (FL)	1	N	1.67	0.41	0.669	0.973	0.027		0	1.67
	2	LN	0.98	0.51	0.331	0.053	0.947		2.34	5.37
CoolingTower1 (CT)	1	N	0.07	0.029	0.656	0.746	0.191	0.063	0	0.07
	2	LN	-2.778	1.023	0.194	0.623	0.295	0.082	0.13	0.24
	3	LN	-1.811	0.945	0.15	0.298	0.085	0.617		
CoolingTower2 (CT)	1	N	0.23	0.077	0.29	0.835	0.155	0.1	0	0.23
	2	N	0.67	0.131	0.438	0.095	0.73	0.176	0	0.67
	3	LN	-1.013	0.963	0.272	0.022	0.272	0.707		
Stacks/Fugitives	1	LN	-0.15	0.56	1	NA			0	1.0068

A second approach for reducing flare emissions is to add more compressor capacity to capture more nearly constant emissions. This approach was modeled by assuming that the nearly constant component of mass flows to all flares in the HG area was reduced by 50% in magnitude. The stochastic inventory generator modified for this task is shown in Table 5.3. To accomplish this, the expected values of the models for nearly constant emissions were reduced by 50%, keeping the shape of the model distributions intact. The expected value for a normal distribution is its mean. Therefore, for models with normal distributions, all nearly constant emission models, except Flare 5 in Table 5.1, means were reduced by 50%. For example, the mean for the nearly constant emission model for Flare 1 in Table 5.1 were reduced from 2.43 to 1.22 as shown in Table 5.3. However, expected values for lognormal distributions are a function of both mean and standard deviation (Expected value = $e^{\mu + \frac{\sigma^2}{2}}$), and the shapes of lognormal distributions are determined by both mean and standard deviation (Variance = $(e^{\sigma^2} - 1)e^{2\mu + \sigma^2}$). Therefore, the only way to reduce expected value of lognormal distributions without changing the shape of the distributions is to move the distributions to the left by reducing shift value of the model. For nearly constant component of Flare 5 in Table 5.3, shift value was reduced so that expected value will be 50% of the original expected value shown in Table 5.1; when the distribution was moved to the left by -449 lbs h⁻¹, the expected value for the distribution was reduced 50%, to 491.6 lbs h⁻¹.

Table 5.3 Parameters used to develop stochastic emissions with nearly constant emissions from flares reduced.

Source Name (Type)	Component	Normal or Lognormal	Mean or Mean (LN Value)	Standard deviation	Normalized proportion	Transition Matrix			Shift	Expected value
Flare1 (FL)	1	N	1.22	0.26	0.603	0.883	0.115	0.001	0	1.22
	2	LN	-0.798	1.05	0.389	0.179	0.813	0.008	2.76	3.54
	3	LN	1.26	0.5	0.008	0.085	0.38	0.535	5.14	9.13
Flare2 (FL)	1	N	0.99	0.64	0.544	0.798	0.196	0.005	0	0.99
	2	LN	0.54	0.97	0.426	0.252	0.729	0.02	2.81	5.56
	3	LN	-0.75	1.65	0.029	0.048	0.333	0.619	11	12.84
Flare5 (FL)	1	LN	6.8	0.305	0.7632	0.951	0.022	0.027	-449	491.61
	2	N	2017	114.8	0.061	0.29	0.557	0.154	0	2017
	3	LN	5.98	0.72	0.1758	0.113	0.058	0.829	2153.2	2665.6
FCCU (FL)	1	N	10.6	3.01	0.9063	0.997	0.002	0.001	0	10.6
	2	N	33.67	2.14	0.0719	0.032	0.958	0.01	0	33.67
	3	LN	0.95	0.69	0.0217	0.003	0.058	0.939	37.56	40.84
General Service1 (FL)	1	N	10.7	1.51	0.9462	0.99	0.009	0.001	0	10.7
	2	LN	-0.572	1.44	0.0402	0.218	0.762	0.02	23.99	25.58
	3	LN	0.404	1.41	0.0135	0.046	0.068	0.886	28.85	32.90
General Service2 (FL)	1	N	8.54	0.94	0.67	0.97	0.027	0.003	0	8.54
	2	N	19.18	0.16	0.25	0.072	0.869	0.059	0	19.18
	3	LN	-1.61	1.48	0.08	0.022	0.186	0.792	19.48	20.08
HCF (FL)	1	N	1.21	0.62	0.974	0.989	0.011		0	1.21
	2	LN	-0.3	0.64	0.026	0.426	0.574		4.01	4.92
Low Pressure (FL)	1	N	12.32	0.918	0.6918	0.988	0.012	0	0	12.32
	2	LN	0.158	0.712	0.298	0.027	0.972	0.001	25.78	27.29
	3	LN	0.079	0.558	0.0102	0.011	0.039	0.95	34.76	36.02
Merox (FL)	1	N	16.0	16.23	0.056	0.896	0.091	0.012	0	16.0
	2	N	500.4	89.45	0.914	0.006	0.991	0.003	0	500.4
	3	LN	4.891	0.242	0.03	0.019	0.082	0.899	622.5	759.5
Olefins Flare (FL)	1	N	0.84	0.41	0.661	0.973	0.027	0	0	0.84
	2	LN	0.98	0.51	0.327	0.053	0.944	0.003	2.34	5.37
	3	LN	0.38	1.02	0.012	0.045	0.045	0.909	16.88	19.34
Cooling Tower1 (CT)	1	N	0.07	0.029	0.656	0.746	0.19	0.063	0	0.07
	2	LN	-2.778	1.023	0.194	0.623	0.295	0.082	0.13	0.24
	3	LN	-1.811	0.945	0.15	0.298	0.085	0.617	0.39	0.65
Cooling Tower2 (CT)	1	N	0.23	0.077	0.29	0.835	0.155	0.01	0	0.23
	2	N	0.67	0.131	0.438	0.095	0.73	0.176	0	0.67
	3	LN	-1.013	0.963	0.272	0.022	0.272	0.707	0.86	1.44
STs/FUs	1	LN	-0.15	0.56	1	NA				1.01

5.2.3 *Air quality modeling*

The effectiveness of the control strategies, described in the previous sub-section of this chapter, was assessed using the Comprehensive Air Quality Model with extensions (CAMx) (Environ, 2004). In this work, a computationally efficient version of CAMx, referred to as a sub-domain model and described in Chapter 3, was used. The overall strategy in developing the sub-domain model was to (1) identify a geographical region (sub-domain) from a full, 3-D photochemical model simulation, (2) create a computationally efficient photochemical model of the sub-domain, and (3) analyze many scenarios of variable emissions using the sub-domain model. Steps 1 and 2 in the development of the model are analogous to the methods used in Chapter 3 and Chapter 4 and are only summarized here. Step 3 is described in the results section of this chapter.

The geographical region (sub-domain) to be modeled is the HG 1 km domain, shown as the region in red in Figure 5.5. CAMx simulations using the full domain, shown in Figure 5.5, were used to develop boundary and initial conditions for the sub-domain. Details of the meteorological modeling and the VOC and NO_x emission inventory development for simulation of the full domain are available from the TCEQ (2006) and are described in Chapter 3. Briefly, meteorological inputs were based on results from the NCAR/Penn State Mesoscale Meteorological Model version 5, MM5. Emission inventories were prepared by the Texas Commission on Environmental Quality (TCEQ). A MOBILE6-based inventory was developed for on-road mobile source emissions. Emissions for non-road mobile and area sources were developed using the U.S. EPA's NONROAD model, using local activity data when available. Biogenic emission inventories were estimated using the GLOBEIS emission model with locally developed land cover data. Point source emissions data were developed with TCEQ's

point source database and special inventory. Approximately 150 tons/day of reactive olefin species were added to approximately 100 point sources in the domain, based on ambient measurements made by aircraft (Ryerson et al., 2003). These point source inventory additions are commonly referred to as the imputed inventory, since the added emissions were estimated based on ambient measurements rather than reported inventories. The imputed point source inventory and the other components of the emission inventory, described above, were used as the base case in this work and will be collectively referred to as the deterministic inventory. Both the sub-domain modeling and the full domain modeling in the region with industrial emissions were performed at a 1 km spatial resolution.

The full domain model was used to establish initial conditions and time varying boundary conditions for the sub-domain model. Calculations reported in Chapter 3 indicate that the sub-domain model responds to temporal variability in industrial emissions in a manner that correlates ($r^2 > 0.96$) with the response of the full domain model.

The sub-domain model was run for 25 August, 2000. This date was selected because there was rapid ozone formation on this date and it shows one of the typical meteorological conditions induced by land/sea/bay effects that lead to high ozone concentrations. Details of the meteorological conditions on this date have been described in Chapter 3.

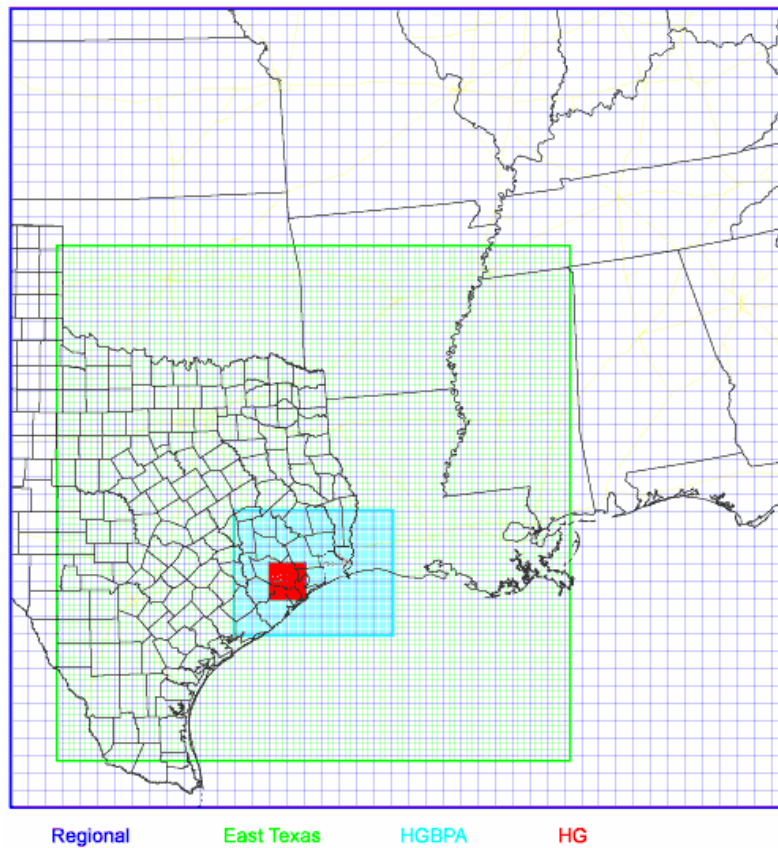


Figure 5.5 Modeling domain used in the study. The Regional, East Texas, Houston-Galveston-Beaumont-Port Arthur (HGBPA), and Houston Galveston (HG) nested domains had 36, 12, 4 and 1 km resolution, respectively.

5.3 Results and Discussion

The Results and Discussion will be presented in two parts. The first part describes the effectiveness of control of allowable episodic component of flare emissions and the second part describes the effectiveness of control of the nearly constant component of flare emissions.

5.3.1 *Control of allowable episodic emissions*

A total of 100 sets of stochastic emission inventories were generated with the models shown in Tables 5.1 and 5.2; 50 sets of inventories for simulation of emission variability without any emission control and 50 sets of inventories for simulation of emission variability with elimination of the allowable episodic emissions. Figure 5.6 shows the difference in ozone concentration between using the 19th stochastic inventory, generated with the models shown in Table 5.1, and using the deterministic inventory. The 19th stochastic inventory led to the largest increase in ozone concentration, as shown in Figure 5.8a. Since the stochastic inventory has both higher and lower VOC emissions across the HG area over the course of the day, ozone concentrations predicted using the stochastic inventory are both higher and lower than using the deterministic inventory without VOC emission variability depending on time of day and location. At conditions that lead to maximum difference in ozone concentration, ozone concentrations predicted using the stochastic inventory are approximately 57 ppb higher than using the deterministic inventory without variable VOC emissions. Ozone concentrations are also up to 7 ppb lower using the stochastic inventory than using the deterministic inventory with constant industrial emissions.

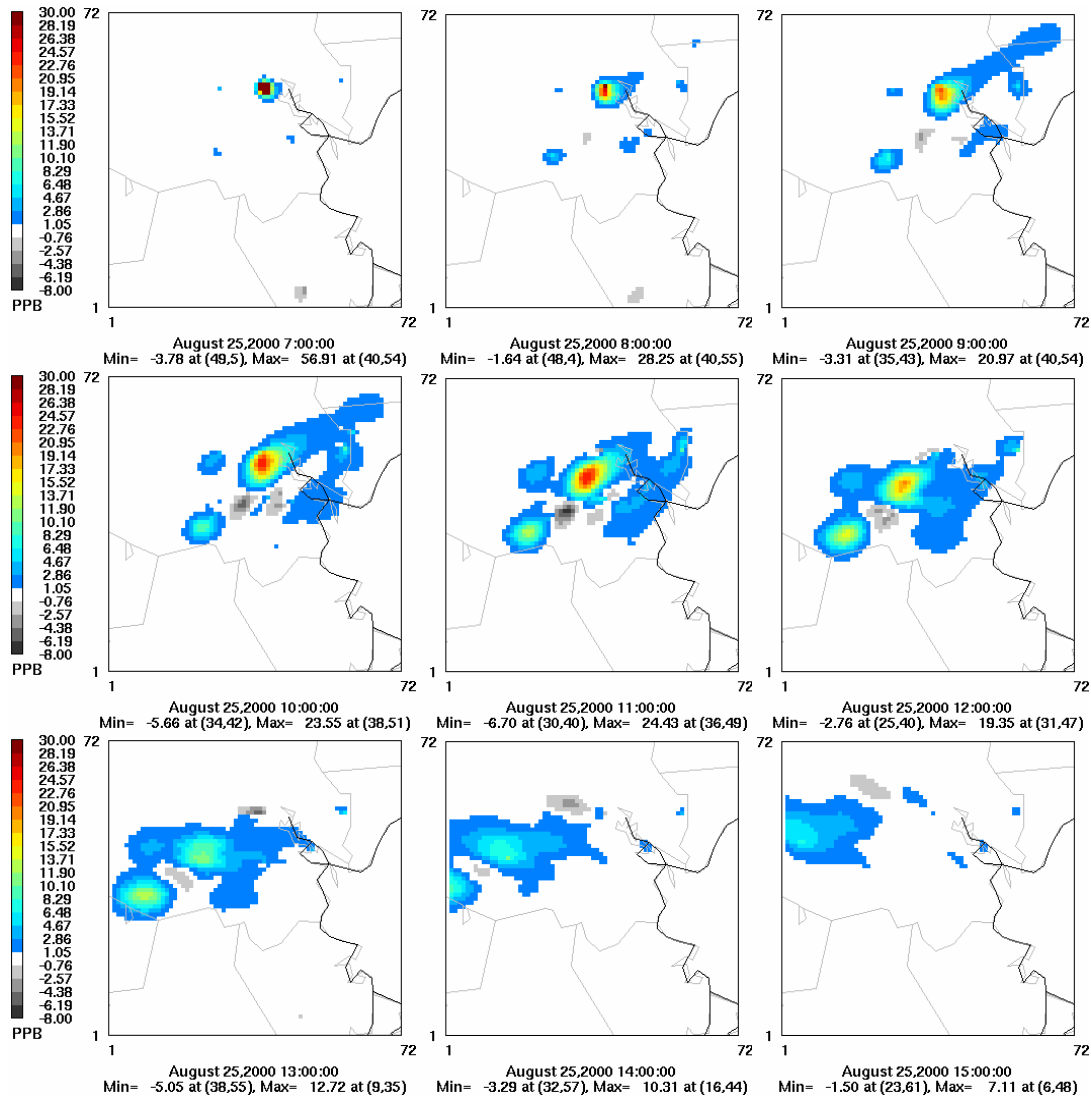


Figure 5.6 Difference in ozone concentrations for 25 August from 700hr to 1500hr between predictions based on the 19th stochastic inventory generated using the models shown in Table 5.1 and predictions based on the deterministic inventory.

This result and those summarized in Figure 5.8a are analogous to the results shown in the previous chapter (Figures 4.12 to 4.14) except that for this chapter the updated version of stochastic inventory generator was used as described in the previous section of this chapter. The difference in maximum ozone concentrations between the two approaches are, on average, about 1.3%; averages of maximum difference (between the stochastic and deterministic inventories) are 24.5 ppb and 24.8 ppb for the results shown in the previous chapter and the results shown in Figure 5.8a, respectively. Their difference in mean was tested using student's t-test and the results indicate that their mean differences are not significantly different; t was calculated as 0.115, which is below the tabled t value, 1.96, at 95% confidence levels, thereby failing to reject null hypothesis, $\mu_1=\mu_2$ (Sokal, et al., 1987). Their coefficient of variance is 0.626 and 0.519 for the results shown in the previous chapter and those in Figure 5.8a, respectively.

Figures 5.7 and 5.8b show the results similar to that shown in Figures 5.6 and 5.8a, however, in this case, the allowable episodic flare emissions were eliminated. Figure 5.7 shows the difference in predicted ozone concentrations on 25 August between using the 10th stochastic inventory, generated with the models that reflect elimination of allowable episodic emissions, and using the deterministic inventory. The 10th stochastic inventory is the inventory that led to the largest increase in ozone concentration, as shown in Figure 5.8b. Compared to the results shown in Figure 5.6, ozone concentration was increased in smaller areas and decreased in larger areas due to emission variability. In addition, the magnitude of increase in ozone concentration was smaller and the magnitude of decrease was larger.

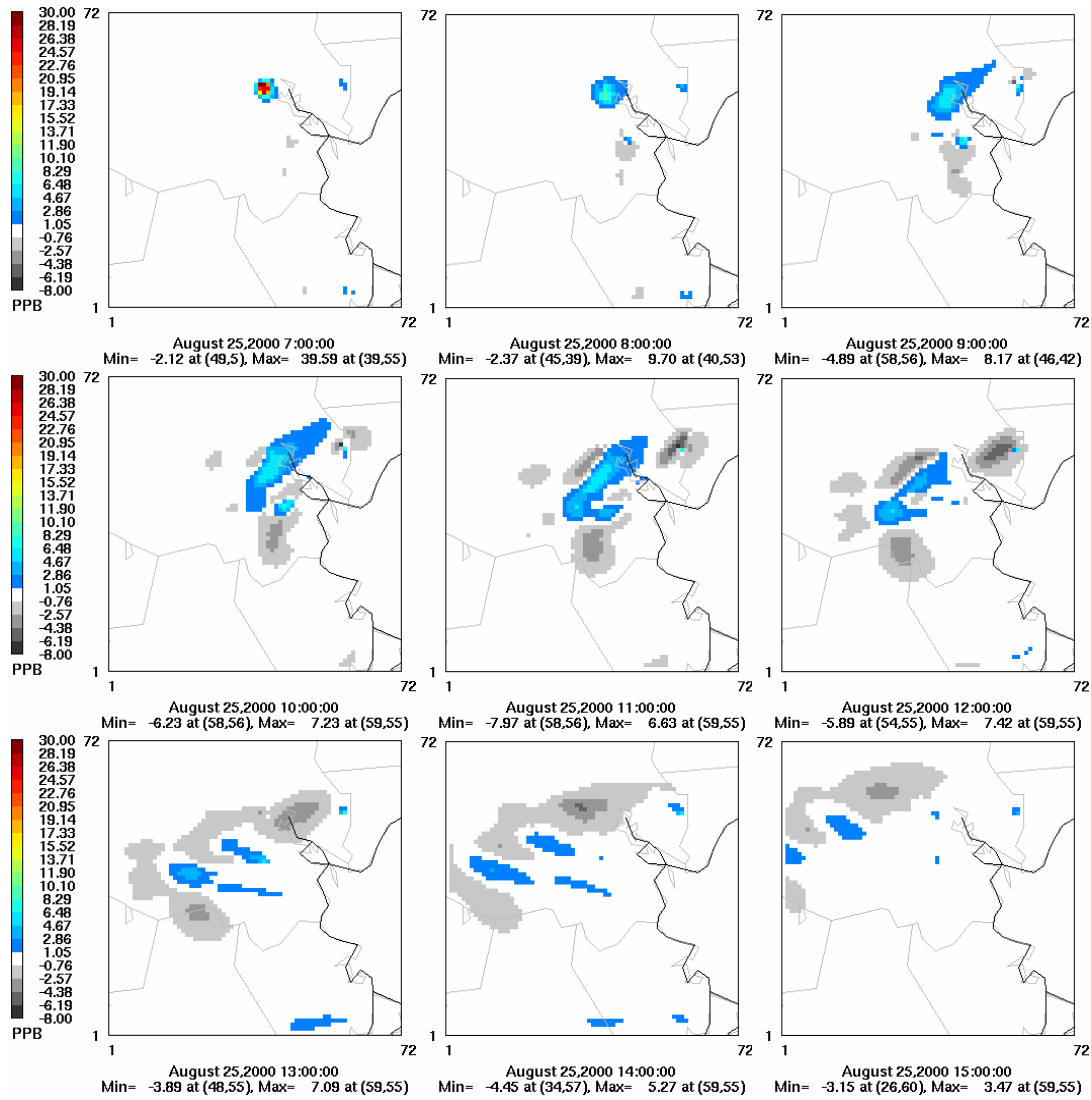


Figure 5.7 Difference in ozone concentration for 25 August from 700hr to 1500hr between predictions based on the 10th stochastic inventory generated using the models shown in Table 5.2 and predictions based on the deterministic inventory. Ozone concentrations are scaled to the results shown in Figure 5.6.

Figure 5.8 summarizes the maximum changes in ozone concentrations, both positive and negative, when all 100 sets of stochastic emission inventories were used for air quality simulations. Specifically, the quantity presented is the maximum difference in ozone concentration over the course of the day between using the stochastic inventory and the deterministic inventory. In the simulation of ozone without any emission control, the maximum difference in ozone concentration is largest when the 19th stochastic inventory was used; the ozone concentrations are 24.5 ppb and 81.4 ppb when the deterministic and the stochastic inventory were used, respectively, at conditions that lead to the maximum increase in ozone concentration. In the simulations of ozone with elimination of allowable episodic emissions, the largest maximum difference in ozone concentration occurred when the 43rd stochastic inventory was used; a 56 ppb decrease in ozone concentration relative to using the deterministic inventory without variable VOC emissions was predicted. The probability distributions of maximum difference in ozone concentration, both positive and negative, are shown in Figure 5.9. The distribution of maximum increases in ozone concentration, shown in Figure 5.9a, has shorter tail to the right for case when allowable episodic emissions are eliminated.

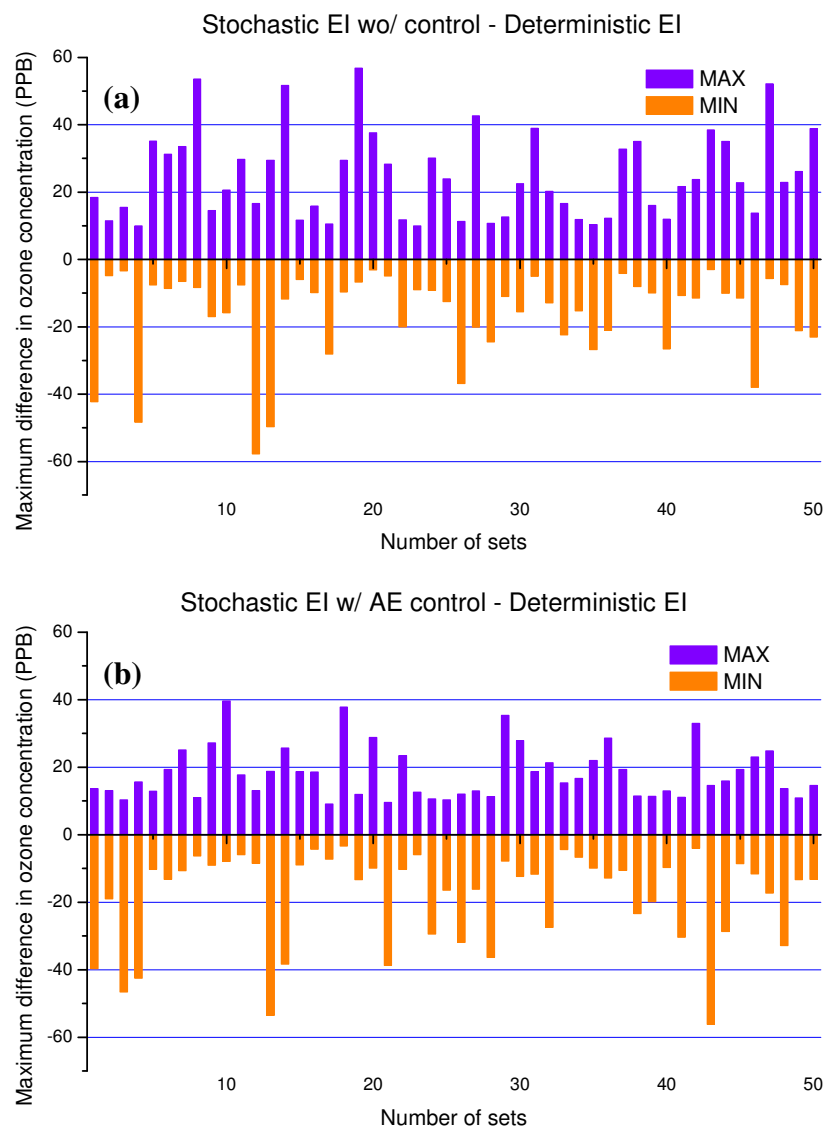


Figure 5.8 Maximum difference in ozone concentration in one day simulations representing 25 August, 2000. The difference is taken between the deterministic inventory with constant industrial emissions and the stochastic inventory for 50 instances of the stochastic inventory with allowable episodic emission control (a) and without the control (b).

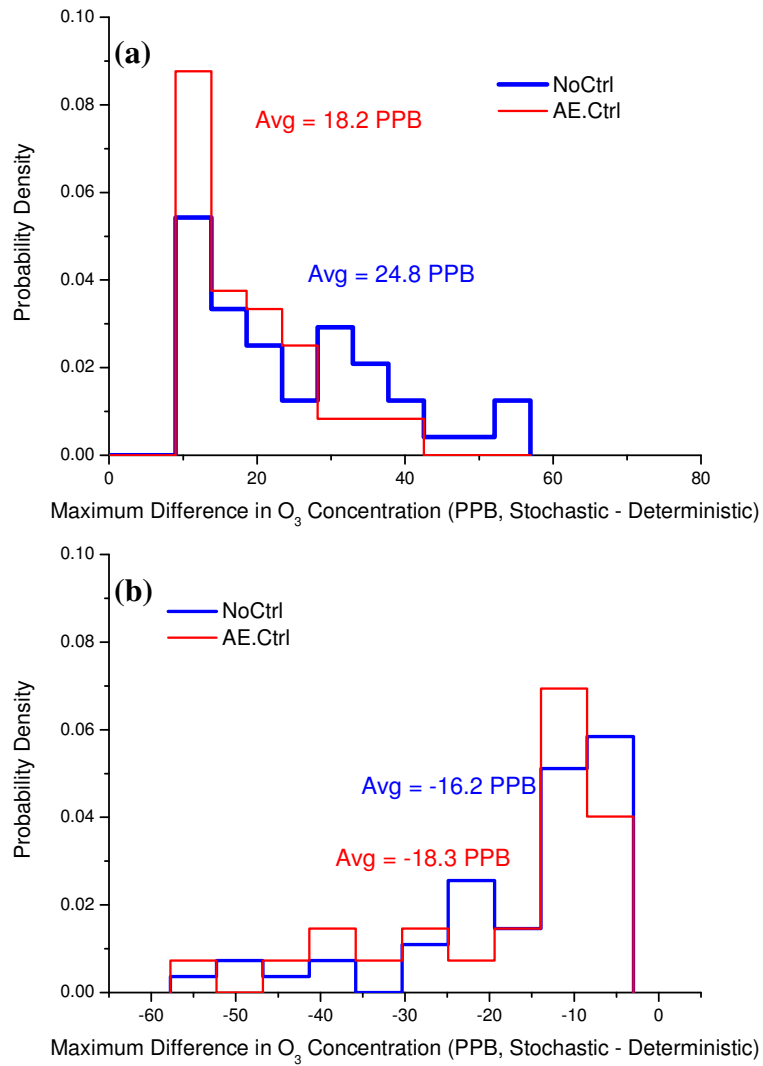


Figure 5.9 Probability distribution of maximum changes in ozone concentration in simulations representing 25 August, 2000 due to variable continuous emissions with allowable episodic emission control (red line) and without the control (blue line) in positive direction (a) and negative direction (b).

Figure 5.10 shows that these changes in ozone concentrations did not always increase or decrease the peak ozone concentration in the 1-km domain over the course of the day. For example, for stochastic inventories without any emission control the daily maximum ozone concentration using the stochastic inventory is up to 5.9 ppb higher and up to 6.7 ppb lower than when the deterministic inventory was used, depending on the stochastic inventory used. The average of daily maximum ozone concentration using the 50 sets of stochastic inventories is 200.9 ppb, compared to a maximum ozone concentration of 200.6 ppb for the deterministic inventory. A total of 28 out of the 50 sets of stochastic inventories led to increases in daily maximum ozone concentration in the sub-domain. For stochastic inventories with allowable episodic emissions eliminated, the daily maximum ozone concentration increased for 20 sets of stochastic inventories, compared to the deterministic inventory. The maximum increase in the peak ozone concentration in the 1-km domain was approximately 3.4 ppb and maximum decrease was approximately 7.3 ppb. Average of daily maximum ozone concentration was 199.4 ppb, approximately 1.5 ppb decrease from average of daily maxima without any emission control.

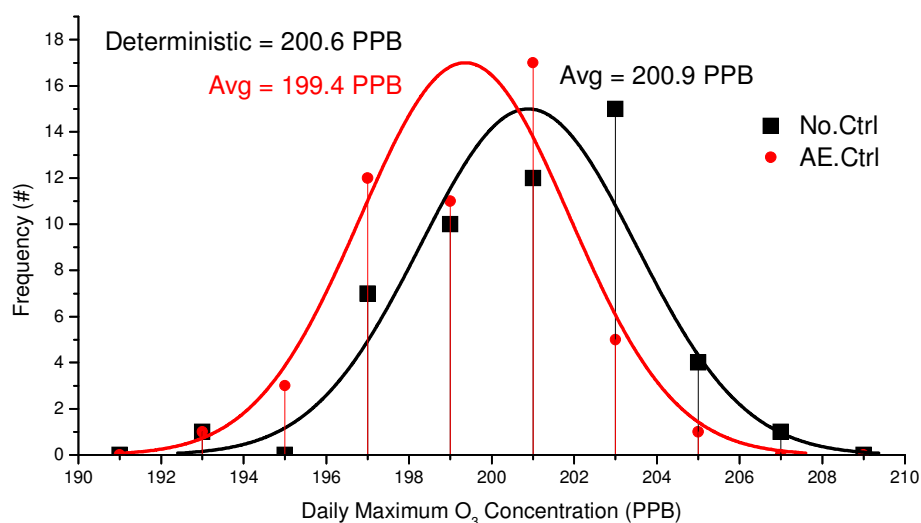


Figure 5.10 Histograms of daily maximum ozone concentration across the HG 1-km domain for no control cases (black) and allowable episodic emission control cases (red).

For comparison purposes, another control scheme was devised so that the same magnitude of reduction in total flare emissions occurred across the domain as when allowable episodic emissions are eliminated, but those reductions are applied to the deterministic inventory. This results in 2.1% and 4.3%, reductions in NO_x and VOC emissions, respectively. Figure 5.11 shows difference in ozone concentration between using the reduced deterministic inventory and using the deterministic inventory. Changes in ozone concentration due to the overall reduction are not significant compared to the results shown in Figures 5.7 and 5.8b. Maximum difference in ozone concentration was approximately 1.4 ppb. Daily maximum ozone concentration was decreased by just 0.1 ppb due to the overall reduction. This reduction in daily maximum ozone is smaller than that due to allowable episodic emission control, as shown in Figure 5.10.

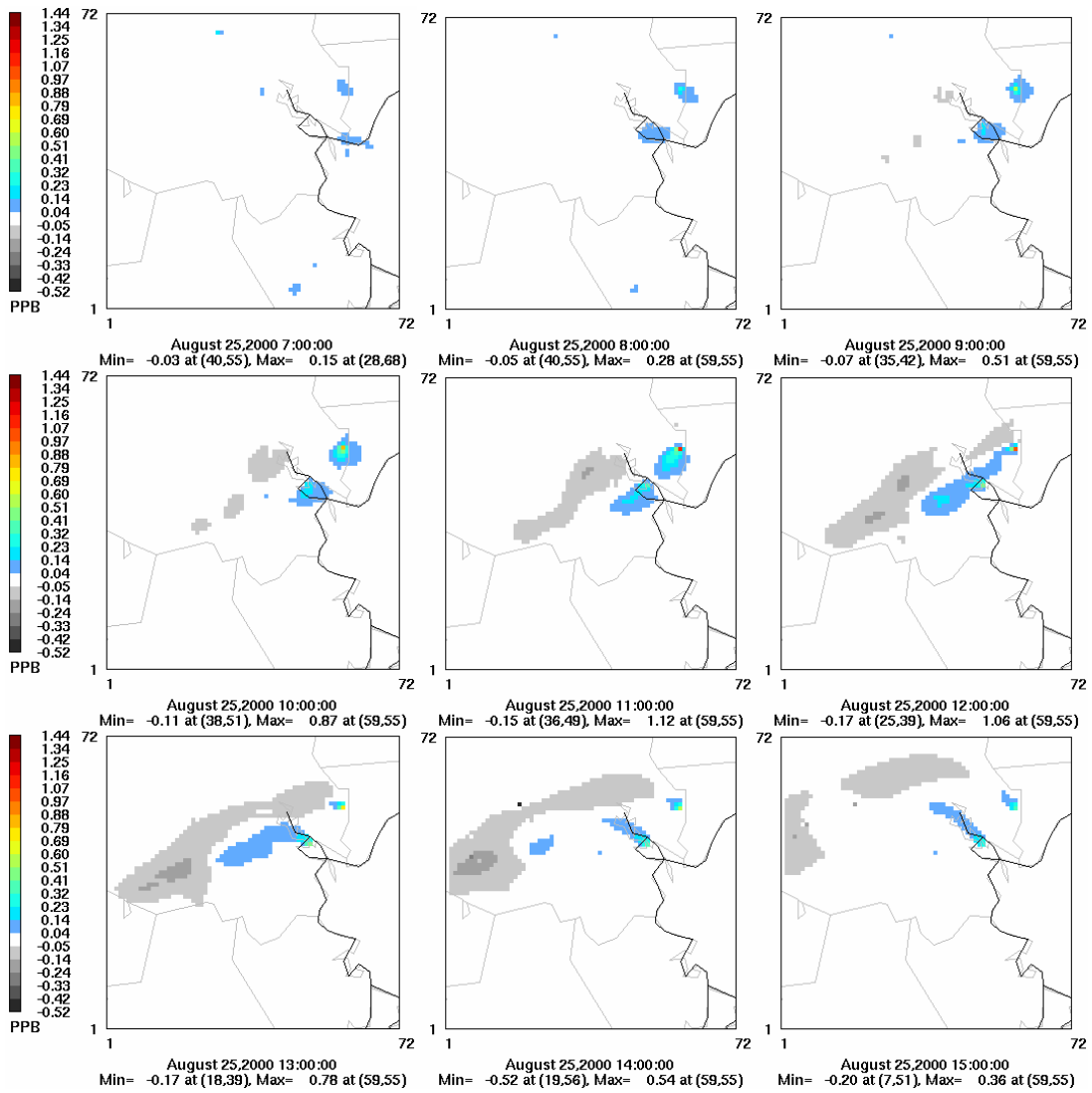


Figure 5.11 Difference in ozone concentration for 25 August from 700hr to 1500hr between predictions based on the reduced deterministic inventory and predictions based on the deterministic inventory. Percentage reduction in emissions was same with that from allowable episodic emission control. Maximum difference, approximately 1.4 ppb, occurred in (59, 55) at 2000hr.

5.3.2 Control of nearly constant emissions

The second control approach involves reduction in nearly constant emissions of NO_x and VOC emissions for all the flares in the HG domain. The stochastic inventory generator was modified to reflect this control scheme, as shown in Table 5.3, and a total of 50 sets of stochastic emission inventories were generated with the models. As described in the previous section of this chapter, expected values of the nearly constant emissions were decreased by 50% by reducing means or shift values, depending on the distribution type (normal or lognormal). Figure 5.12 shows the difference in ozone concentration between using the 38th stochastic inventory with 50% reduction in nearly constant emissions and using the deterministic imputed inventory. The 38th stochastic inventory is the inventory that led to largest additional ozone formation as shown in Figure 5.13. Compared to the results shown in Figure 5.6 (base case stochastic inventory), ozone concentration was increased in smaller areas and decreased in larger areas over the course of the day. The maximum difference in ozone concentration was larger, both positive and negative, than the results shown in Figure 5.7 (allowable episodic emission control); maximum increase in ozone was approximately 11 ppb larger, and maximum decrease in ozone was approximately 9 ppb larger than those shown in Figure 5.7.

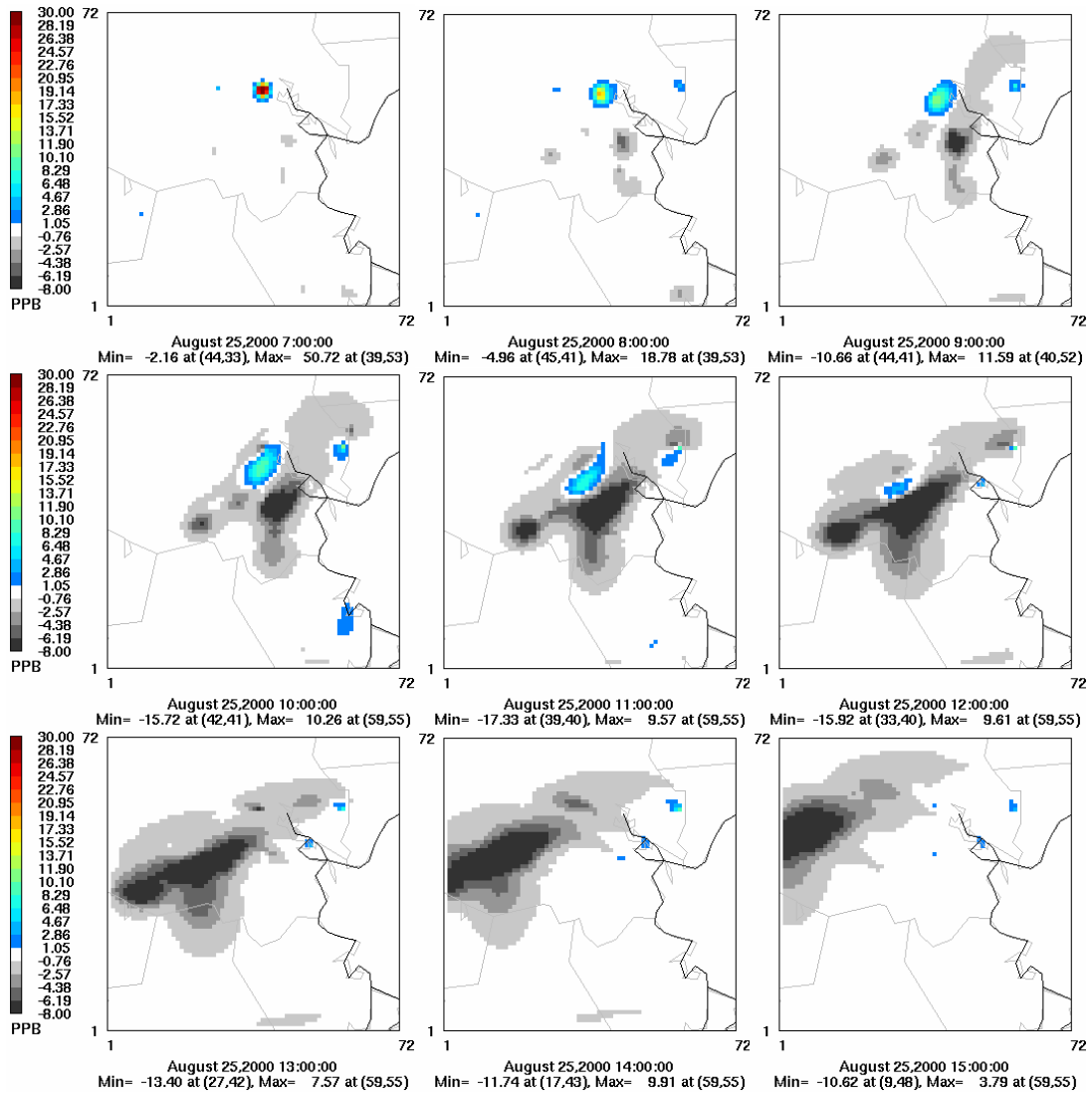


Figure 5.12 Difference in ozone concentration for 25 August from 700hr to 1500hr between predictions based on the 38th stochastic inventory generated using the models shown in Table 5.3 and predictions based on the deterministic inventory. Ozone concentrations are scaled to the results shown in Figures 5.6 and 5.7.

Figure 5.13 summarizes the maximum changes in ozone concentrations, both positive and negative, when the 50 sets of stochastic emission inventories with a 50% reduction in nearly constant flare emissions were used for simulations. The maximum difference in ozone concentration is largest when the 38th stochastic inventory was used; the ozone concentrations are 47.4 ppb and 98.1 ppb when the deterministic and the stochastic inventory were used, respectively, at conditions that lead to the maximum increase in ozone concentration. Figure 5.14 compares the maximum difference in ozone concentration, both positive and negative, for eliminating allowable episodic emissions, 50% reduction in nearly constant emissions and no control cases. The maximum increase in ozone concentration has longer tail to the right for 50% reduction in nearly constant emissions cases than eliminating allowable episodic emission cases; controlling the nearly constant emissions is not as effective in eliminating large maximum increases in ozone as controlling the allowable episodic emissions. Maximum decreases in ozone concentration, shown in Figure 5.14b, have the longest tail for the control of nearly constant emissions.

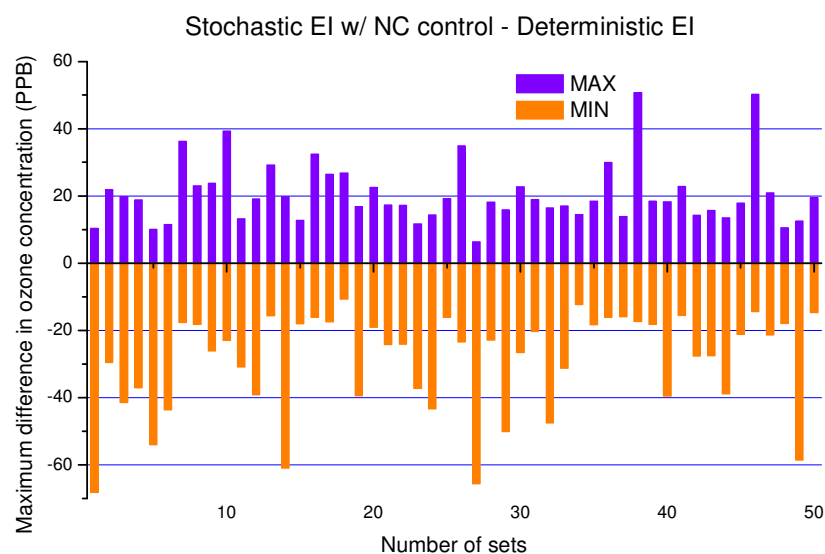


Figure 5.13 Maximum difference in ozone concentration in one day simulations representing 25 August, 2000. The difference is taken between the deterministic inventory with constant industrial emissions and the stochastic inventory for 50 instances of the stochastic inventory with a 50% reduction in nearly constant flare emissions. Maximum difference in ozone concentration was scaled to the results shown in Figure 5.8.

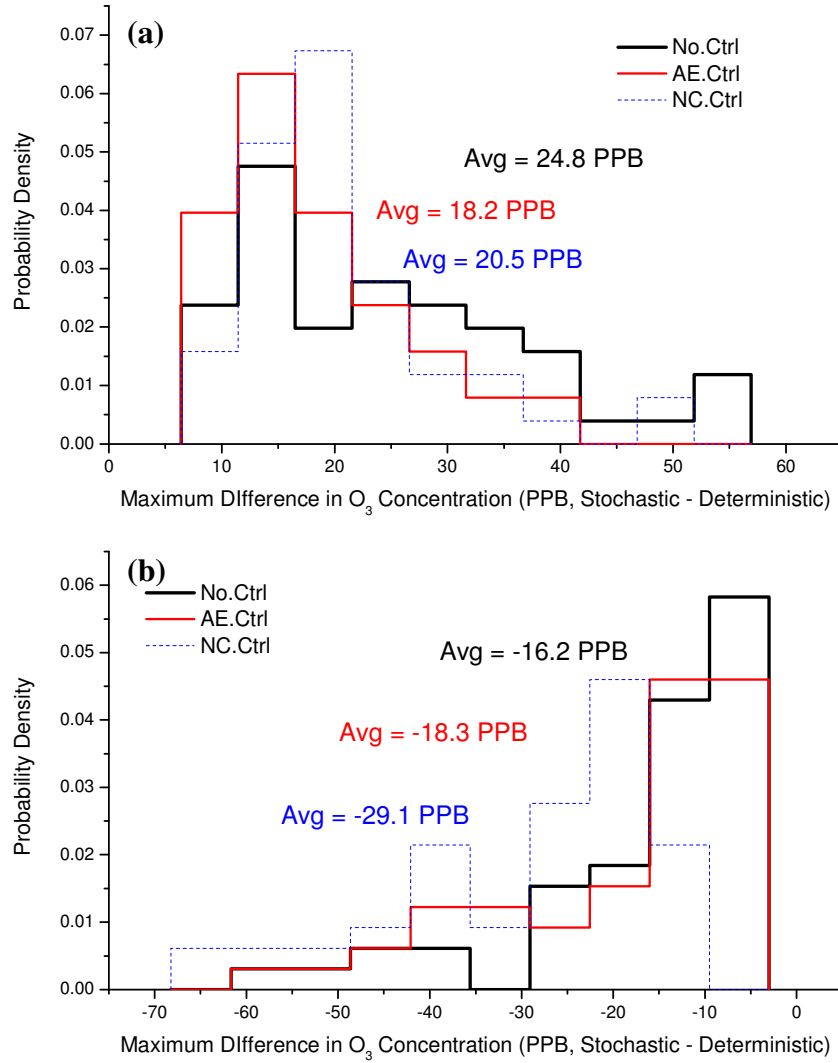


Figure 5.14 Probability distributions of maximum changes in ozone concentration in simulations representing 25 August, 2000 due to variable continuous emissions with allowable episodic emission control (red line), with nearly constant emission control (blue line) and without the control (black line) in positive direction (a) and negative direction (b).

Figure 5.15 compares daily maximum ozone concentration in the HG domain for no control, allowable episodic emission control, and nearly constant emission control cases. On average, total flare emissions across the domain were decreased, due to control of allowable episodic emissions, by 1.4 tons and 0.12 tons for VOC and NO_x, respectively, relative to no control cases. Reduction in daily maximum ozone concentration due to the control is 1.07 ppb per ton of VOC reduction ($1.5 \text{ ppb} / 1.4 \text{ tons}$) and 12.07 ppb per ton of NO_x reduction ($1.5 \text{ ppb} / 0.12 \text{ tons}$). Control of nearly constant emissions reduced total flare emissions by 9.73 tons and 1.47 tons, for VOC and NO_x, respectively. Reduction in daily maximum ozone concentration is 1.08 ppb per ton of VOC reduction ($10.5 \text{ ppb} / 9.73 \text{ tons}$) and 7.14 ppb per ton of NO_x reduction ($10.5 \text{ ppb} / 1.47 \text{ tons}$) due to the nearly constant emission control. In terms of daily maximum ozone reduction per amount of VOC reduction, control of allowable episodic emissions and control of nearly constant emissions are similarly effective. In terms of daily maximum ozone reduction per amount of NO_x reduction, control of allowable episodic emissions are more effective than control of nearly constant emissions.

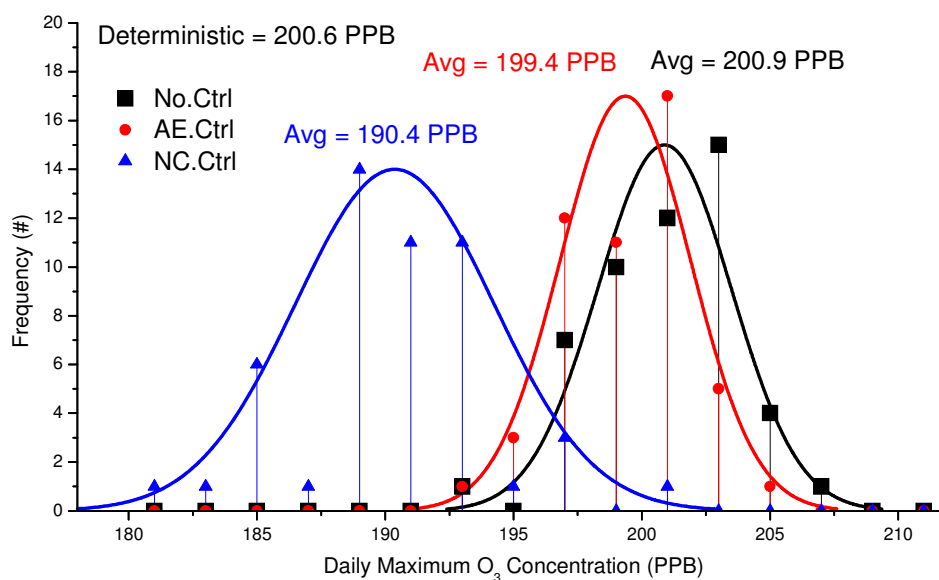


Figure 5.15 Histograms of daily maximum ozone concentration across the HG 1-km domain for no control cases (black), allowable episodic emission control cases (red), and nearly constant emission control cases (blue).

For comparison purposes, the same magnitude of reduction in total flare emissions, due to nearly constant emission control, were applied to the deterministic inventory. The average percentage reductions for NO_x and VOC emissions from flares due to the reduction of the nearly constant emissions are 24.7% and 30.1%, respectively.

Figure 5.16 shows difference in ozone concentration between using the reduced deterministic inventory and using the deterministic inventory. Maximum changes in ozone concentration due to the overall reduction are approximately +9.4 ppb and -2.6 ppb. These maximum increases and decreases in ozone concentration are smaller by a factor of 2 and 11, respectively, relative to averages of maximum increase and decrease shown in Figure 5.14. Daily maximum ozone concentration using the reduced deterministic inventory was about 198.7 ppb, approximately 1.9 ppb lower than using

deterministic inventory. This decrease in daily maximum ozone concentration was more than a factor of 5 smaller than the average decrease in daily maximum ozone shown in Figure 5.15. On average, in terms of both daily maximum ozone concentration and maximum changes in ozone concentration, control of nearly constant emissions of flares is more effective in ozone reduction than overall reduction in flare emissions assuming constant industrial emissions of NO_x and VOC.

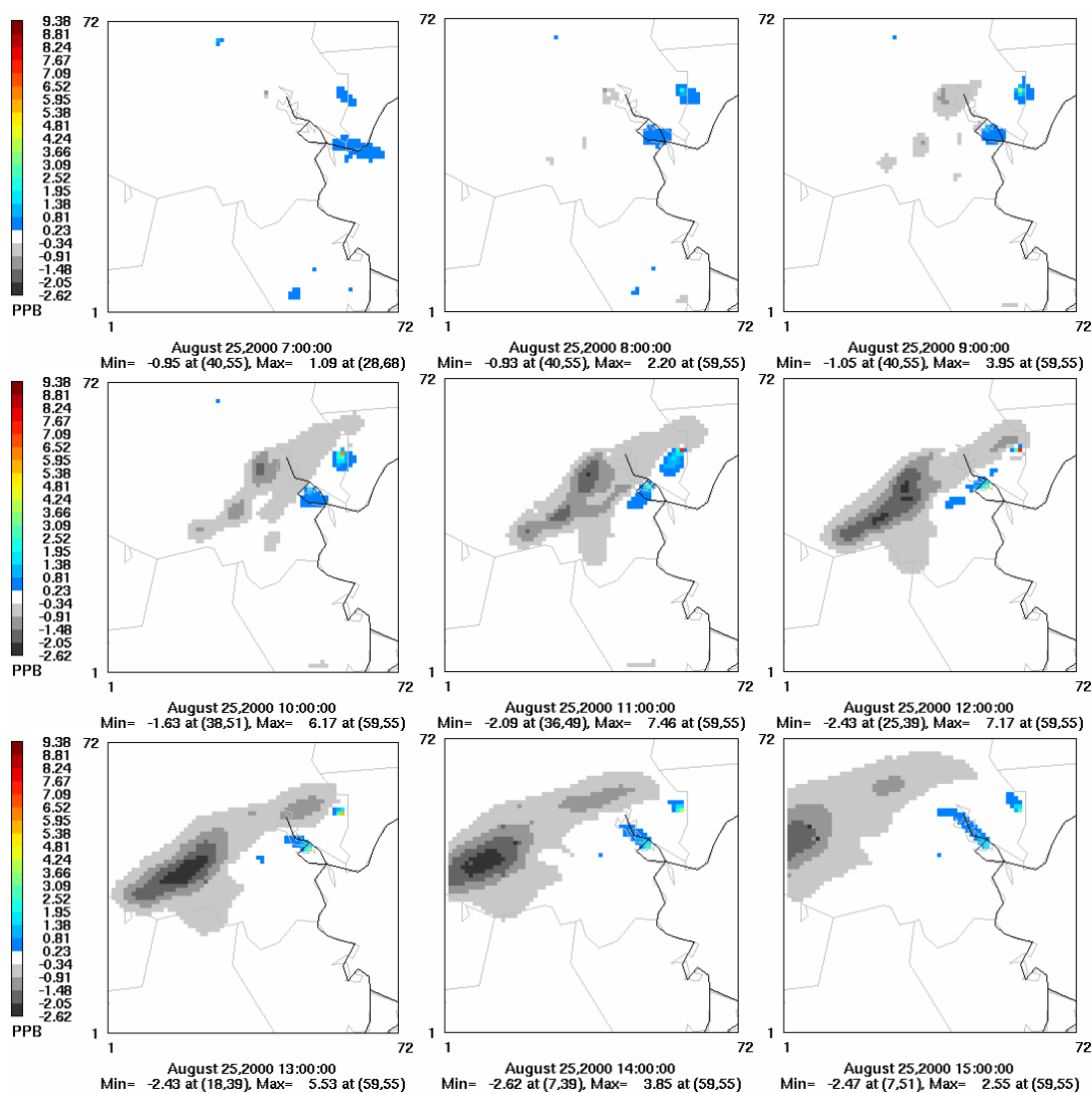


Figure 5.16 Difference in ozone concentration for 25 August from 700hr to 1500hr between predictions based on the reduced deterministic inventory and predictions based on the deterministic inventory. Percentage reduction in emissions was same with that from nearly constant emission control. Maximum difference, approximately 9.4 ppb, occurred in (59, 55) at 2000hr.

5.4 Conclusions

This chapter evaluated two flare reduction scenarios as examples of alternative strategies for reducing ozone concentrations due to variable industrial emissions. The first control strategy involved reducing large magnitude, infrequent emissions (allowable episodic emissions) from flares and the second strategy involved reducing continuous, and relatively constant, emissions (nearly constant emissions) from flares.

In terms of maximum difference in ozone concentration, control of allowable episodic emissions is more effective in eliminating large increases in ozone than control of nearly constant emissions. In contrast, control of nearly constant emissions is more effective in achieving maximum decreases in ozone concentration than control of allowable episodic emissions. For both control cases, maximum increases and decreases in ozone concentrations were significantly larger than those due to equivalent reductions in VOC and NO_x emissions applied to deterministic inventories.

Control of allowable episodic emissions and control of nearly constant emissions are similarly effective in reducing daily maximum ozone concentration per amount of VOC reduction in flare emissions. In contrast, decreases in daily maximum ozone concentration per amount of NO_x reduction are larger in the simulations with control of allowable episodic emissions than those with control of nearly constant emissions. These decreases in daily maximum ozone concentration due to both control strategies were significantly larger than those due to similar reductions in VOC and NO_x emissions applied to deterministic inventories.

5.5 References

- Bay Area Air Quality Management District (BAAQMD), 2005. Flare Monitoring at Petroleum Refineries, Accessed January 2007 at <http://www.baaqmd.gov/dst/regulations/rg1211.pdf>
- Bay Area Air Quality Management District (BAAQMD), 2006. Flares at Petroleum Refineries, Accessed January 2007 at <http://www.baaqmd.gov/dst/regulations/rg1212.pdf>
- Kleinman, L.I., Daum, P.H., Imre, D., Lee, Y.N., Nunermacker, L.J., Springston, S.R., Weinstein-Lloyd, J., Rudolph, J., 2003. Correction to "Ozone production rate and hydrocarbon reactivity in 5 urban areas: A cause of high ozone concentration in Houston". Geophys. Res. Lett. 30 (12), 1639.
- Murphy, C.F., Allen, D.T., 2005. Hydrocarbon emissions from industrial release events in the Houston-Galveston area and their impact on ozone formation. Atmospheric Environment 39(21), 3785-3798.
- Nam, J., Kimura, Y., Vizuite, W., Murphy, C.F., Allen, D.T., 2006. Modeling the impacts of emission events on ozone formation in Houston, Texas. Atmospheric Environment 40 (28), 5329-5341.
- Ryerson, T.B., Trainer, M., Angevine, W.M., Brock, C.A., Dissly, R.W., Fehsenfeld, F.C., Frost, G.J., Goldan, P.D., Holloway, J.S., Hubler, G., Jakoubek, R.O., Kuster, W.C., Neuman, J.A., Nicks, D.K., Parrish, D.D., Roberts, J.M., Sueper, D.T., Atlas, E.L., Donnelly, S.G., Flocke, F., Fried, A., Potter, W.T., Schauffler, S., Stroud, V., Weinheimer, A.J., Wert, B.P., Wiedinmyer, C., Alvarez, R.J., Banta, R.M., Darby, L.S., Senff, C.J., 2003. Effect of petrochemical industrial emissions of reactive alkenes and NO_x on tropospheric ozone formation in Houston, Texas. J. Geophys. Res. 108 (D8), 4249.
- Shell Oil Products US, 2006. Shell Martinez Refinery Flare Minimization Plan.
- Sokal, R.R., Rohlf, F.J., 1987. *Introduction to Biostatistics*. W.H. Freeman & Company, NY.
- Texas Commissions on Environmental Quality (TCEQ), 2004. Revisions to the State Implementation Plan for the Houston-Galveston-Brazoria nonattainment area. Accessed February 2007 at <http://www.tceq.state.tx.us/assets/public/implementation/air/sip/sipdocs/2004-05-HGB/execsumm.pdf>

Vizuete, W., 2005. Implementation of Process Analysis in a three dimensional air quality model, PhD thesis, University of Texas.

Webster, M., 2007. Updates on Stochastic Emission Inventory Generator

Webster, M., Nam, J., Kimura, Y., Jeffries, H., Vizuete, W., Allen, D.T., 2007. The effect of variability in industrial emissions on ozone formation in Houston, Texas. Submitted to Atmospheric Environment

CHAPTER 6

SUMMARY, CONCLUSIONS, AND RECOMMENDATIONS

6.1 Summary

The primary objective of this thesis was to investigate impacts of variability in industrial hydrocarbon emissions on ozone formation in the Houston Galveston (HG) area. Variability in industrial emissions of hydrocarbons was characterized as due to either episodic emission events or to variability in continuous emissions. The effect of each of these components of variability on ozone formation in the HG area was investigated with computationally efficient versions of 3-D photochemical grid models developed for this study. An emission event database for the HG area, compiled by the Texas Commissions on Environmental Quality (TCEQ, 2004), was utilized to determine event characteristics examined for this study. Variable continuous emissions were simulated with stochastic models based on observations of emission variability from a group of sources in the HG area. Also, the effectiveness of controlling emission variability was assessed.

6.2 Conclusions

1. Emission events have the potential to lead to substantial ozone formation in the HG area, creating localized regions where ozone concentrations are enhanced by more than 100 ppb.
2. Large emission events can, by themselves, cause exceedances of the air quality standards for ozone.
3. Ozone formation and accumulation due to emission events have a complex dependence on event magnitude, composition, duration, and timing as well as the specific meteorology at the time of events.
4. Temporal variability in continuous emissions from industrial sources has the potential to cause increases and decreases of 10~50 ppb, or more, in ozone concentrations over large areas.
5. Temporal variability in continuous emissions can increase region wide maximum ozone concentration by up to several ppb, on average; therefore decreasing variability can reduce region wide maximum ozone concentrations by several ppb.
6. Control of emission variability can be more effective in ozone reduction relative to across the board reduction in average emission rates in terms of both maximum changes in ozone concentration and region wide maximum ozone concentration.

6.3 Recommendations for future work

Impacts of variability in continuous emissions of hydrocarbons on ozone formation were investigated based on the assumption of constant combustion efficiency of flares. However, flares may operate with combustion efficiencies that vary in time due to crosswinds and other factors (Levy et al., 2006; Castineira, 2006). Crosswinds can reduce flame temperature and shorten the residence time of the waste gas in the flame, degrading combustion efficiency of flares. Because industrial flares are designed and used for control of emission spikes, decreases in destruction efficiencies, by even a small amount, can lead to significant air quality impacts. Therefore, it is recommended to investigate the impacts on ozone formation of incomplete combustion products of waste gas, such as formaldehyde, from flares.

6.4 References

Castineira, D., 2006. A computational fluid dynamics simulation model for flare analysis and control, PhD thesis, University of Texas.

Levy, R.E., Randel, L., Healy, M., Weaver, D. 2006. Reducing emissions from plant flares. *Proceedings of the Air & Waste Management Association's Annual conference*, Paper #61.

Texas Commissions on Environmental Quality (TCEQ), 2004. Air emission event reports. Accessed March 2007 at http://www.tceq.state.tx.us/compliance/field_ops/eeer/

APPENDIX A

Summary of emission events reported for TCEQ region 12 from 2003 to 2005

Table A.1 Summary of emission events reported by industrial facilities in the TCEQ region 12 from 2003 to 2005 (TCEQ, 2006). TCEQ region 12 is 13 counties around Houston. HRVOC was defined as ethylene, propylene, 1,3-butadiene, and isomers of butene by Texas Air Quality regulation for their significant roles in ozone formation.

	2003	2004	2005
Total Number of events	1,894	1,988	1,722
Number of HRVOC events	759	654	574
Total Emissions (kilo-lb)	12,018	23,129	14,227
HRVOC Emissions (kilo-lb)	1,743	1,457	1,830
Proportions of HRVOC events (Number / Mass)	40.1% / 14.5%	32.9% / 6.3%	33.3% / 12.9%
Ethylene	58%	50%	64%
Propylene	33%	37%	25%
1,3-Butadiene	3%	7%	5%
Butenes	6%	6%	6%

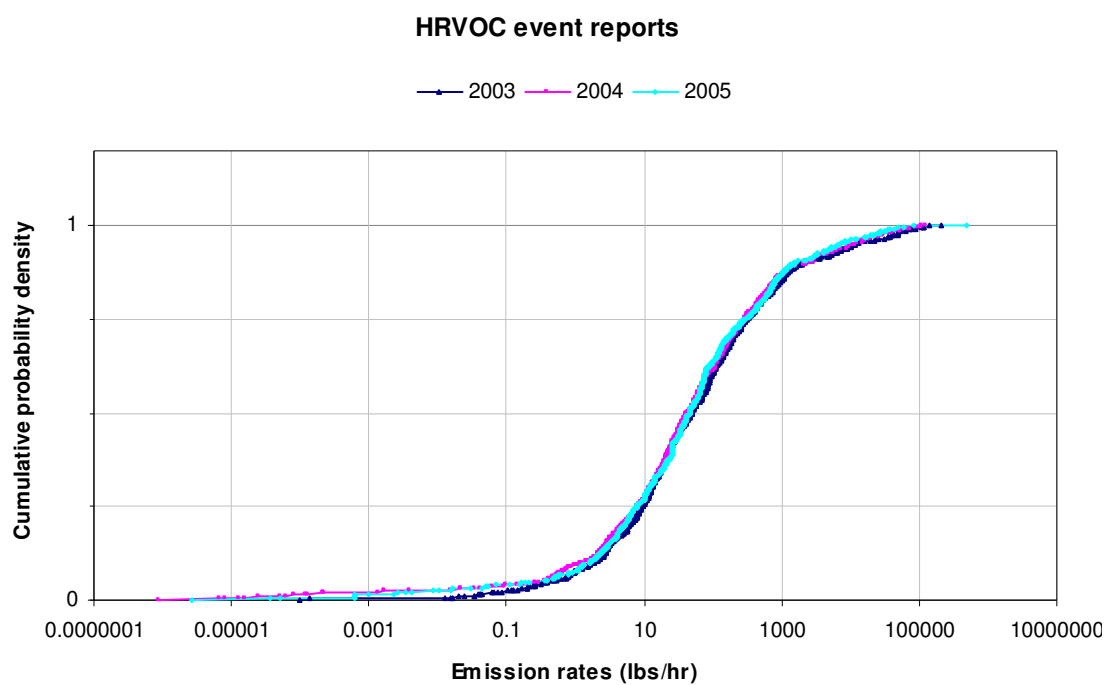


Figure A.1 Cumulative distribution function of event emission rates for 2003, 2004, and 2005

APPENDIX B

Evaluation of the sub-domain model for 30 August, 2000

Figures B.1 to B.4 provide a comparison similar to those shown in Figures 3.4 to 3.6; the data shown are for 30 August, 2000. Figure B.1 compares the spatial distribution of ground level ozone concentrations predicted by the sub-domain model to ground level ozone concentrations predicted by the full domain simulation for the same time and locations. Figure B.2 presents a scatter plot comparing predictions of ozone concentrations in all ground level cells from the full domain model and sub-domain simulation. Figure B.3 compares the changes in ozone concentration due to the emission event, predicted by the sub-domain and full domain model. The emission event released 5819 lbs per hour of propylene from 10 am to 12 pm 30 August, 2000, at ground level, near the center left portion of Figure B.3. Figure B.4 shows a scatter plot comparing differences in predicted ozone concentrations between the simulation that included the emission event and the base case. The scatter is greater in Figure B.4 than the data shown in Figure 3.6. This is because the event plume on this date was more affected by boundary conditions, which are the major cause of the differences between the sub-domain and full domain simulation, as described in Chapter 3.

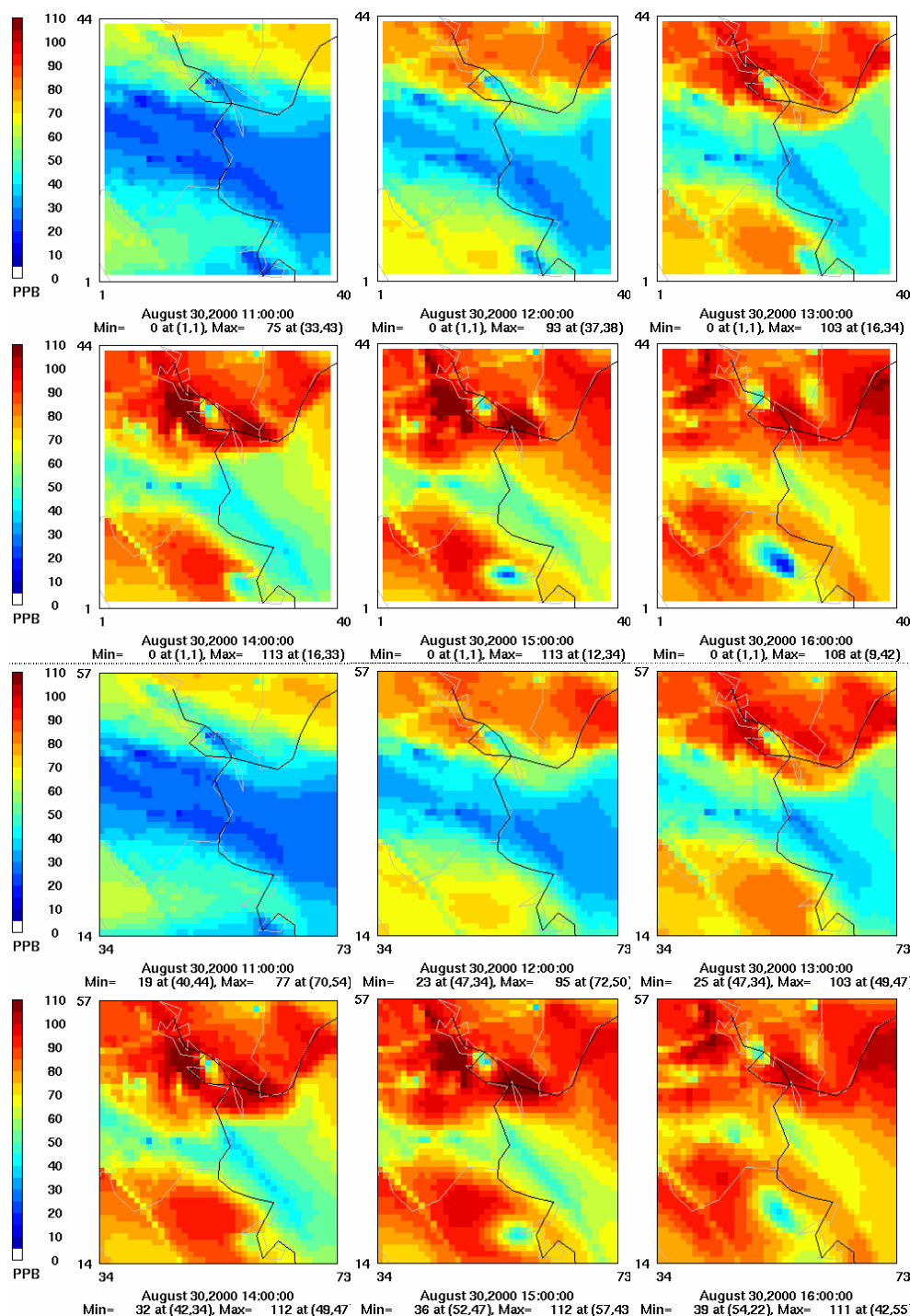


Figure B.1 Ozone concentration for 30 August from 1100hr to 1600hr using the basecase inputs, predicted by the sub-domain model (top 6 figures) and full-domain model (bottom 6 figures)

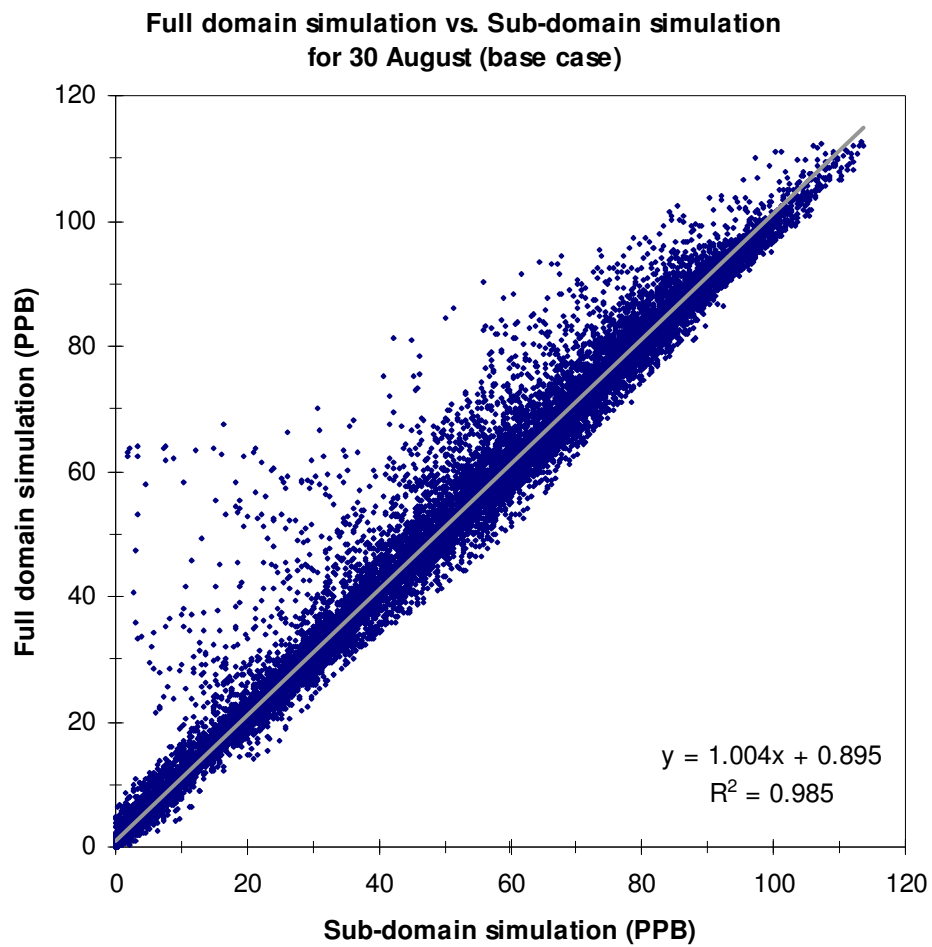


Figure B.2 Comparison of ozone concentration predictions for the 30 August base case simulation using the sub-domain and the full domain

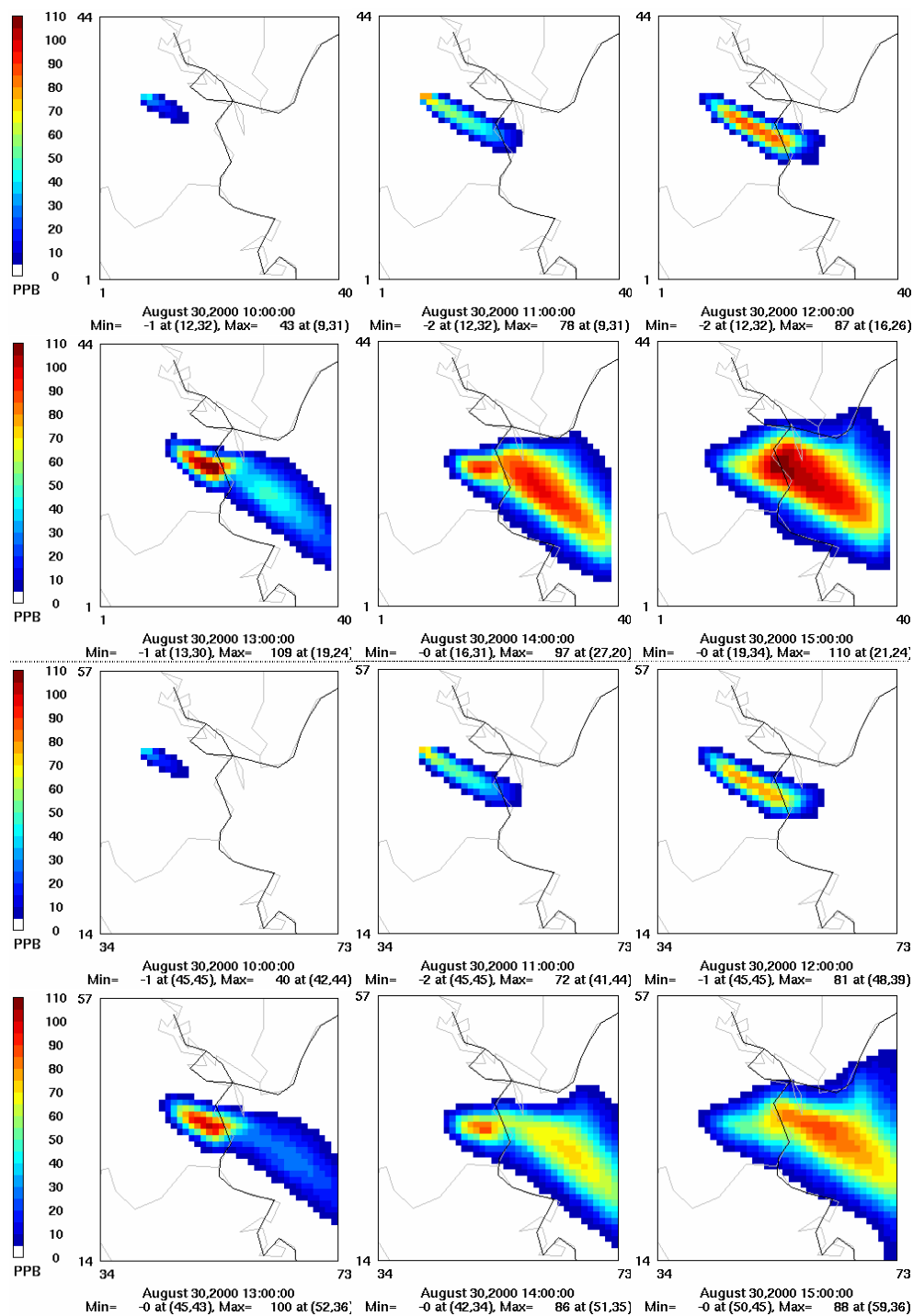


Figure B.3 Ozone difference plots for 30 August from 1000hr to 1500hr between emission event case and basecase with sub-domain model (top 6 figures) and full-domain model (bottom 6 figures)

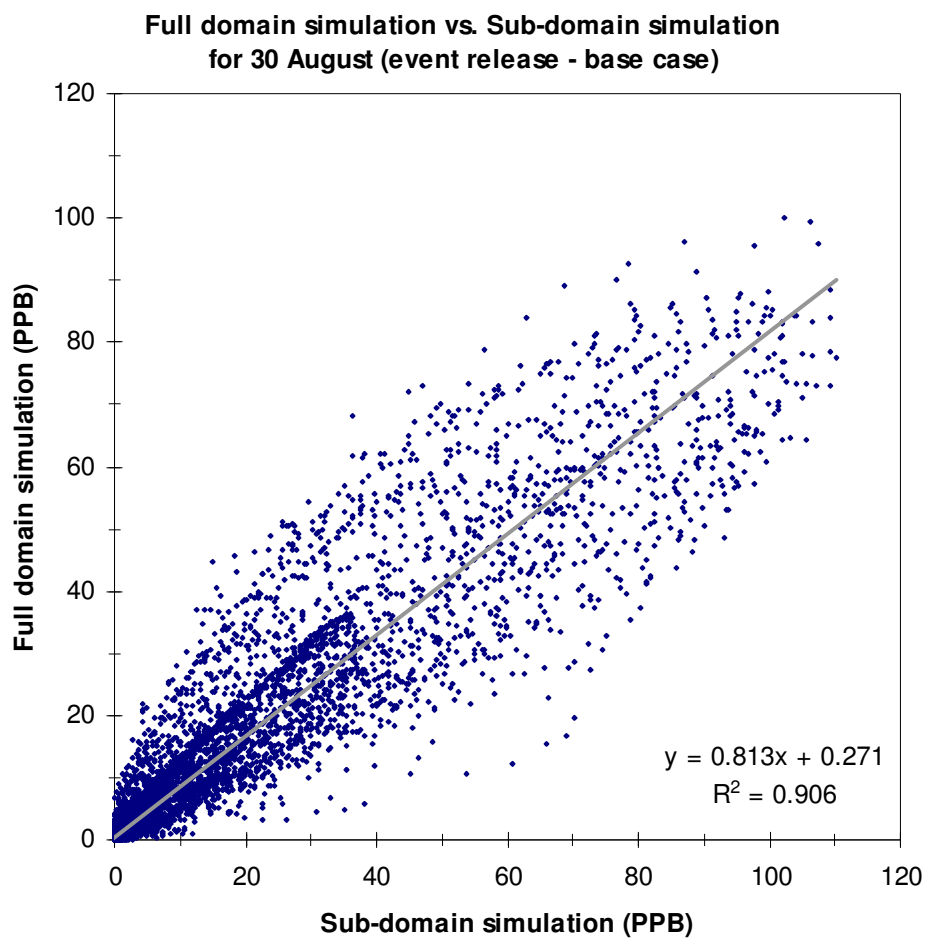


Figure B.4 Comparison of the difference between the emission event and the base case in the full domain simulation to the difference between the emission event and the base case in the sub-domain simulation. Emission event is a propylene release at a rate of 5819 lb h^{-1} from 10 am to 12 pm near the center left portion of Figure B.3.

APPENDIX C

Summary of linear relationships between maximum additional ozone formation and event characteristics examined for Monte-Carlo simulation in Chapter 3

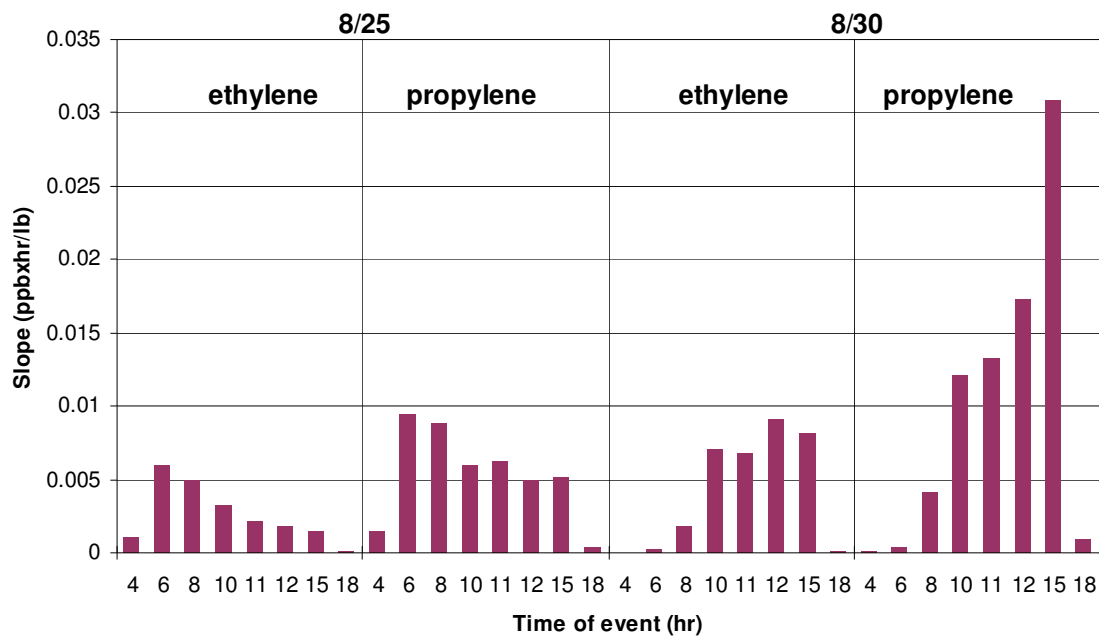


Figure C.1 Slopes of linear relationships between maximum additional ozone formed and event magnitude for each compound, each day, and each time of release. Slopes are based on the results from zero release and 1,000 lb release of event, instead of trend line of multiple simulation results like those shown in Figure 3.8.

APPENDIX D

Impacts of variable continuous emissions on ozone formation using the regular emission inventory

Analyses similar to those shown in Figures 4.12 to 4.14 were conducted with the regular emission inventory. The main difference between the regular inventory and the imputed inventory used in Chapter 4 lies in the amount of olefin emissions; olefin species were added to the regular inventory, based on observations, to create the imputed inventory. Using the regular inventory, without additional olefin emissions, the effect of variable continuous emissions on ozone formation was investigated.

A total of 10 sets of stochastic emission inventory were generated with the models described in the Methods section of Chapter 4 and simulations representing 25 August and 30 August, 2000 were performed using them. Figure D.1 shows the differences in ozone concentration on the 25 August between using the 7th stochastic regular inventory and the regular inventory without VOC emission variability. The 7th stochastic inventory is the largest inventory in terms of total VOC emissions in a day, although the difference from the regular inventory is less than 2%. Since the stochastic inventory has both higher and lower VOC emissions across the HG area over the course of the day, ozone concentrations using the stochastic inventory are higher or lower than using the regular inventory depending on time of day and location. At conditions that lead to maximum difference in ozone concentration, ozone concentrations predicted using the stochastic inventory are approximately 5.5 ppb higher than using regular

inventory. Ozone concentrations are also up to 1.8 ppb lower using stochastic inventory than using the regular inventory with constant VOC emissions.

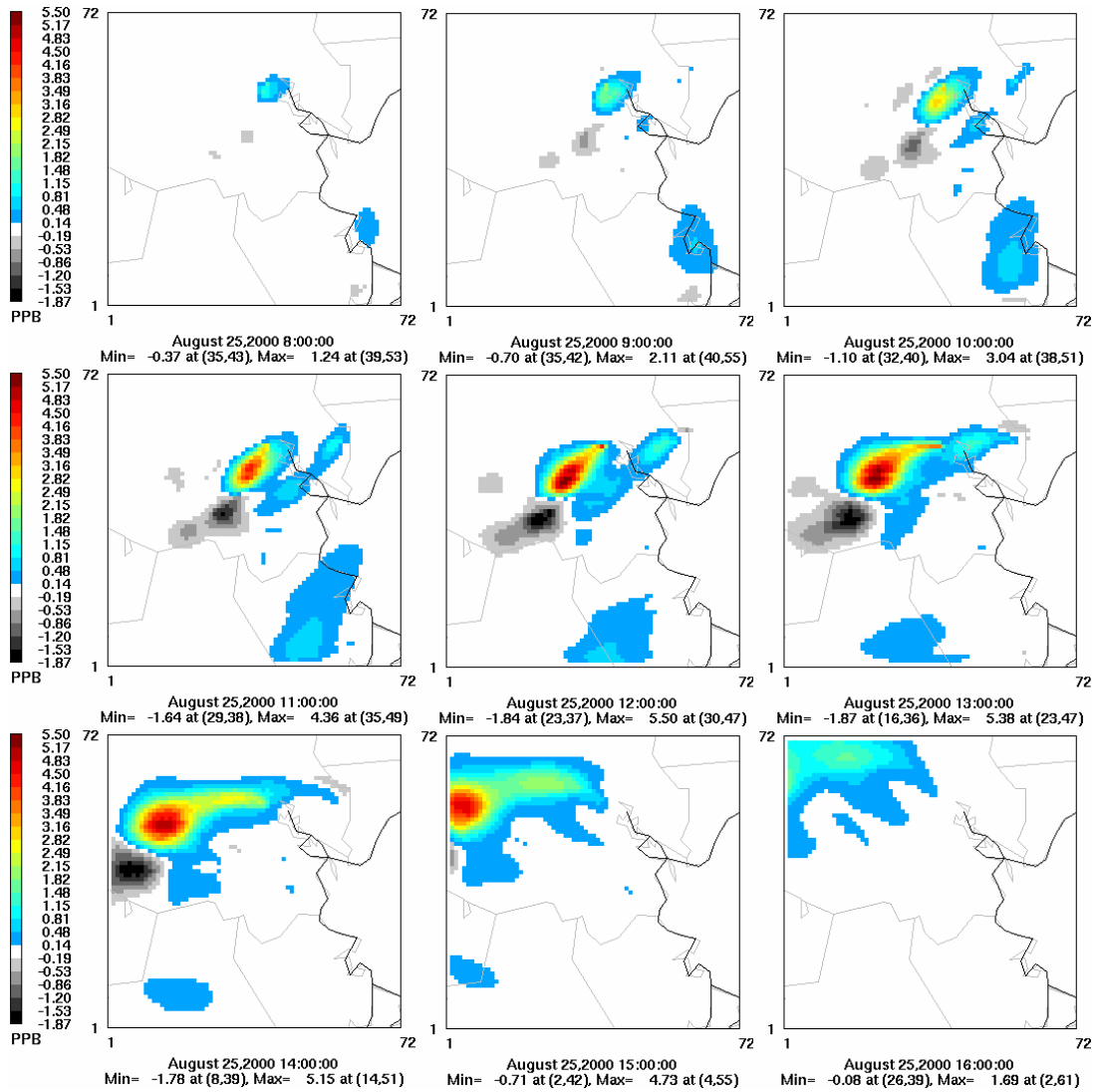


Figure D.1 Difference in ozone concentration for 25 August from 800 hr to 1600 hr between using the 7th stochastic regular emission inventory and using the regular inventory with constant VOC emission, regular inventory

Figure D.2 summarizes the maximum changes in ozone concentrations, both positive and negative, when all the ten stochastic emission inventories were used for simulations on 25 August and 30 August, 2000. Specifically, the quantity presented is the maximum difference in ozone concentration between using the stochastic inventory and the regular inventory. Inside each column, ozone concentration for the stochastic inventory, at the time when the maximum difference occurred, is indicated in ppb. In the simulations of 25 August, the maximum difference in ozone concentration is largest when the 7th stochastic emission inventory was used; the ozone concentrations are 43 ppb and 48.5 ppb when the regular and the stochastic inventory were used, respectively, at conditions that lead to the maximum difference in ozone concentration. In the simulations of 30 August, the largest maximum difference in ozone concentration occurred when the 3rd stochastic inventory was used; an 8 ppb increase in ozone concentration relative to the regular inventory was predicted. Compared to the results using the imputed inventory shown in Figures 4.12 to 4.14, both the maximum increase and the maximum decrease in ozone due to VOC emission variability were approximately 10 times smaller, on average, when the regular inventory was used than when the imputed inventory was used.

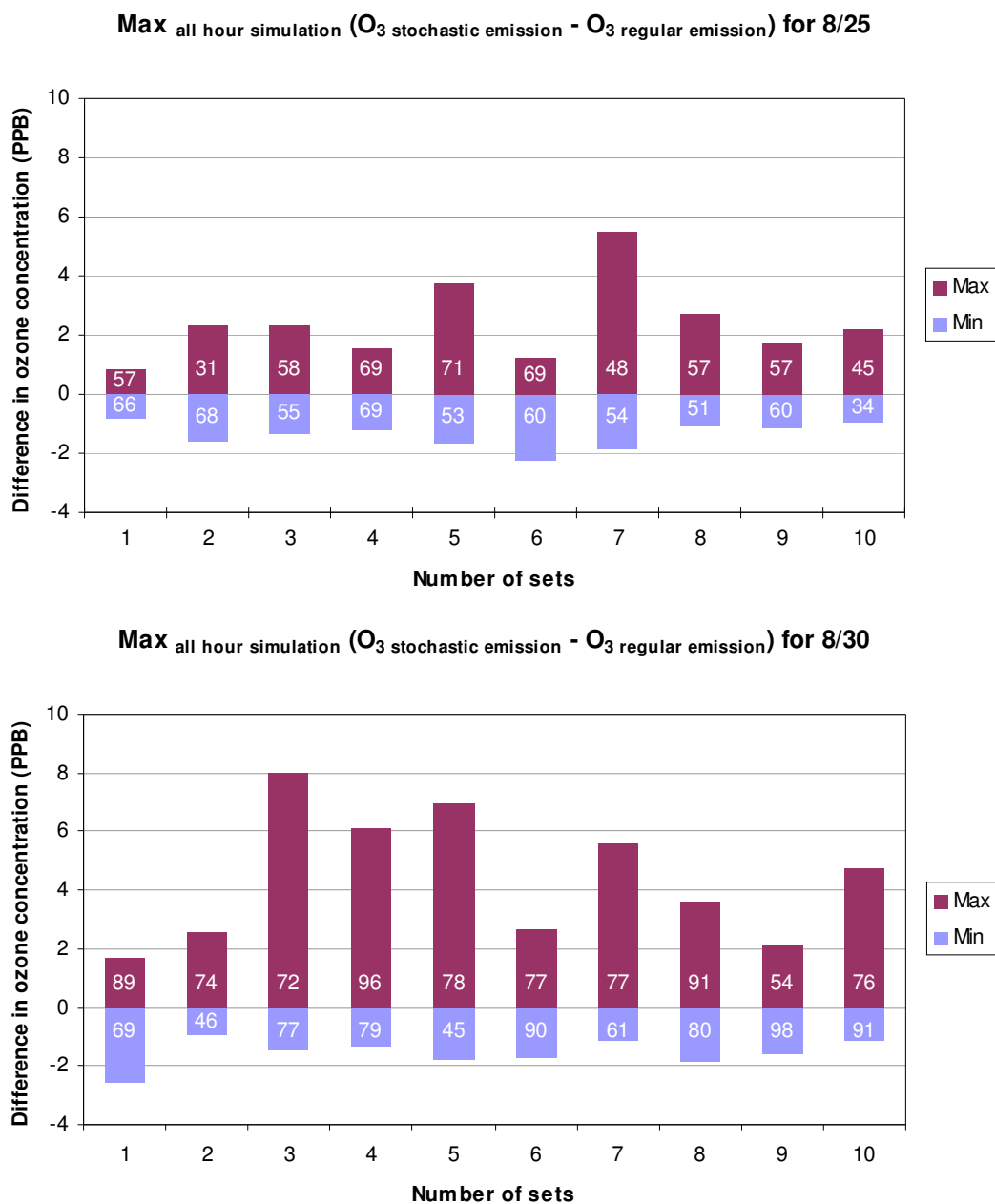


Figure D.2 Maximum difference in ozone concentration in all hours of simulations representing 25 August and 30 August, 2000 between using regular inventory and stochastic regular inventory for 10 sets of stochastic inventory. Ozone concentrations using the stochastic regular inventory are indicated in ppb inside each column.

Simulations of the two episode days exhibit different responses of ozone formation due to variable VOC emissions. For example, the 7th stochastic inventory led to a maximum difference in ozone concentration of 5.5 ppb in a grid cell which is the 30th to the east and the 47th to the north from the southwest corner of the region in red, shown in Figure D.1, at 12pm 25 August. At the same time of day and location on 30 August, the ozone concentration was not affected by variable VOC emissions. Distinctly different meteorological conditions on the two days led to these different behaviors of ozone formation for the same stochastic emission inventory.

With the exception of the 6th and the 1st stochastic inventory for 25 August and 30 August, respectively, the maximum difference in ozone concentration (stochastic EI case – regular EI case) is, in absolute values, larger in the positive direction than in the negative direction, as shown in Figure D.2. Figure D.3 shows that this change in ozone concentration did not always increase the peak ozone concentration in the sub-domain over the course of the day. For example, on 25 August the daily maximum ozone concentration using the stochastic inventory is up to 2.6 ppb higher and up to 0.6 ppb lower than when the regular inventory with constant VOC emissions was used, depending on the stochastic inventory used. This can be contrasted with a maximum increase of 5.5 ppb and a maximum decrease of 2.3 ppb, shown in Figure D.2. A total of 5 out of the 10 sets of stochastic inventories led to increases in daily maximum ozone concentration in the sub-domain. For 30 August, the daily maximum ozone concentration increased for three sets of stochastic inventories. The maximum increase in the peak ozone concentration is approximately 1.3 ppb and maximum decrease is approximately 0.2 ppb.

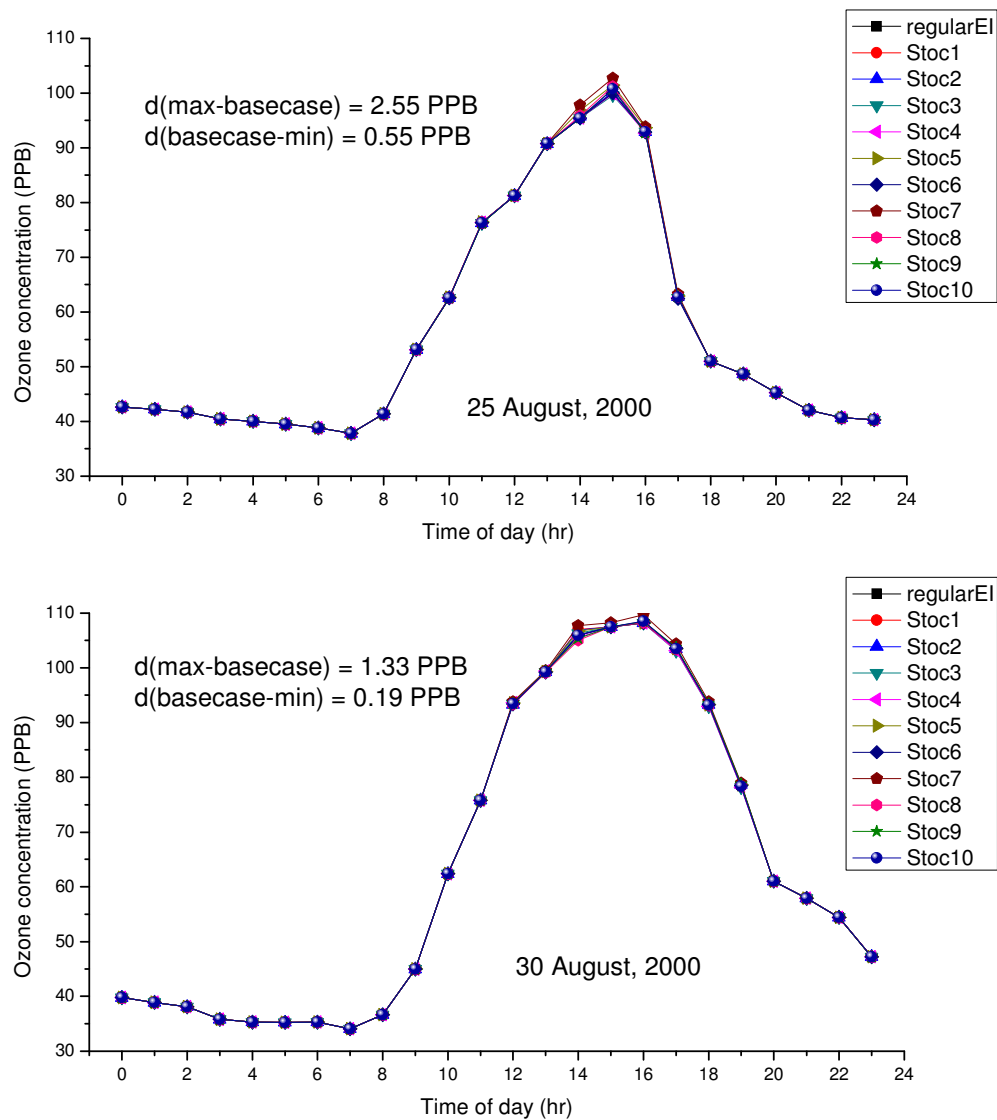


Figure D.3 Domain-wide maximum ozone concentration for 10 sets of stochastic regular emission inventory for both episode days

APPENDIX E

Impacts of VOC emission variability on effectiveness of ozone control strategies

The response of ozone to across the board emission reductions, using variable industrial VOC emissions, was compared to the response of ozone to emission reductions when industrial VOC emissions were constant. Scenarios of 25% NO_x reduction, 50% NO_x reduction and 25% VOC reduction from all the emission sources across the HG area were investigated. For this task, simulation with the 7th stochastic inventory on 25 August was selected as representative of the simulation with a stochastic inventory. The results will be presented in two parts. The first part describes the effect of industrial VOC emission variability using the regular emission inventory. The second describes the effect of industrial VOC emission variability using the imputed emission inventory.

E.1 Impacts of VOC emission variability using regular emission inventory

Figure E.1 compares ozone concentrations using the stochastic inventory with 25% NO_x reduction and using the stochastic inventory without the control. When NO_x was reduced by 25% in emissions from all the sources across the HG area, ozone concentration increased in a large area, by up to 41 ppb. When the regular inventory with constant VOC emissions was used to investigate the response of ozone to the same NO_x control, a similar result was observed; the spatial distribution and magnitude of ozone difference largely agree with those using the stochastic inventory, shown in Figure

E.1. If NO_x was reduced by 25% in all the emission sources in the HG area, ozone concentration would be increased significantly in large portion of the area whether VOC emissions from industrial point sources were constant or variable. This is indicative of NO_x rich conditions of the Houston area, where effective control of high ozone levels in the area could be achieved using VOC control. This is partly due to underestimated VOC emissions in the regular emission inventory used for this study, and the effect of this underestimation will be examined in the next section.

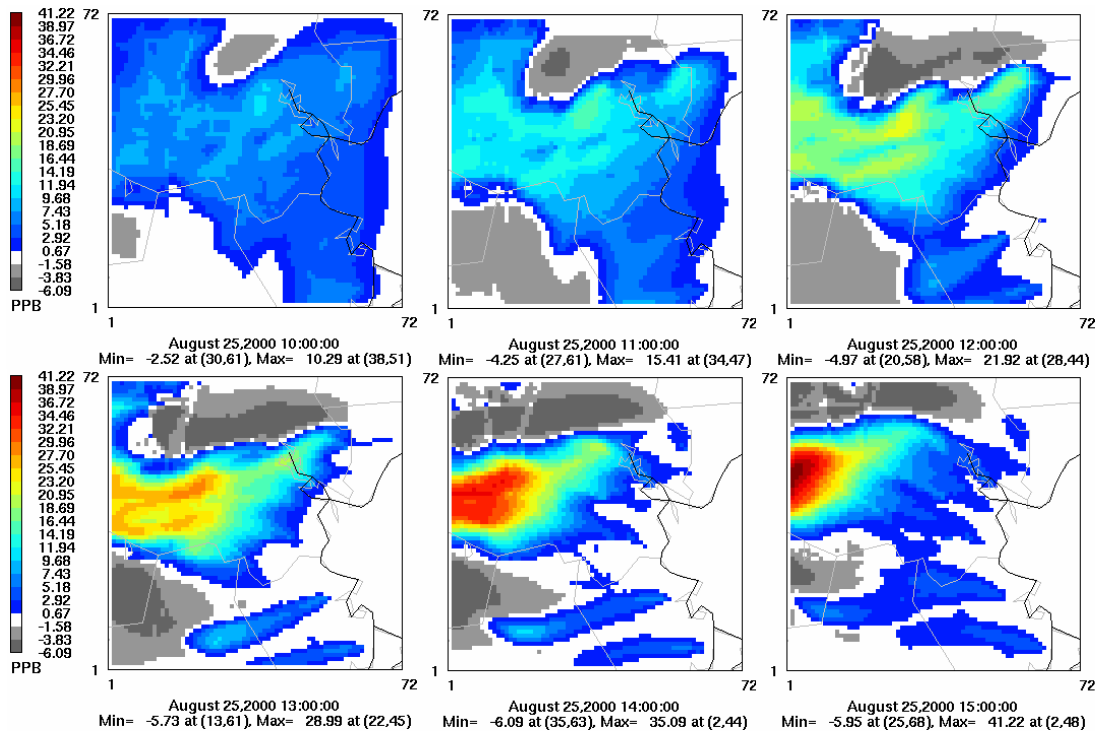


Figure E.1 Ozone difference plots between using the 7th stochastic regular inventory with 25% NO_x reduction and using the stochastic regular inventory without control

The difference in the response of ozone concentration is shown in Figure E.2. Specifically, the quantity reported is:

$$\{ \text{Ozone}_{\text{using stochastic regular inventory with control}} - \text{Ozone}_{\text{using stochastic regular inventory without control}} \} - \{ \text{Ozone}_{\text{using regular inventory with control}} - \text{Ozone}_{\text{using regular inventory without control}} \} \quad (\text{Eqn. E.1})$$

The quantity is positive or negative depending on location and time of day. Under conditions when the quantity is positive, the response of ozone to NO_x controls is larger when the stochastic inventory was used than when regular inventory was used. The maximum difference in response of ozone is approximately 2.6 ppb.

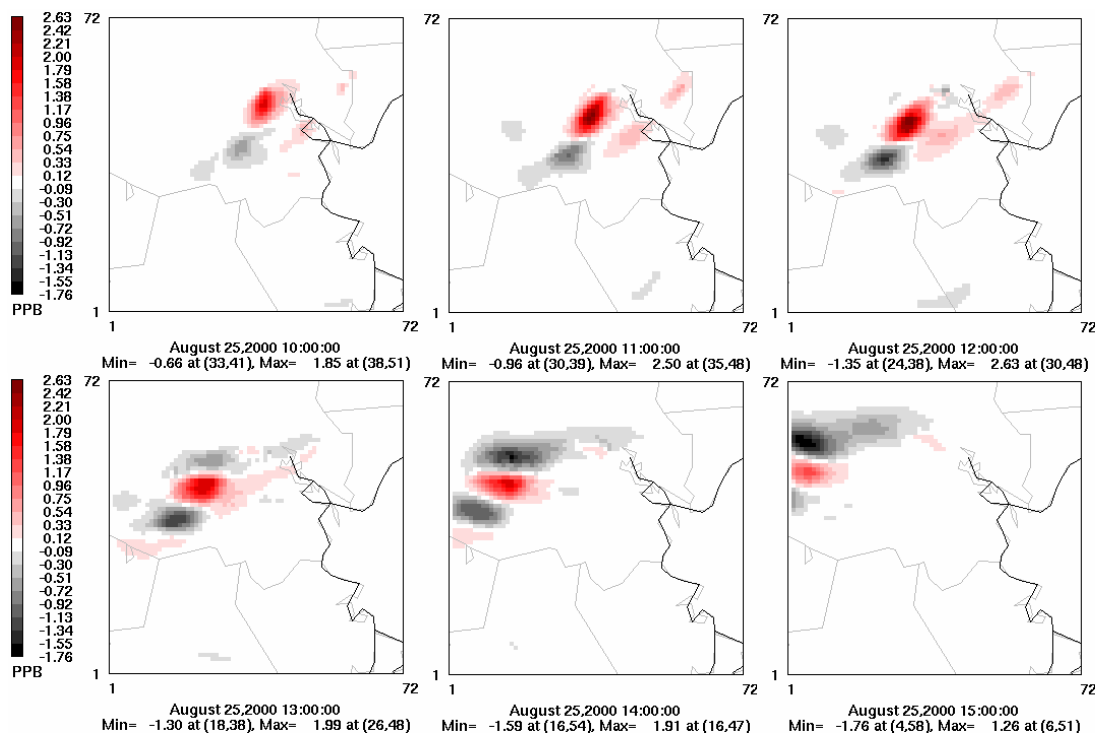


Figure E.2 Ozone difference plots showing difference in response of ozone to 25% NOx reduction across the sub-domain between using the 7th stochastic inventory and using regular inventory

For the control strategy of 50% NOx reduction in all the emissions across the HG area, a comparison similar to that shown in Figure E.2 was performed and is shown in Figure E.3. When NOx was reduced by 50%, the spatial pattern of ozone difference between using the inventory with the control and without the control appeared comparable to when NOx was reduced by 25%, although the magnitude of difference is larger in 50% NOx reduction cases than 25% NOx reduction cases.

The maximum difference in response of ozone to 50% NOx reduction was observed earlier in the day, at 11 am, relative to 25% NOx reduction cases. With less

NOx available across the area, NOx was depleted sooner. The maximum difference in response of ozone is approximately 5.8 ppb between the constant industrial VOC emissions and the variable industrial VOC emissions.

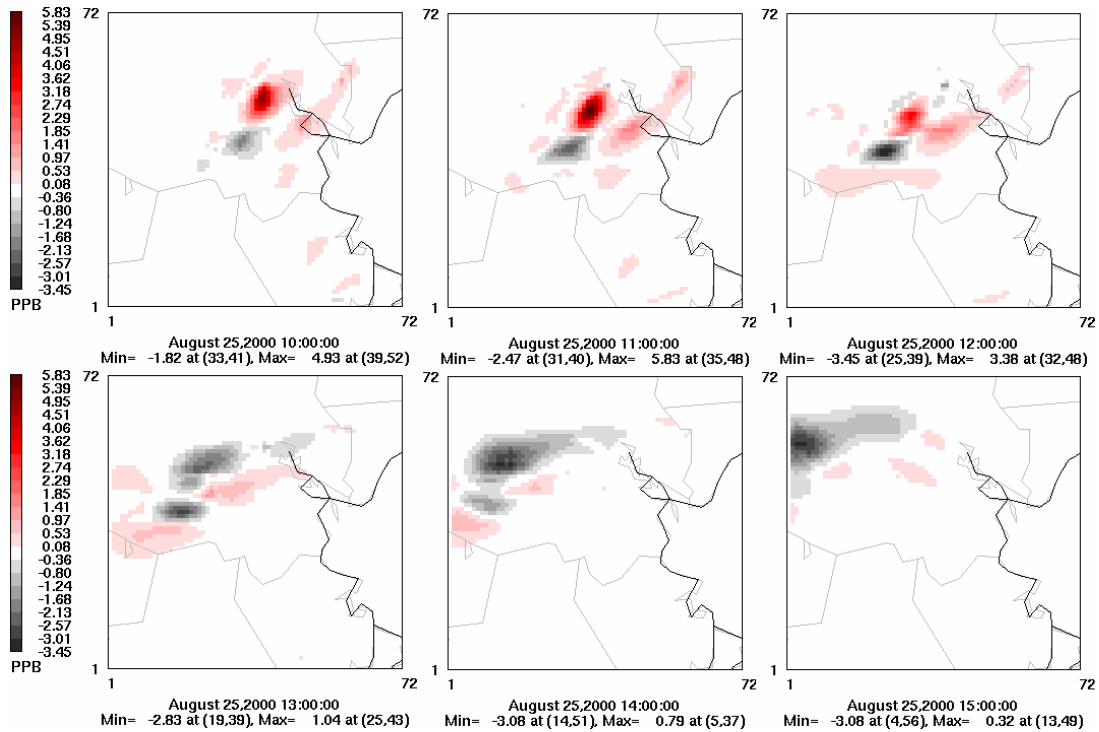


Figure E.3 Ozone difference plots showing difference in response of ozone to 50% NOx reduction across the sub-domain between using the 7th stochastic inventory and using regular inventory

Finally, a control strategy of 25% VOC reduction in all the emissions across the HG area was examined. Figure E.4 compares ozone concentration using the stochastic inventory with the VOC control and without the control. When VOC was reduced by

25% in all the emissions across the area, ozone was decreased in a large area, by up to 21 ppb. Simulation using the regular inventory with constant VOC emissions exhibits similar patterns of ozone response. The maximum decrease of ozone is approximately 20 ppb.

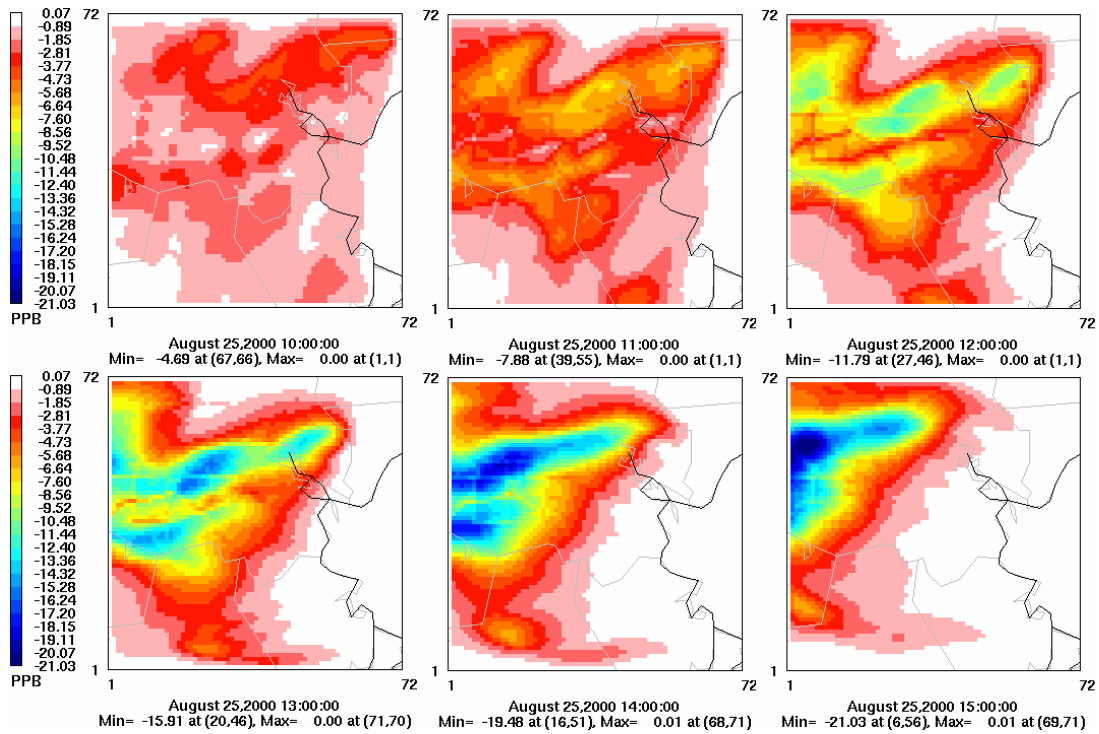


Figure E.4 Ozone difference plots between using the 7th stochastic inventory with 25% VOC reduction and using the stochastic inventory without control

Figure E.5 compares the response of ozone concentration to 25% VOC emission reduction, using the stochastic regular inventory and the regular inventory with constant VOC emissions. The spatial distribution of the difference in response of ozone to the

VOC control has high resemblance to the results of NO_x emission reduction by the same percentage, shown in Figure E.2, but the quantity reported is opposite in sign. This is due to the fact that VOC emission reduction led to overall decreases in ozone concentration, while NO_x emission reductions led to overall increases in ozone concentration. The absolute magnitude of response to the VOC control is larger when stochastic inventory was used than when regular inventory was used. The maximum difference in absolute response of ozone concentration between using the stochastic and regular inventory is approximately 2.2 ppb.

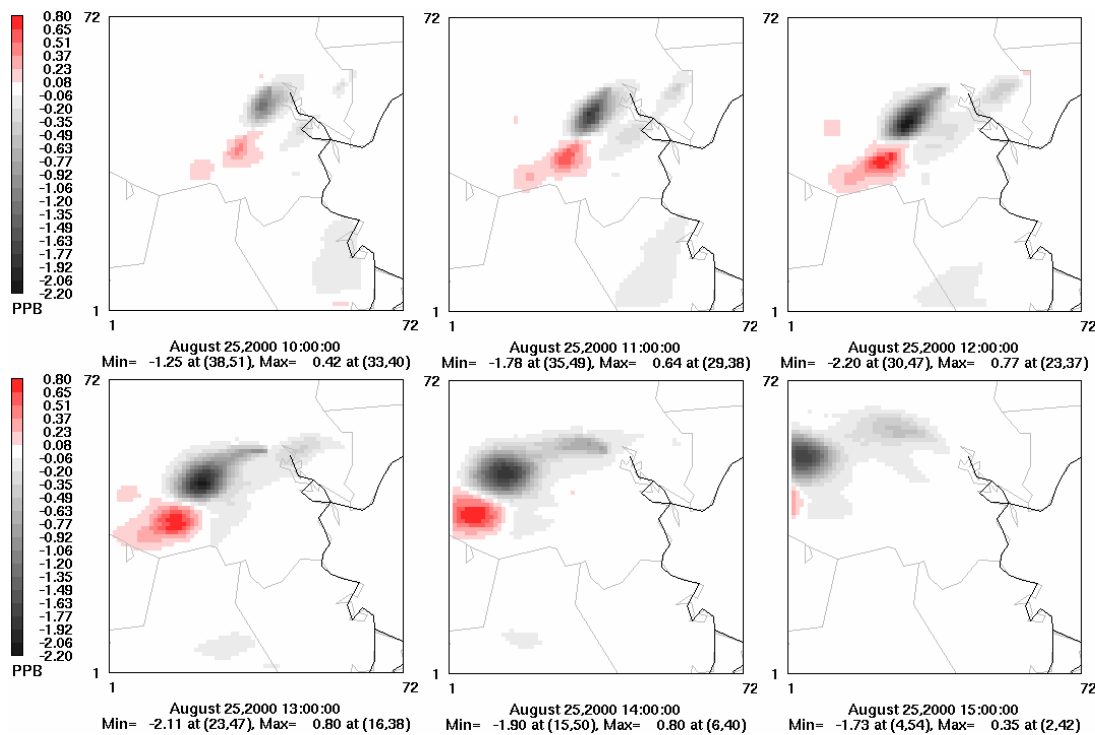


Figure E.5 Ozone difference plots showing difference in response of ozone to 25% VOC reduction across the sub-domain between using the 7th stochastic inventory and using regular inventory

In summary, the increases in ozone concentration due to NO_x reductions and the decreases in ozone due to VOC reduction were larger in regions of 200-300 km² when the stochastic regular inventory was used than when regular inventory, with constant VOC emissions, was used for simulating ozone concentration.

E.2 Impacts of VOC emission variability using imputed emission inventory

This section describes the effect of VOC emission variability on the effectiveness of various control strategies using the imputed emission inventory. The three ozone control strategies described in the previous section were assessed using the 7th stochastic imputed inventory and the imputed inventory with constant VOC emissions. The 7th stochastic imputed inventory was generated so that the added olefin emissions for each emission point are varied synchronously with the variable VOC emissions in the 7th stochastic regular inventory. That is, emission points in a facility that experienced high variability of VOC emissions in the stochastic regular inventory has also the same high variability of the added olefin emissions.

Figure E.6 presents changes in ozone concentration due to 25% NO_x reductions for all the emissions across the modeling domain using the 7th stochastic imputed inventory. Similar to the results using the regular inventory, ozone concentration was increased in a large portion of the modeling domain, by up to 56 ppb. The maximum decrease due to the control is approximately 10 ppb. Compared to the results shown in Figure E.1, the maximum increase in ozone is roughly 40% larger when using the stochastic imputed inventory. The maximum decrease in ozone concentration is 63%

larger using the imputed inventory than using the regular inventory. Besides the maximum increase observed in the early morning, high ozone concentration was observed earlier in the day using the imputed inventory than using the regular inventory. When the imputed inventory with constant VOC emissions was used for the simulations, similar response of ozone concentration was observed; maximum increase due to the control is approximately 56 ppb and maximum decrease is 9.5 ppb.

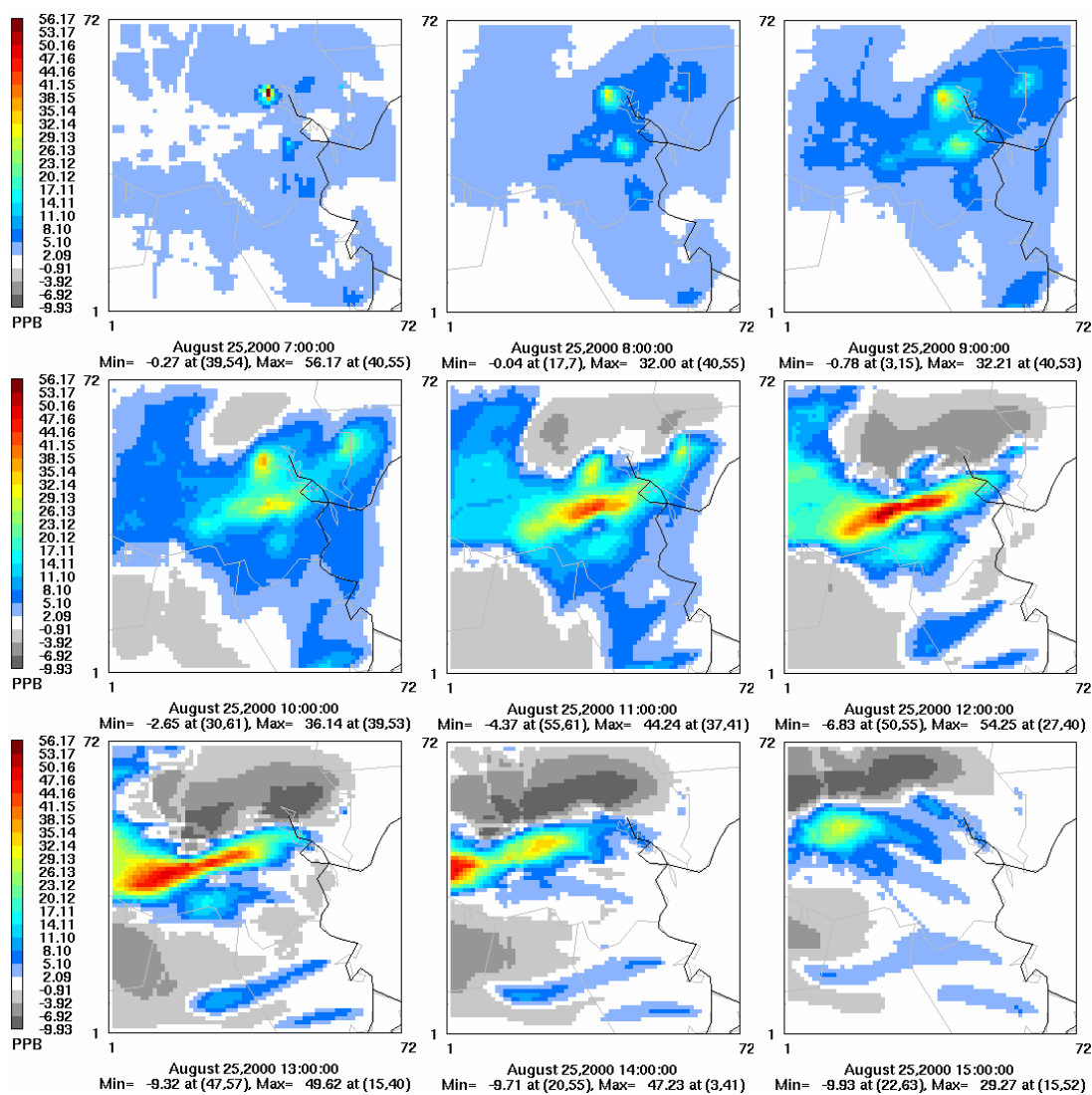


Figure E.6 Ozone difference plots between using the 7th stochastic imputed inventory with 25% NO_x reduction and using the stochastic imputed inventory without control

Figure E.7 shows the difference in response of ozone to 25% NO_x reduction of all the emissions across the domain between using the 7th stochastic imputed inventory and using the imputed inventory with constant VOC emissions. The quantity reported is as shown in Eqn. E-1, except that this set of simulations used the imputed inventory instead of the regular inventory. The difference in response of ozone to the NO_x control is dependent on time of day and location. The maximum difference in the response of ozone using the two versions of inventory is approximately 19 ppb. Compared to the results with the regular inventory shown in Figure E.2, the difference in response of ozone to the control is more than 7 times larger using the imputed inventory.

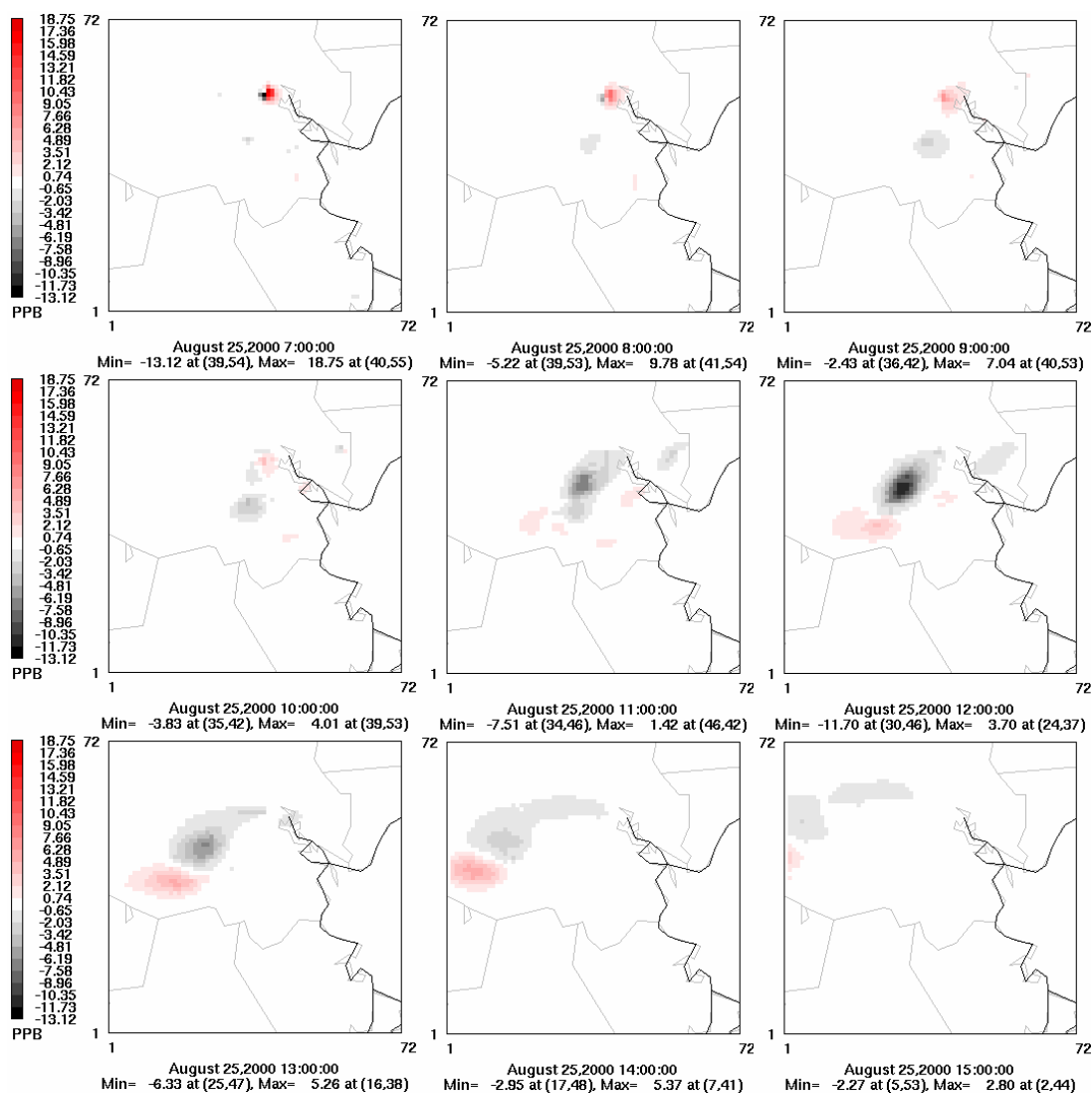


Figure E.7 Ozone difference plots showing difference in response of ozone to 25% NO_x reduction across the sub-domain between using the 7th stochastic imputed inventory and using the imputed inventory with constant VOC emissions

An ozone control strategy of 50% NO_x reduction of all the emissions across the area was assessed using the 7th stochastic imputed inventory and the imputed inventory without varying VOC emissions. When NO_x was reduced by 50%, the spatial distribution of ozone difference between using the inventory with the control and without the control exhibits a pattern comparable to the spatial pattern of ozone when NO_x was reduced by 25%, whether VOC emissions were constant or variable. However, the increase in ozone concentration due to the NO_x control is up to 92 ppb and 91 ppb using the stochastic and non-stochastic imputed inventory, respectively. Maximum decrease in ozone concentration is approximately 27 ppb and 25 ppb when using the stochastic and non-stochastic imputed inventory, respectively. Compared to the results using the regular inventory, high ozone concentration was observed earlier in the day using the imputed inventory.

Figure E.8 shows difference in response of ozone concentration to 50% NO_x reduction between the stochastic and non-stochastic imputed inventory. As shown in the figure, the results are similar to the case of 25% NO_x emission reduction. Maximum difference in response of ozone is approximately 32 ppb. Compared to the results using the regular inventory shown in Figure E.2, the maximum difference in response of ozone is more than 5 times higher using the imputed inventory than using the regular inventory.

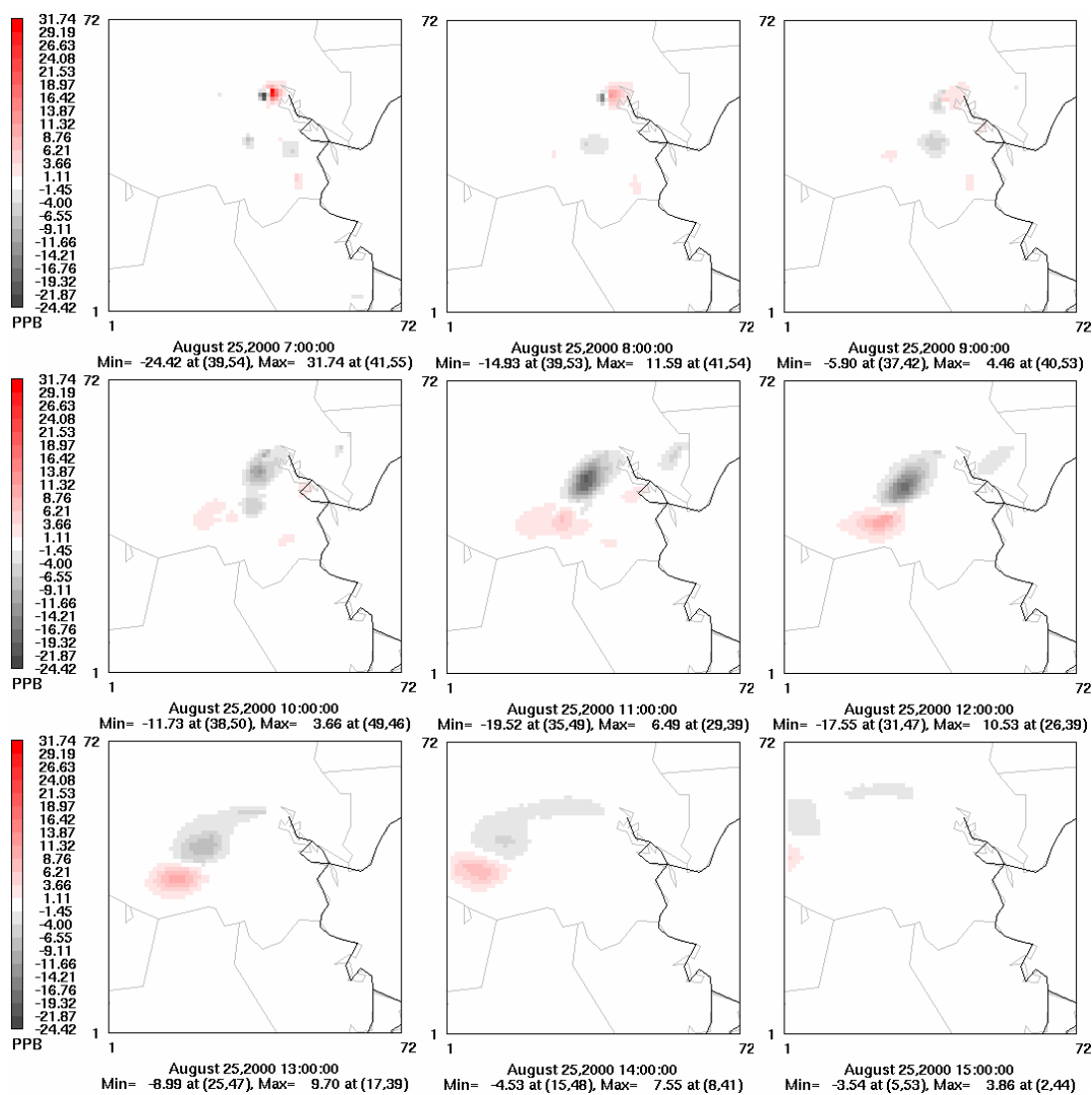


Figure E.8 Ozone difference plots showing difference in response of ozone to 50% NO_x reduction across the sub-domain between using the 7th stochastic imputed inventory and using the imputed inventory without varying VOC emissions

Finally, a control strategy of 25% VOC reduction was assessed using the stochastic and non-stochastic imputed emission inventory. Figure E.9 shows changes in ozone concentration due to the VOC control using the stochastic imputed inventory. With the VOC control, ozone was decreased in large portion of the area, by up to 61 ppb, while increases in ozone are negligible. This decrease in ozone concentration is nearly 3 times larger than using the regular inventory. When the imputed inventory with constant VOC emissions was used for the analysis, similar results were observed; the maximum decrease in ozone concentration was 63 ppb.

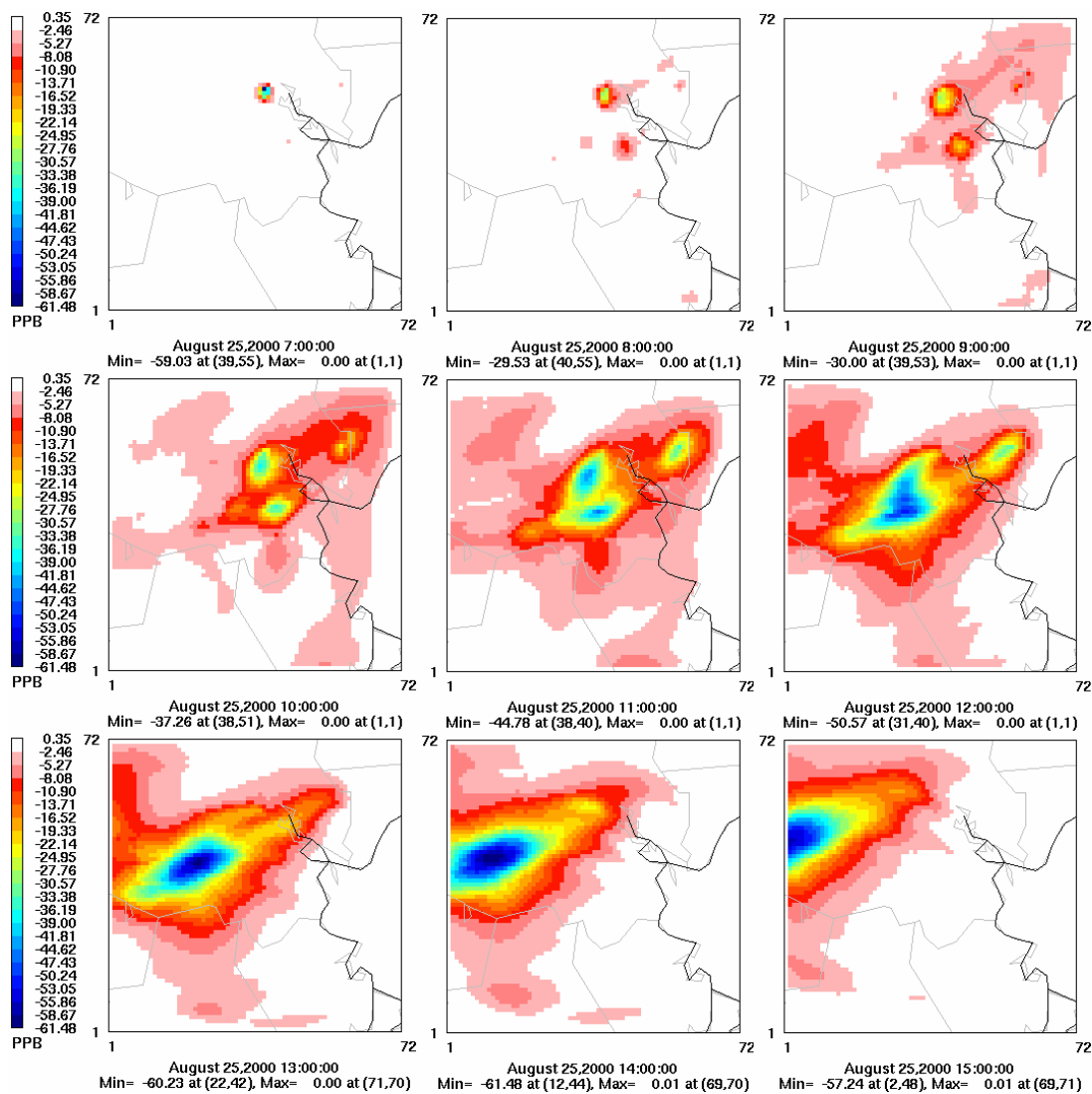


Figure E.9 Ozone difference plots between using the 7th stochastic imputed inventory with 25% VOC reduction and using the stochastic imputed inventory without control

The differences in the response using the two versions of imputed inventory are shown in Figure E.10. The magnitude of the difference in response is dependent on time of day and location. Maximum differences in both positive and negative direction are

observed at 7 am in the upper center portion of the domain and they are approximately 22 ppb in both cases.

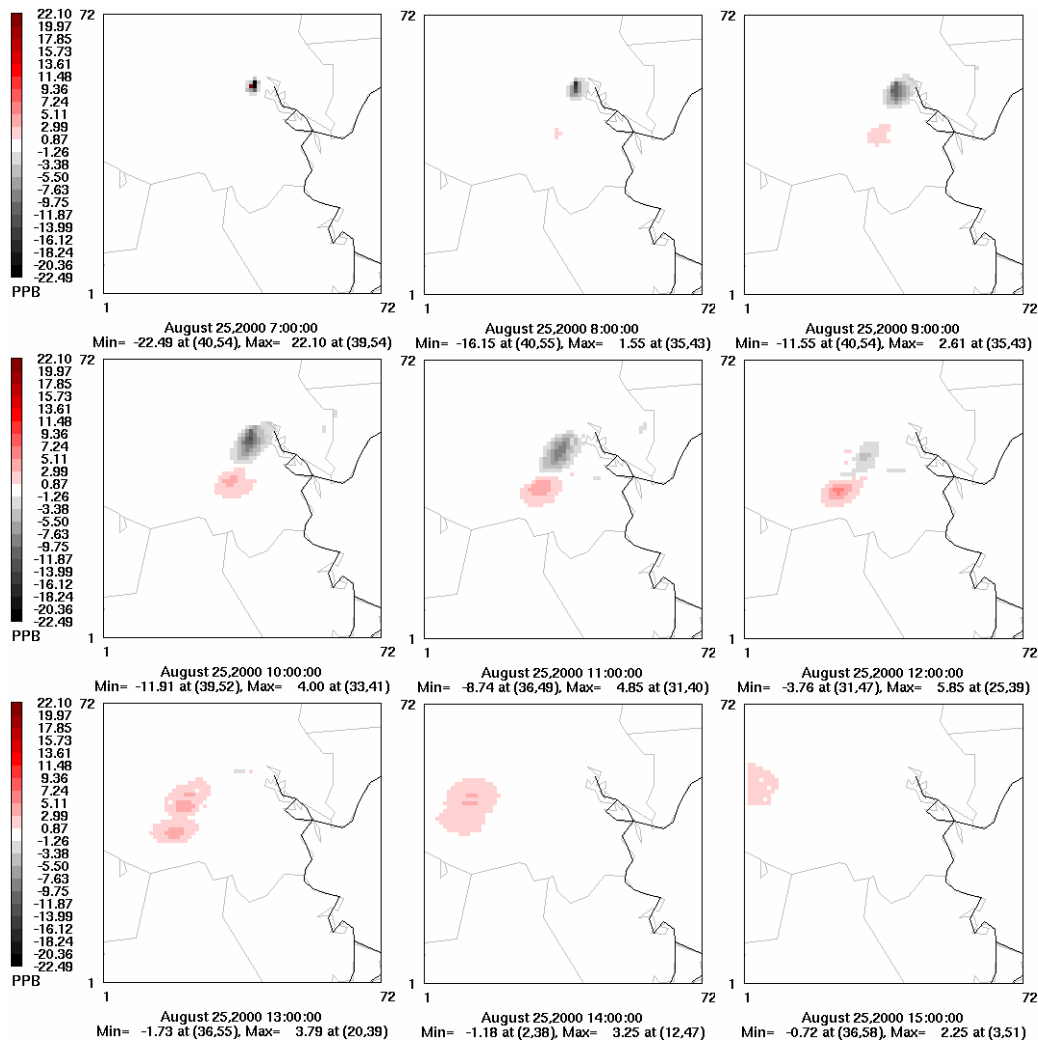


Figure E.10 Ozone difference plots showing difference in response of ozone to 25% VOC reduction across the sub-domain between using the 7th stochastic imputed inventory and using the imputed inventory without varying VOC emissions

In summary, response of ozone concentration to NO_x or VOC reductions were larger, in regions of 100-150 km², when the stochastic imputed inventory was used than when the imputed inventory, with constant VOC emissions, was used for simulating ozone concentration. Compared to the results using the regular inventory, the regions with larger response to VOC or NO_x reduction in stochastic inventory relative to the inventory with constant VOC emissions are small by a factor of two. If the stochastic imputed inventory used for this analysis represents real VOC emissions in the Houston area, control strategies associated with VOC reduction could be more effective, in the regions of 100-150 km², than is currently believed.

REFERENCES

- Abdel-Aziz, A., Frey, H.C., 2003. Quantification of Hourly Variability in NO_x Emissions for Baseload Coal-Fired Power Plants. J. Air & Waste Manage. Assoc. 53, 1401-1411.
- Allen, D., Murphy, C., Kimura, Y., Vizuite, W., Edgar, T., Jeffries, H., Kim, B.-U., Webster, M., Symons, M., 2004. Inventories of HRVOC Emissions & Impact of Emission Magnitude & Variability on Ozone Formation in H/G Area. Houston Advanced Research Center, H13.2003 Final Report, April 16, 2004, available at <http://www.harc.edu/harc/Projects/AirQuality/Projects/ShowProject.aspx?projectID=27>
- Bay Area Air Quality Management District, 2005. Flare Monitoring at Petroleum Refineries accessed February 2007 at <http://www.baaqmd.gov/dst/regulations/rg1211.pdf>
- Bay Area Air Quality Management District, 2006. Flares at Petroleum Refineries, Accessed January 2007 at <http://www.baaqmd.gov/dst/regulations/rg1212.pdf>
- Berkowitz, C.M., Jobson, T., Jiang, G., Spicer, C.W., Doskey, P.V., 2004. Chemical and meteorological characteristics associated with rapid increases of O₃ in Houston, Texas. J. Geophys. Res. 109, D10307
- Cardelino, C., 1998. Daily Variability of Motor Vehicle Emissions Derived from Traffic Counter Data. J. Air & Waste Manage. Assoc. 48, 637-645.
- Castineira, D., 2006. A computational fluid dynamics simulation model for flare analysis and control, PhD thesis, University of Texas.
- Carter, W.P.L., 1994. Development of ozone reactivity scales for volatile organic compounds, J. Air & Waste Manage. Assoc., 44, 881-899.
- Chi, T.R., Unal, A.D., Tian, R.A., 2004. Uncertainty of NONROAD emissions in Georgia. *13th Annual Emission Inventory Conference*, Clearwater, FL.
- Cornell, J., 2002. *Experiments with mixtures: designs, models, and the analysis of mixture data*. Wiley, New York.
- Daum, P.H., Kleinman, L.I., Springston, S.R., Nunnermacker, L.J., Lee, Y.-N., Weinstein-Lloyd, J., Zheng, J., Berkowitz, C.M., 2003. A comparative study of O₃

formation in the Houston urban and industrial plumes during the 2000 Texas Air Quality Study. J. Geophys. Res. 108 (D23), 4715

Daum, P.H., Kleinman, L.I., Springston, S.R., Nunnermacker, L.J., Lee, Y.-N., Weinstein-Loyd, J., Zheng, J., Berkowitz, C.M., 2004. Origin and properties of plumes of high ozone observed during the Texas 2000 Air Quality Study (TexAQS 2000). J. Geophys. Res. 109, D17306.

Environ International Corporation (Environ), 2004. User's Guide: Comprehensive Air Quality Model with Extensions (CAMx), Version 4.03, Document and model are available online at <http://www.camx.com>

Environ International Corporation (Environ), 2006. Comprehensive Air Quality Model with Extensions (CAMx) Pre-processors, Accessed January 2006 at <http://www.camx.com/download/support.php>

Environmental Protection Agency, 1998. Handbook for Air Toxics Emission Inventory Development, Vol. 1. Stationary Sources. EPA 454/B-98-002. Office of Air Quality Planning and Standards, Research Triangle Park, NC.

Environmental Protection Agency, 2003a. MOBILE6 Model, Accessed March 2007 at <http://www.epa.gov/otaq/models/mobile6/mobile62.zip>

Environmental Protection Agency, 2003b. Biogenic Emission Inventory System (BEIS), Accessed March 2007 at <ftp://ftp.epa.gov/amd/asmd/beis3v12>

Environmental Protection Agency, 2004. NONROAD2004 Model, Accessed March 2007 at <http://www.epa.gov/otaq/nonrdmdl.htm>

Environmental Protection Agency, 2007. AP-42: Compilation of Air Pollutant Emission Factors, Accessed February 2007 at <http://www.epa.gov/ttn/chief/ap42/index.html>

Frey, H.C., 1997. Variability and Uncertainty in Highway Vehicle Emission Factors. *Proceedings of the Air & Waste Management Association's Annual Meeting & Exhibition*, 208-219.

Frey, H.C., Bammi, S., 2002. Quantification of variability and uncertainty in lawn and garden equipment NO_x and Total hydrocarbon emission factors. J. Air and Waste Manag. Assoc. 52(4), 435-448.

Frey, H.C., Bammi, S., 2003. Probabilistic Nonroad Mobile Source Emission Factors. J. Environmental Engineering. 129(2). 162-168.

Frey, H.C., Li, S., 2003. Methods for quantifying variability and uncertainty in AP-42 emission factors: case studies for natural gas-fueled engines. J. Air and Waste Manage. Assoc. 53(12).

Frey, H.C., Song, L., 2003. Methods for Quantifying Variability and Uncertainty in AP-42 Emission Factors: Case Studies for Natural Gas-Fueled Engines. J. Air & Waste Manage. Assoc. 53, 1436-1447.

Frey, H.C., Zhao, Y., 2004. Quantification of variability and uncertainty for air toxic emission inventories with censored emission factor data. Environ. Sci. Technol. 38, 6094-6100.

Frey, H.C., Zheng, J., 2002. Probabilistic Analysis of Driving Cycle-Based Highway Vehicle Emission Factors. Environ. Sci. Technol. 36, 5184-5191.

Harley, R.A., Marr, L.C., Lehner, J.K., Giddings, S.N., 2005. Changes in Motor Vehicle Emissions on Diurnal to Decadal Time Scales and Effects on Atmospheric Composition. Environ. Sci. Technol. 39, 5356-5362.

Kleinman, L.I., Daum, P.H., Imre, D., Lee, Y.-N., Nunnermacker, L.J., Springston, S.R., 2003. Correction to "Ozone production rate and hydrocarbon reactivity in 5 urban areas: A cause of high ozone concentration in Houston". Geophys. Res. Lett. 30 (12).

Kleinman, L.I., Daum, P.H., Imre, D., Lee, Y.N., Nunnermacker, L.J., Springston, S.R., Weinstein-Lloyd, J., Rudolph, J., 2002. Ozone production rate and hydrocarbon reactivity in 5 urban areas: A cause of high ozone concentration in Houston. Geophys. Res. Lett. 29 (10).

Kleinman, L.I., Daum, P.H., Imre, D., Lee, Y.N., Nunnermacker, L.J., Springston, S.R., Weinstein-Lloyd, J., Rudolph, J., 2003. Correction to "Ozone production rate and hydrocarbon reactivity in 5 urban areas: A cause of high ozone concentration in Houston". Geophys. Res. Lett. 30 (12), 1639.

Levy, R.E., Randel, L., Healy, M., Weaver, D. 2006. Reducing emissions from plant flares. *Proceedings of the Air & Waste Management Association's Annual conference*, Paper #61.

Miller, A.C., Hidy, G., Hales, J., Kolb, E.C., Werner, S.A., Haneke, B., Parrish, D., Frey, H. C., Rojas-Bracho, L., Deslauriers, M., Pennell, B., Mobley, D.J., 2006. Air Emission Inventories in North America: A Critical Assessment. J. Air & Waste Manage. Assoc. 56, 1115-1129.

Murphy, C.F., Allen, D.T., 2005. Hydrocarbon emissions from industrial release events in the Houston-Galveston area and their impact on ozone formation. Atmospheric Environment 39(21), 3785-3798.

Nam, J., Kimura, Y., Vizuite, W., Murphy, C.F., Allen, D.T., 2006. Modeling the impacts of emission events on ozone formation in Houston, Texas. Atmospheric Environment 40 (28), 5329-5341.

NARSTO, 2000. An Assessment of Tropospheric Ozone Pollution: A North American Perspective. Palo Alto, CA: EPRI.

NARSTO, 2005. Improving Emission Inventory for Effective Air Quality Management Across North America: A NARSTO assessment, NARSTO-05-001.

National Research Council, 2004, Air Quality Management in the United States. National Academy Press, Washington, D.C.

Rhodes, D.S., Frey, H.C., 1997. Quantification of variability and uncertainty in AP-42 emission factors using bootstrap simulation. Presented at the *Emission Inventory Planning for the Future. Air and Waste Management Association: Pittsburgh, Pennsylvania, October*, 147-161.

Ryerson, T.B., Trainer, M., Angevine, W.M., Brock, C.A., Dissly, R.W., Fehsenfeld, F.C., Frost, G.J., Goldan, P.D., Holloway, J.S., Hubler, G., Jakoubek, R.O., Kuster, W.C., Neuman, J.A., Nicks, D.K., Parrish, D.D., Roberts, J.M., Sueper, D.T., Atlas, E.L., Donnelly, S.G., Flocke, F., Fried, A., Potter, W.T., Schauffler, S., Stroud, V., Weinheimer, A.J., Wert, B.P., Wiedinmyer, C., Alvarez, R.J., Banta, R.M., Darby, L.S., Senff, C.J., 2003. Effect of petrochemical industrial emissions of reactive alkenes and NO_x on tropospheric ozone formation in Houston, Texas. J. Geophys. Res. 108 (D8), 4249.

Seinfeld, J.H., Pandis, S.N., 1998. Atmospheric chemistry and physics. John Wiley & Sons, Inc. New York.

Shell Oil Products US, 2006. Shell Martinez Refinery Flare Minimization Plan.

Sokal, R.R., Rohlf, F.J., 1987. *Introduction to Biostatistics*. W.H. Freeman & Company, NY.

Texas Commissions on Environmental Quality (TCEQ), 2004. Air emission event reports. Accessed March 2007 at http://www.tceq.state.tx.us/compliance/field_ops/eer/

Texas Commissions on Environmental Quality (TCEQ), 2004. Revisions to the State Implementation Plan for the Houston-Galveston-Brazoria nonattainment area. Accessed

February 2007 at

<http://www.tceq.state.tx.us/assets/public/implementation/air/sip/sipdocs/2004-05-HGB/execsumm.pdf>

Texas Commission on Environmental Quality (TCEQ), 2006. Houston-Galveston-Brazoria Ozone SIP Mid-Course Review Modeling, Accessed January 2006 at <http://www.tceq.state.tx.us/implementation/air/airmod/data/hgb1.html>

Texas Commission on Environmental Quality (TCEQ), 2006a. Houston-Galveston-Brazoria State Implementation Plan (SIP) Revision, Accessed March 2006 at <http://www.tceq.state.tx.us/implementation/air/sip/hgb.html>

Texas Commission on Environmental Quality (TCEQ), 2006b. General air pollution and meteorological data, Accessed May 2006 at <http://www.tceq.state.tx.us/assets/public/compliance/monops/air/sigevents/03/event2003-10-23hou.html>

Texas Commission on Environmental Quality (TCEQ), 2006c. Air emission event reports, Accessed March 2006 at http://www.tceq.state.tx.us/compliance/field_ops/eer/

University of North Carolina, 2004. Stochastic Emission Inventories of Continuous Emissions. Houston Advanced Research Center, H13.2003 Final Report Appendix B, available at <http://files.harc.edu/Projects/AirQuality/Projects/H013.2003/H13AppendixB.pdf>

University of Texas at Austin, 2006. Comprehensive Air Quality Model with Extension (CAMx) Preprocessor for Albedo/haze/ozone column and Land use extraction

Vizuite, W., 2005. Implementation of Process Analysis in a three dimensional air quality model, PhD thesis, University of Texas.

Webster, M., 2004. Stochastic Emission Inventories of Continuous Emissions. Houston Advanced Research Center, H13.2003 Final Report Appendix B, available at <http://files.harc.edu/Projects/AirQuality/Projects/H013.2003/H13AppendixB.pdf>

Webster, M., 2007. Updates on Stochastic Emission Inventory Generator

Webster, M., Nam, J., Kimura, Y., Jeffries, H., Vizuite, W., Allen, D.T., 2007. The effect of variability in industrial emissions on ozone formation in Houston, Texas. Submitted to Atmospheric Environment

Zhao, Y., Frey, H.C., 2004. Development of probabilistic emission inventories of air toxics for Jacksonville, Florida, USA. J. Air and Waste Manag. Assoc. 54(11), 1405-1421.

VITA

Junsang Nam was born on September 30, 1975 in Seoul, Korea, the son of Bong-Gil Nam and Young-Hwa Lee. He attended Kyungmoon High School in Seoul, Korea and graduated in February, 1994. After high school he enrolled in Kyunghee University, Suwon, Korea and received Bachelor of Science degree in February, 2001. He entered the Master's program at The University of Texas at Austin in September, 2002. After completing his master's program, he entered the Ph.D. program at The University of Texas at Austin in December, 2004.

Permanent address: 809-31 Bangbae4dong Seochogu, Seoul, Korea

This dissertation was typed by the author.